GFRP STAY IN PLACE (SIP)

FLEXIBLE FORMWORK FOR CURVED SLABS

A Thesis Submitted in Fulfillment of the Requirement for the Award of the Degree of

MASTER OF ENGINEERING

IN

STRUCTURAL ENGINEERING

Submitted by:

SHIVANG GAUR

801624027

Under Supervision of

Dr. REEMA GOYAL
Lecturer

Dr. SHRUTI SHARMA
Associate Professor

Department of Civil Engineering

THAPAR INSTITUTE
OF ENGINEERING & TECHNOLOGY
(Deemed to be University)

CIVIL ENGINEERING DEPARTMENT

THAPAR INSTITUTE OF ENGINEERING & TECHNOLOGY

(A DEEMED TO BE UNIVERSITY), PATIALA, PUNJAB

JUNE, 2018

DECLARATION

I, Shivang Gaur hereby declare that the work presented in this thesis entitled "**GFRP STAY IN PLACE (SIP) FLEXIBLE FORMWORK FOR CURVED SLABS**" in fulfilments of the requirement for the award of degree of **Master of Engineering** in **Structural Engineering** submitted at Civil Engineering Department, Thapar Institute of Engineering & Technology (Deemed to be University), Patiala is an authentic record of work carried out under supervision of **Dr. Reema Goyal, Lecturer** and **Dr. Shruti Sharma, Associate Professor,** Department of Civil Engineering, Thapar Institute of Engineering & Technology (Deemed to be University), Patiala from January to July,2018.

The matter presented in this has not been submitted either in part or full to any other university or institute for the award of any other degree.

Date: 25/7/2018

SHIVANG GAUR

Roll No.: 801624027

(25/7/2018)

Dr. Reema Goyal
Lecturer
Department of Civil Engineering
Thapar Institute of Engineering & Technology
(A Deemed To Be University), Patiala, Punjab

25/7/2018

Dr. Shruti Sharma
Associate Professor
Department of Civil Engineering
Thapar Institute of Engineering & Technology
(A Deemed To Be University), Patiala, Punjab

ACKNOWLEDGEMENT

Time has provided me the cherished opportunity to express my heartfelt gratitude to my guides Dr. Reema Goyal, Lecturer and Dr. Shruti Sharma, Associate Professor, CED, Thapar University, Patiala, who permitted me to carry out research work under their able guidance. I shall ever remain indebted to them for their meticulous guidance, constructive criticism, clear thinking, keen interest, constant encouragement and forbearance right from the beginning of this research to its completion.

I wish to express my sincere thanks to Dr. Prem Pal Bansal, Associate Professor and Head, CED, Thapar University, Patiala, who has been a constant source of inspiration for me throughout this thesis work. The cheerful support of my friends and colleagues is sincerely appreciated. Special words of appreciation go to Sh. Ram Simran, Sh. Virender Singh and other laboratory colleague who helped me in my experimental work. I am also thankful to all the staff members of Civil Engineering Department for their full cooperation and help.

Above all, I thank my parents, whose love and affectionate blessing have been a constant source of inspiration in making this manuscript a reality. I render my gratitude to the almighty who bestowed self-confidence, ability and strength in me to complete this work.

SHIVANG GAUR

ABSTRACT

One of the important purpose of construction research is to develop a creative, ingenious, economical and efficient method of construction. Stay-in-place (SIP) formwork is such a system that is not required to be removed upon hardening of concrete. SIP structural formwork is a permanent participating formwork system which is structurally integrated with concrete. It acts as self-supporting formwork during construction and remains to act as reinforcement after the concrete hardens.

This research is in continuation with previous study which investigated the role of FRP stay-in-place formwork for concrete straight slabs. In this study aim was to check the behavior of GFRP planks as SIP formwork as well as reinforcement for curved slabs.

Experimental investigation regarding the suitability of the plank as SIP formwork for curved slab was done in two stages- casting stage testing and cured concrete flexural testing. In casting stage testing, sand and concrete loading tests were conducted to check if the planks has sufficient strength and stiffness for obtaining desirable curvature of slab. Performance of plank was tested as formwork for both straight and curved slabs

In the second stage testing the role of SIP formwork as reinforcement for curved slabs was investigated through cyclic flexural tests. For this test three slabs were casted out of which two are curved and one is straight with two types of bond treatments- aggregate bonding and adhesive bonding were compared. Ultimate load carrying capacity, deflection and strains level in GFRP and concrete were measured under two-point cyclic loading. Acoustic emission technique was used to monitor the cracks development during flexural testing. Finally, numerical validation of the experimental data was performed using non-linear finite elements method. A three-dimensional finite element model was prepared using software ATENA to simulate the behaviour of the bond treated GFRP-concrete interface.

Load carrying capacity of curved slab is around 25% higher than straight slabs. From the failure mode of all the three slabs, it was concluded that failure mode is brittle in case of both straight slabs and curved slabs. This study demonstrates that the bond treated FRP plank has the potential to serve as formwork and as tensile reinforcement for appropriately sized curved slabs concrete slabs provided the ductility issue is solved.

CONTENTS	Page No.

LIST OF FIGURES

LIST OF TABLES

CHAPTER 1

INTRODUCTION TO FRP STAY IN PLACE (SIP) FORMWORK

1.1 GENERAL

The applications of advanced composite materials in the civil engineering has been growing slowly, particularly due to economic reasons. Their main advantages, such as free form and tailorable design attribute, strength-to-weight ratios that outstandingly exceed those of conventional civil engineering materials and a high degree of chemical resistance in most civil environments are lost in high manufacturing costs. Furthermore, complete replacement of conventional structural member with overall advanced composite components has shown that it is difficult to justify the use of advanced composites in civil construction, not only economically, but structurally also. However, several developments have changed this scenario over the past few years. Techniques such as resin transfer molding, pultrusion, filament winding and semiautomated manufacturing of large components have led to advancements in low cost FRP (Fibre Reinforced Polymer) manufacturing. Also designs of these new materials in conjunction with conventional structural materials rather than individual component replacement or complete advanced composite designs, have shown that technical efficiency can be achieved within competitive economical constraints.

Fibre reinforced polymer composites, developed mainly for the aerospace and defense industries, are a class of materials with great potential to use in civil construction. Since the construction of the very first composite bridge superstructure in Miyun, China, in 1982, have led to wide range of acceptance from civil engineers as a new composite construction material. In last few years, Fibre reinforced polymer composites have proved their usefulness in a few areas of applications: mainly in form of strips and sheets for retrofitting of existing bridge structures, and also as reinforcing bars and eliminating steel as reinforcement used in concrete. In recent years large number of constructions have been done, in which traditional materials have been replaced by FRP composites materials for structural elements.

One of the important purpose of construction research is to develop a creative, ingenious, economical and efficient method of construction. Conventional reinforced concrete structures are fabricated by using temporary forms which are generally made of wood or steel in which casting of concrete is done. These forms are generally held in place by temporary shoring or scaffolding structures. Upon hardening of the concrete, the forms are removed, exposing the concrete structure within. In recent years the use of Stay-in-Place (SIP) forms,

also known as permanent forms which remains structurally integrated with the concrete and provides structural strength to the overall system is gaining popularity. Instead of being removed after setting, these forms become a part of the permanent structure. The forms acts as a self-supporting formwork during construction stage, and acts as structural reinforcement throughout the lifetime of the structure. The primary advantage of SIP form construction is the additional speed and ease of construction which they offer over conventional formwork. These SIP forms are most commonly either corrugated cold rolled steel or precast concrete. Erection and removal of conventional formwork and its associated falsework is often expensive, potentially hazardous and in some instants presents significant technical challenges. In some situation the use of SIP permanent formwork might significantly lower down these costs and risks. Moreover, the elimination of conventional rebar cages can significantly simplify the engineering and detailing process (Ralph and Denton, 2004), as well as saving a great deal of time and effort during construction. It can also help to improve the longevity of the system by eliminating steel reinforcements that are susceptible to corrosion.

Structural system with FRP SIP forms will make appropriate use of FRP in tension and concrete in compression. The elimination of typical reinforcement can significantly simplify the engineering and detailing process, as well as saving a great deal of time and effort during construction. It can also help to improve the longevity of the system by eliminating steel reinforcements that are susceptible to corrosion. In recent years various open structural formwork that can be used as SIP formwork and having corrosion resistant property have been explored. It should be noted that FRP materials still have a relatively short track record in structural applications, relative to steel. As such, their long-term durability is yet to be confirmed. These types of formwork are prefabricated in factories using a technique called pultrusion and their mass production is important as they have to be used in large numbers at the site. It is also relatively light weight, so forms can be shipped, maneuvered, and installed by a few workers without the aid of heavy machinery. Since these forms have excellent stiffness and dimensional stability, the need for scaffolding or shoring is greatly reduced or eliminated completely. In order to compensate the high initial cost of FRP forms it is required consider its various advantages like advanced construction activity and erection speed, and reduction in maintenance cost of the structure due to superior life cycle and durability.

1.2 ORIGIN OF THE PROJECT

From the previous studies it was found out that the use of FRP planks as permanent formwork serving both as formwork and reinforcement performs well when some bond treatment is provided between cast in place concrete and FRP formwork. This bond treatment is required to achieve composite action between the two. However, the previous study was limited to straight flexural members. Thus, in order to cast structural members with complicated configuration from aesthetic and structural point of view, there is need of research on performance of FRP plank as SIP formwork for different configuration of structural members.

In this study, one configuration of curved slabs with flat top and concave bottom surface has been selected. The most important parameter is to check the flexibility of GFRP formwork. Experimental investigations regarding the suitability of the plank as SIP formwork for curved slab was done in two stages- casting stage testing and cured concrete flexural testing. Basic aim of this research is to use the GFRP plank as permanent flexible formwork and also as reinforcement for curved concrete flexural members.

1.3 OBJECTIVES

The primary objective of this study is to study the performance of pultruded GFRP sections as stay-in-place structural open formwork for concrete flexural members, as well as to investigate some of the logistical details that arose while developing such a structural system. The main topics addressed by this study are:

1. To evaluate experimentally the ability of proposed GFRP plank as formwork and as reinforcement for curved slabs.

2. To compare the performance of GFRP plank as reinforcement for curved and conventional straight slabs.

3. To compare the performance of aggregate bonding and adhesive bonding bond mechanisms.

4. To monitor the cracks and investigate the cracking pattern and failure mechanism of the GFRP concrete hybrid slabs during flexural testing through Acoustic emission.

5. To develop Finite Element Model of the proposed FRP plank as formwork and as reinforcement.

1.4 OUTLINE OF THESIS

Chapter 2: In this chapter literature review of various properties of GFRP plank like bond performance, durability, flexural properties and as flexible forms and how Acoustic Emission Technique (AET) is used for monitoring damage pattern in concrete structures is presented.

Chapter 3: This chapter gives details of the experimental program and various experimentation procedure conducted on GFRP plank.

Chapter 4: The results of the experimentatal analysis and the results obtained are presented and discussed.

Chapter 5: FEM simulation of GFRP slabs is attempted and comparison with experimental result is presented.

Chapter 6: In this chapter various conclusions drawn from the present research work is presented.

CHAPTER 2

LITERATURE REVIEW

2.1 GENERAL

This chapter generally reviews the research that has been performed on stay-in-place open structural formwork for reinforced concrete flexural members. Firstly, a brief introduction about stay in place formwork is presented. Then a brief introduction about open stay in place formwork is presented. In particular, the chapter addresses about the various bond mechanisms between FRP SIP formworks and concrete and also about the FRP profiles that have potential to be used as structural forms. It also reviews about the various new techniques by which FRP SIP formwork is used in bridge decks.

Fiber-reinforced polymers (FRPs) includes of load-bearing fibers implanted in a polymer matrix and the reason for using reinforced polymers is to obtain maximum advantage from the reinforcement fibers. The properties of FRPs can be engineered over a wide range due to the large selection of fiber reinforcements, orientations, and polymer matrices. The reinforcement fibers usually dominate the mechanical properties, especially the tensile strength and stiffness of the composite. The volume fraction of fibers determines dimensional stability and resistance to creep under load. Two types of polymer resins are used as matrices in FRPs: thermoplastics and thermosetting polymers. Thermoplastics melt when heated and solidify when cooled. In contrast thermosets cure permanently through irreversible cross-linking at elevated temperatures. Mainly thermosets are used for FRP structures today, and the most important of these are unsaturated polyester (UP) resins, epoxy (EP) resins, vinylester (VE) resins and phenolic resins. The polymer encapsulates the fiber in order to fix the fibers in the desired direction, transfer the loads to the fibers and prevent buckling of the fibres. At the same time it seals the fiber surface and prevents moisture to drop off along the fiber.

SIP formwork is not required to be removed after the concrete has been cast. With the use of permanent formwork construction speed increases as time for the removal of the forms is saved. It also results in the saving of labour cost. With the use of SIP formwork the durability properties of concrete also improves. The formwork is assembled on site, connected with different connections available, bracing is also done and then concrete is poured. After the setting of concrete the bracing is set aside and SIP form remains at its place and provides exterior casing. With the use of SIP formwork the accidents which used to occur while removing forms are prevented. Thus, the use of SIP formwork results in fast, economical and safe construction.

Stay in place (SIP) formwork bifurcates into two categories:

(a) Stay in place Structural formwork – These are the type of formworks that shows composite behavior with the structure and take part in resisting the live loads during service as well as load during casting. Simply it can be said that they act both as reinforcement as well as formwork for the framing system.

(b) Stay in place Non-structural formwork – These are the type of formwork that resist only the loads coming at the time of casting and also the live loads during construction till the time when concrete has been set. Economically Structural SIP forms are more sound when compared to non-structural SIP forms as they reduces the amount of material due to the reduction in cost of material that is required as reinforcement.

In recent years FRP has marked its place in construction industry as a material for retrofitting and structural integrity ***(Ramana et al. (2000); Hadi et al. (2003))***. In the current scenario FRP is not only restricted to retrofitting material but also as structural material like reinforcement for bridge decks in the form of FRP rods and gratings ***(Alagusundaramoorthy et al. (2006); Grace et al.(2013))***. Due to the advancements in the field of FRP, the abstraction of FRP structural stay in place forms system has been taken into account. A state-of-the-art article has been disseminate that majorly discuss the application of FRP stay in place form for bridge decks (***Nelson et al. (2014))***. There are various field application regarding the use of FRP that have been discussed in the literature, some of them includes Greene County Bridge which was constructed in Missouri ***(Matta et al. (2006))***, Salem Avenue Bridge constructed in Ohio ***(Reising et al. (2004))***, the Black River Falls Bridge that was constructed in Wisconsin ***(Olivia et al. (2007))*** and Route US-151 Bridge which was constructed in Wisconsin ***(Berg et al. (2006))***.

2.2 BOND MECHANISM BETWEEN FRP SIP STRUCTURAL FORMWORK AND CONCRETE

Hall et al. (1998) worked on a hybrid concrete-FRP section using FRP stay- in-place open formwork. Corrugated FRP sheets can be used as floor panels, which is integrated with tensile reinforcement can be used as floor panels and as permanent open SIP structural formwork for the concrete slab, as shown in Fig.2.1**.** The casted hybrid beam made of concrete-FRP was then tested with four-point bending. At the very initial stage it was found out that there was some horizontal shear slippage between the surface of concrete and FRP. This horizontal shear

slippage critically reduces the flexural capacity of the member because of the existence of large strain lag between the surface of concrete and FRP.

In an attempt to deal with the above mentioned problem, adhesive bonding was applied. This was achieved by applying adhesive (epoxy mortar) directly over the surface of the FRP formwork before pouring of the concrete. This adhesive was specially manufactured for bonding with fresh wet concrete. The resultant system showed monolithical behaviour during positive bending. Plot for mean shear stress versus slip is represented in Fig.2.2. The failure mode observed was diagonal tension shear cracking, which occurred due to the absence of shear reinforcement within the concrete. Tension cracking of concrete was critical in the absence of the longitudinal stiffening ribs of the FRP sheet. Overall, the concept of applying adhesive to the formwork before pouring of concrete appears to have provided positive results. It was an advantageous technique from a fabrication standpoint because it reduced the use of mechanical shear studs or the use of aggregate bonding on the surface of the formwork, because both of them are very much time consuming to install than adhesive bonding.

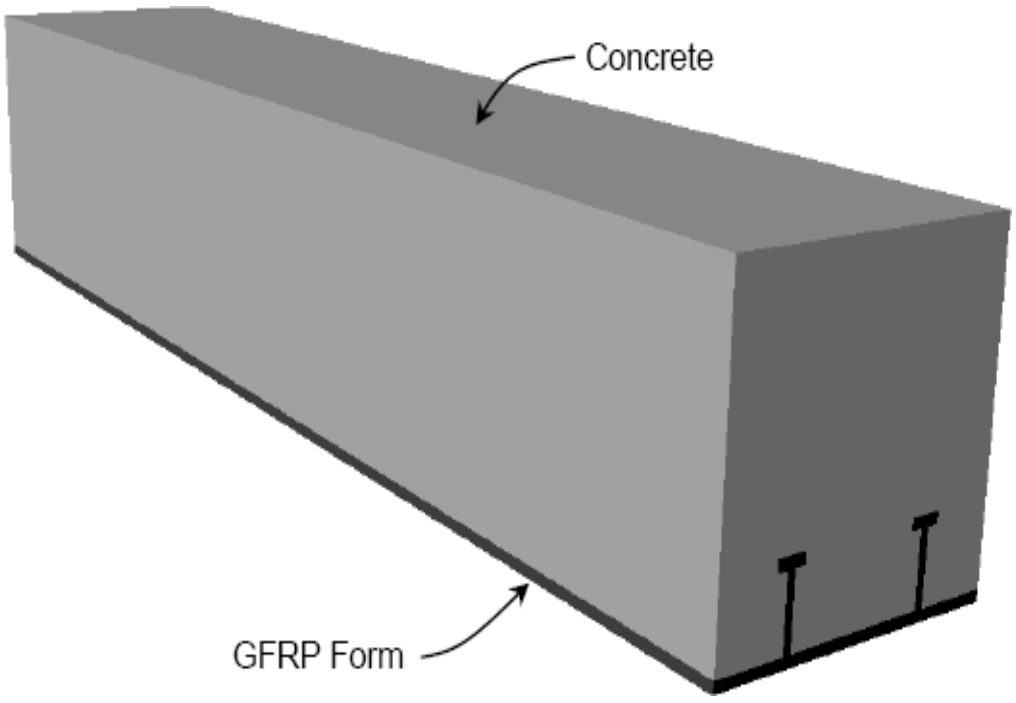

Fig.2.1 Concrete and GFRP Ribbed Sheet Hybrid Section ***(Hall et al. (1998))***

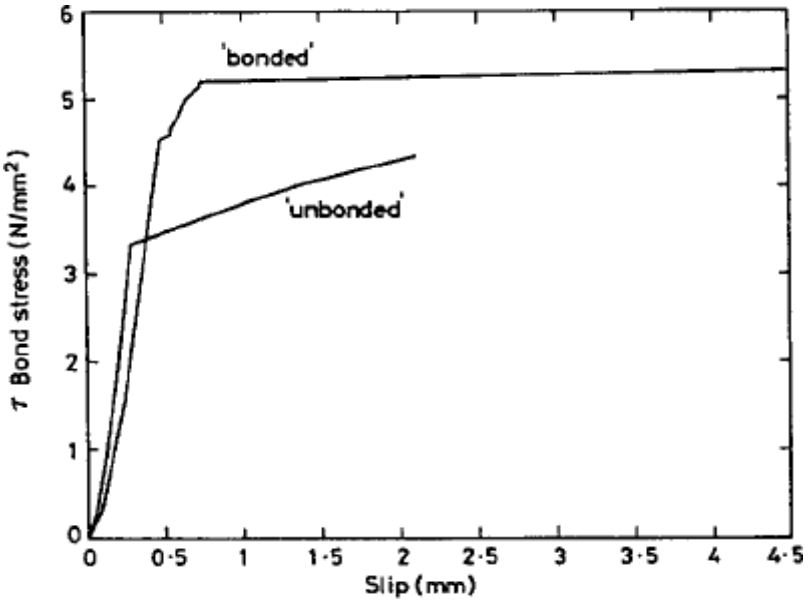

Fig.2.2 Average Bond Stress with Slip ***(Hall et al. (1998))***

Dieter et al. (2002) carried out study on different FRP formworks and FRP reinforcement for the bridge deck. Hybrid concrete-FRP stay-in-place open structural formwork and FRP grid reinforcement were used. A pultruded FRP sheet with hollow FRP box sections (Fig.2.3) running along the length provide stiffness and is being used as tensile reinforcement and play the role of stay-in-place structural open formwork for the concrete slab casted. For the regions where negative bending moments occur a bi- direction grid incorporated with pultruded FRP elements provides the top longitudinal reinforcement. In order to obtain sufficient amount of bond between the FRP stay-in-place formwork and the concrete slab casted over it, the FRP formwork surface is required to be roughened before pouring of the concrete along with the coating of a mixture which consist of epoxy and gravel. This was found to have a decreasing effect on the bond performance. A very critical slippage was found between the surface of FRP and concrete slab at the places where bond mechanism was absent. Consequently, the regions where bonding was absent the flexural crack pattern was very much predominent than the regions where bonding was provided.

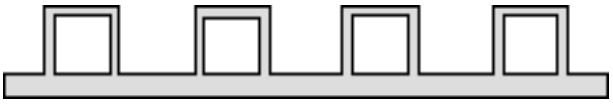

Fig.2.3 Selection of Formwork used **(*Dieter et al. (2002)*)**

Bank et al. (2006) discussed about the pultruded fiber reinforced polymer (FRP) plank that can be used as formwork and also as a reinforcement in the tensile region for a concrete member. The study was influenced by the construction of new bridge that was being constructed in Wisconsin in FRP planks were being used as both permanent formwork and also as reinforcement. For the composite action to be achieved between FRP plank and the concrete the main requirement was to have a bond between concrete and the FRP plank (Fig.2.4). To achieve this bond at the interface, aggregates bonding was adopted. Two kinds of aggregates were used that is gravel and sand. A commercially available adhesive was used to achieve the aggregate. Concrete beams of different lengths were casted using pultruded FRP plank and limits the use of flexural or shear reinforcement in the beams. For control specimens two beams were casted. One control beam was without aggregate bonding and the other control beam was casted in a traditional manner with the use of reinforcement and without FRP plank**.**

The beams were loaded up to their ultimate capacity by central patch load. Fig.2.5 shows dimension of fabricated FRP plank reinforced beam specimens. Suitable bond between the FRP plank and the concrete was achieved and depends upon the length of the beam, shear or flexural failures that occurred while testing. As per the results the initial cracking moment capacity of a concrete beam was increased in case of coated FRP plank and proved to be a benefit for a bridge deck as far as servicibility factors are concerned. The sand coated FRP plank specimen depicted higher initial cracking capacity than the gravel coated FRP plank specimen which shows there is an even interface or smooth surface in case of sand coated specimen. With the use of aggregate bonding it was found out that it is proved to be a mechanism to distribute cracks and to transfer bond stress at the surface between the plank and the concrete.

It was found out that the aggregate bonded FRP plank can be used as an effective tension reinforcement and shows the distribution of flexural cracks in a very similar way as shown by internal steel reinforcements. As far as initial cracking moment capacity, ability to distribute flexural cracks and ultimate load carrying capacity are concerned the aggregate bonded FRP plank specimens shows better results than the steel reinforcement. The specimens which were casted without any surface treatment resulted in significant slip between concrete and FRP and very much less capacity during testing. The aggregate coated FRP plank specimens showed higher ultimate capacity than that of the control specimens**.** The failure mode of all the specimens is shown in Fig.2.6 and Fig.2.7. This study shows that the FRP plank can be used as formwork and has the potential to serve as tensile reinforcement for concrete beams.

Fig.2.4 12 Inches Wide Pultruded FRP Plank ***(Bank et al. (2006))***

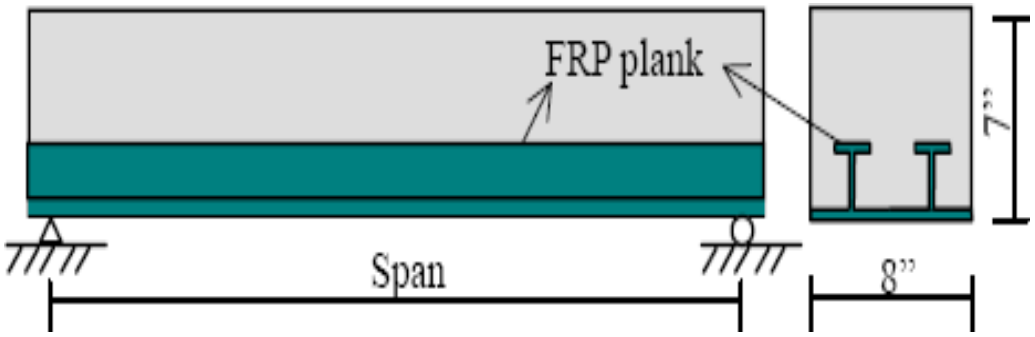

Fig.2.5 Dimension of FRP Plank Reinforced Beam Specimens ***(Bank et al. (2006))***

Table 2.1 Dimension of fabricated FRP plank reinforced beam specimens ***(Bank et al. (2006))***

Specimen I.D.	Span	Tensile Reinforcement	Compressive Strength(Psi)
1	3"7"	Gravel coated FRP Plank	3,740
2	3"7"	Sand coated FRP plank	3,740
3	3"7"	Sand coated FRP plank	3,550
C1	3"7"	FRP plank	3,740
4	6"	Sand coated FRP plank	4,650
5	6"	Sand coated FRP plank	4,860
C2	6"	Sand coated FRP plank	4,775

a) Shear failure of specimen 1

b) Shear failure of specimen 2

c) Shear failure of specimen 3

d) Flexural failure of specimen C1

Fig.2.6 Specimens 1-3 and C1 after Test **(*Bank et al., 2006)***

1) Hybrid failure mode of specimen 4

2) Hybrid failure mode of specimen 5

3) Flexural failure of specimen C2

Fig.2.7 Specimens 4-5 and C2 after Test **(*Bank et al., 2006)***

Fam et al. (2009) presented a study on a trapezoidal pultruded glass fiber-reinforced polymer (GFRP) section which has been used as a structural formwork for concrete girder. Pin- and-eye connection was used in order to ensure continuity in transverse direction. For the study of different bond systems the performance in positive and negative bending girders with different dimensions were casted and tested for flexure. Fig.2.8 depicts the GFRP profile and the different profiles which are filled with concrete. The bond systems that were used are (a) adhesive bond to freshly casted concrete (b) aggregates bonding and (c) mechanical shear studs which are anchored to the GFRP flanges). Steel wire meshes were welded close to the upper surface of the slab, and have the main purpose of shrinkage crack control.

The concrete and GFRP section showed no slippage but delamination occurred within the concrete layer that remained attached to plank. The pull-out test resulted in failure of the mechanical studs. Concrete and GFRP achieved approximately 47–75% of their full strengths at ultimate bond failure. This was also proved that the adhesive bonding showed equivalent strength as that of other systems and its ease to apply.

A “moment-curvature” analytical model, incorporating a strong bond failure criterion, was developed, validated, and utilized in a constant study. Stiffness or the bond failure load was influenced by the increasing compressive strength of the concrete. As far as concrete compression failure is concerned flexural strength is increased. With the increase in the thickness of the GFRP flanges the flexural strength and stiffness of the specimen increases considerably on the other hand there was no possible effect on the bond failure load.

The hollow concrete core in the tension region had minimal effect on stiffness. Due to the hollow concrete core the void is created and runs through the bottom GFRP flange which in turns reduced the bond are and also resulted in reduction of the strength by an amount of 13% but the overall strength -to- self weight ratio of the voided section is almost 30% more than the filled section. Fig.2.9 depicts the load-deflection responses of the different specimens. Critical values were found for shear span-to-depth ratio, shear strength of cement mortar, concrete strength, and width of the top GFRP flange, after which, the required flexural failure mode comes prior to bond failure.

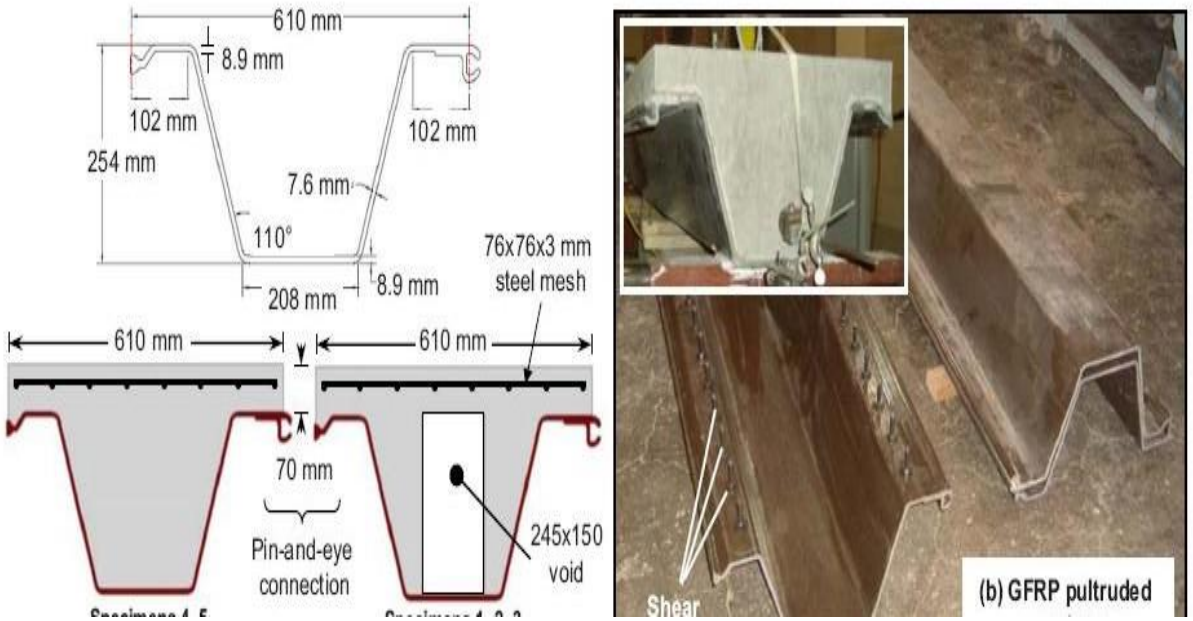

Fig.2.8 GFRP Profile and Concrete Fill Configuration ***(Fam et al. (2009))***

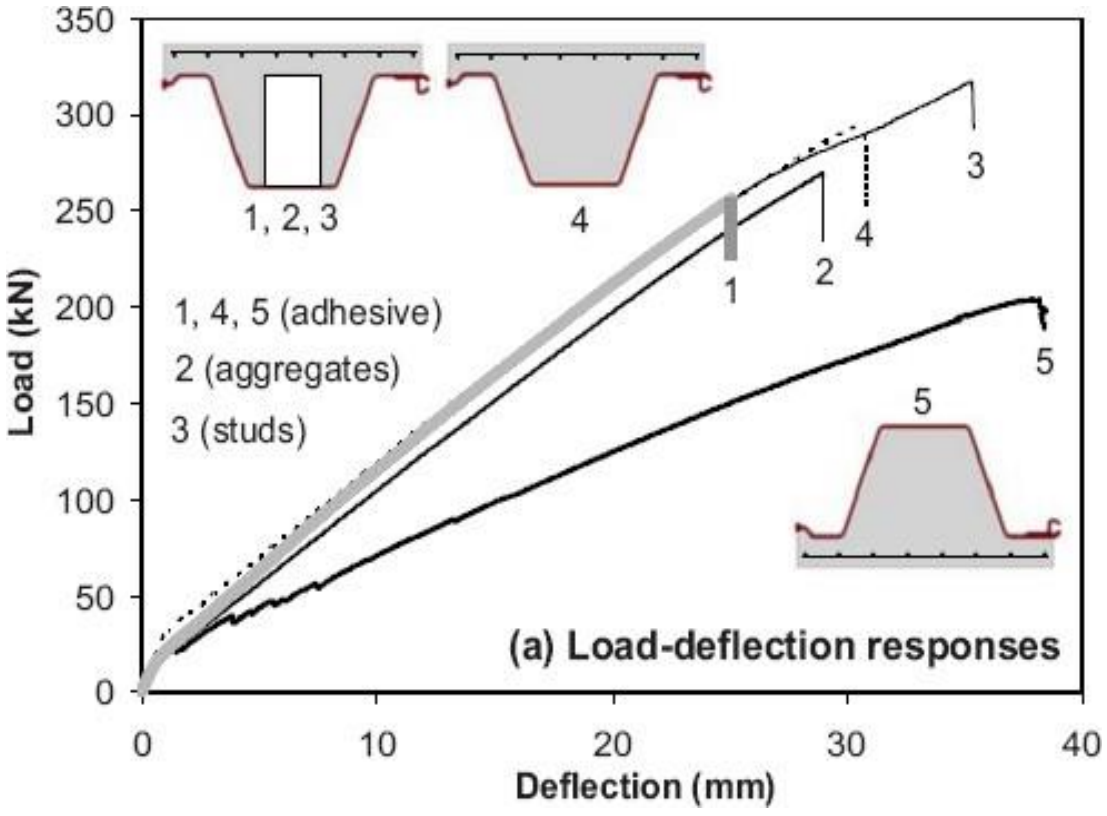

Fig.2.9 Load Deflection Response ***(Fam et al. (2009))***

Goyal et al. (2016) have explored the use of FRP stay-in-place formwork to culverts with three different adhesives and two different techniques of application, adhesive bonding and aggregate bonding. The FRP used as SIP is a commercially available pultruded GFRP profile consisting of plates with T-shaped ribs shown in Fig.2.10. A Self-compacting concrete with compressive strength of 50 MPa. and manufacturer specified mechanical properties of the adhesives were used. Specimen of concrete with FRP formwork with and without adhesive coating were prepared as shown in Fig.2.11 and were placed in universal testing machine(UTM) and subjected to upward pull resulting in tension in FRP and compression in concrete. The result shows two major modes of failure (a) Failure of the interface (b)Failure of concrete. Very less failure load of control concrete shows the importance of bond treatment at the interface between FRP and concrete for the FRP formwork to perform successfully. The failure mode and the load capacity varries with the use of adhesive as shown in Table.2.2. Load displacement behaviour given in Fig.2.12 shows that initial stiffness of samples with mixed mode failure (AB, GB) was about 2.5 times more than that of the samples failing through FRP-adhesive interface failure (AA, GA) but the initial stiffness of AC and GC was similar to that of AB and GB respectively. Overall, the concept of using adhesive to the formwork before pouring of concrete appears to have provided the positive results. Most of the adhesives that are available in the market are manufactured for bonding with cured concrete whereas in the case of adhesive bonding wet concrete is poured over the adhesive. This fundamentally alters the process of polymerisation. Therefore, depending on manufacturer's data sheet is not good enough and the adhesives should be specifically tested for their application. It was a beneficial technique as far as fabrication is concerned because it eliminated the need for mechanical shear studs or a bonded coarse aggregate coating on the surface of the formwork, both of which would be far more time consuming to install than an adhesive coating.

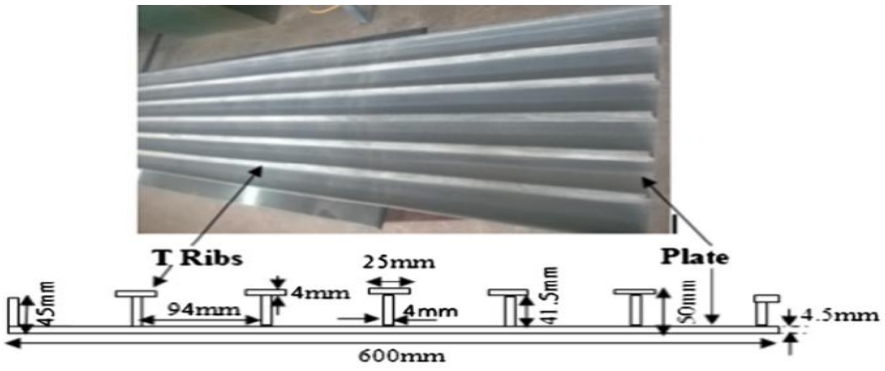

Fig.2.10 FRP Plank ***(Goyal et al. (2016))***

Table 2.2 Load Capacities and Failure Modes ***(Goyal et al. (2016))***

Series	Load capacity (kN)	Standard Deviation	Failure mode
C	5	0.328	FRP-concrete interface failure
AA	33	1.140	FRP-adhesive interface failure
GA	19.5	1.843	FRP-adhesive interface failure
AB	44	1.702	FRP-adhesive and Concrete-adhesive mixed failure
GB	43.6	1.740	FRP-adhesive and Concrete-adhesive mixed failure
AC	46.18	1.472	Concrete failure
GC	45.2	0.758	Concrete failure

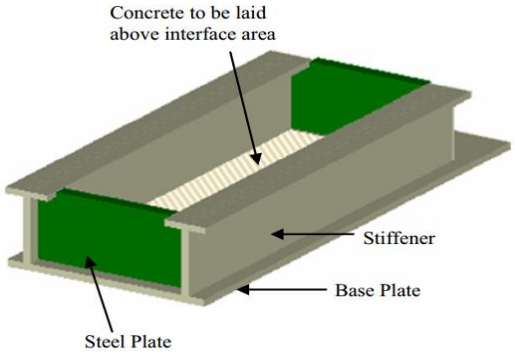

Fig.2.11 FRP Formwork with Bond Coating ***(Goyal et al. (2016))***

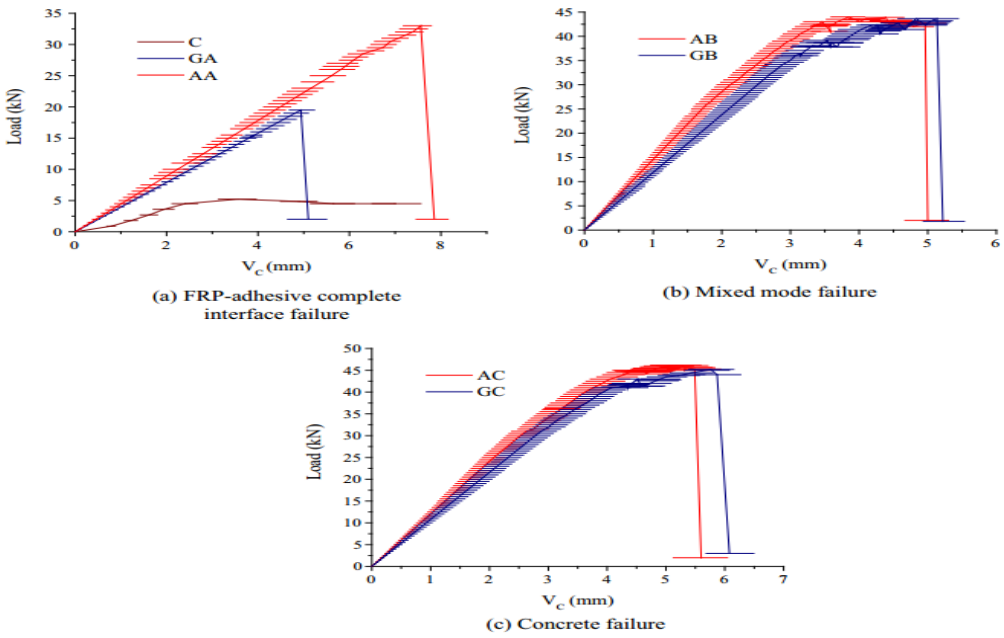

Fig.2.12 Load vs Concrete Displacement for Different Failure Modes ***(Goyal et al. (2016))***

Goyal et al. (2016) investigated the bond between FRP and cast-in-place concrete with two major objectives (a) to understand the performance of commercially available adhesives for

bonding; and (b) to compare the performance of adhesive bonding and aggregate bonding. To study the bond properties push out tests is conducted. Concrete was loaded with uniform compression at top. The entire force transfers through the bonded FRP-concrete interface as shear. All specimens were tested in displacement control mode with rate of loading 0.2mm/min. The result depicts that adhesive bonding achieved higher bond strength than aggregate bonding and is time saving and easy to apply. Fig.2.13 shows the load–vc (concrete displacement measured by digital dial gauge II) plots for the different systems. The control sample showed the lowest stiffness. The FRP-adhesive interface failure specimen shows two times more stiffness as compared to that of control samples. The concrete-adhesive interface failure specimen achieved about three times more stiffness than the specimens failed through FRP-adhesive interface failure. Stiffness of the specimens having material failure was similar to that of the specimens with concrete-adhesive interface failure. Clearly, it is believed that the adhesive type has an impact the failure mode and the specimen stiffness. It was also found out that ultimate load of the samples increases with increasing bond length. However, the average shear stress decreases with increasing area of bond as shown in Fig.2.14. The main reason for local failure is the non-uniform distribution of shear stress occurring in the bonded area. Thereafter, an increase in the bond area is observed due to the initiation of various failure modes. Further with the increase in the bond length a considerable decrease in the increase in failure load was noticed.

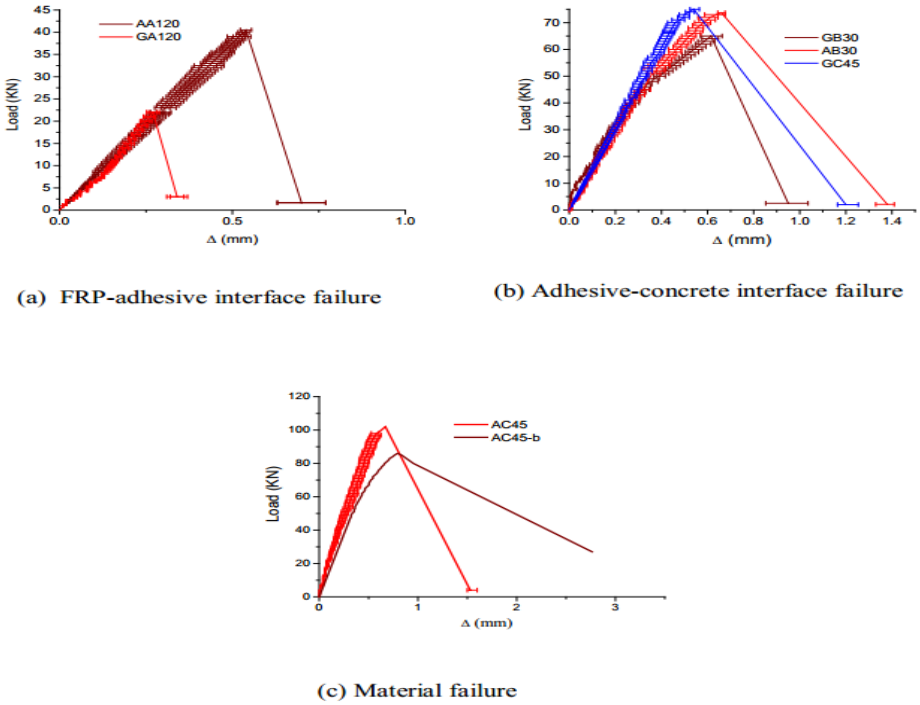

(a) FRP-adhesive interface failure

(b) Adhesive-concrete interface failure

(c) Material failure

Fig.2.13 Load-Concrete Displacement Plot for Different Failure Modes ***(Goyal et al. (2016))***

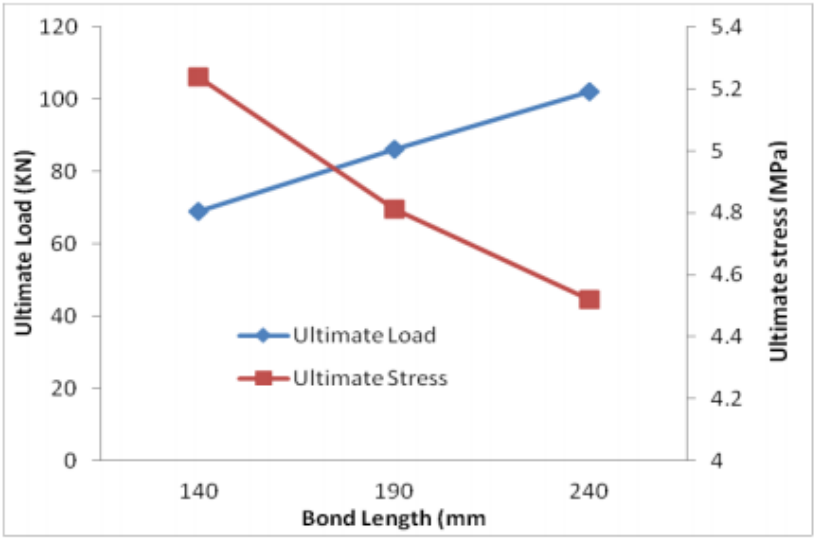

Fig.2.14 Effect of Bond Length on Ultimate Load and Ultimate Stress ***(Goyal et al. (2016))***

2.3 FLEXURAL BEHAVIOUR

Fam et al. (2012) investigated role of different interlocking joints in GFRP SIP formwork for bridge decks. The GFRP formwork comprised of corrugated panels with pin-and-eye joints as shown in Fig.2.15. All the specimens were tested for failure under a single load. In this paper importance was given to the connection between deck and the supporting girders and their construction details. To check the practicability of using GFRP SIP forms for an overhanging section a specimen was constructed and tested. The study mainly focused on the interfacial adhesive bonding at concrete and formwork interface and its thickness depending on the orthogonal mesh of steel bar at top and bottom. The result depicts that the deflections of all interior span of the decks installed with GFRP SIP formwork at service loads shows deflection below the span/1,600 limit as per the code. Also, at service loads the GFRP formwork shows strain less than 2% of ultimate. The major Failure criteria of all interior span GFRP formed deck panel was mainly by punching shear which was very much similar to the RC control deck panel. The web of the GFRP formwork was failed by inclined crack resulting from the tearing at supports near the corner between the web and the bottom flange which was basically initiated by punching shear and associated de-bonding. The pin-and-eye connections that were installed in transverse direction continued without any failure and damage. There was no slip between GFRP SIP formwork and girders. In this paper it has been proved that adhesive bonding resulted in remarkably increased in the stiffness but very small increase in ultimate strength.

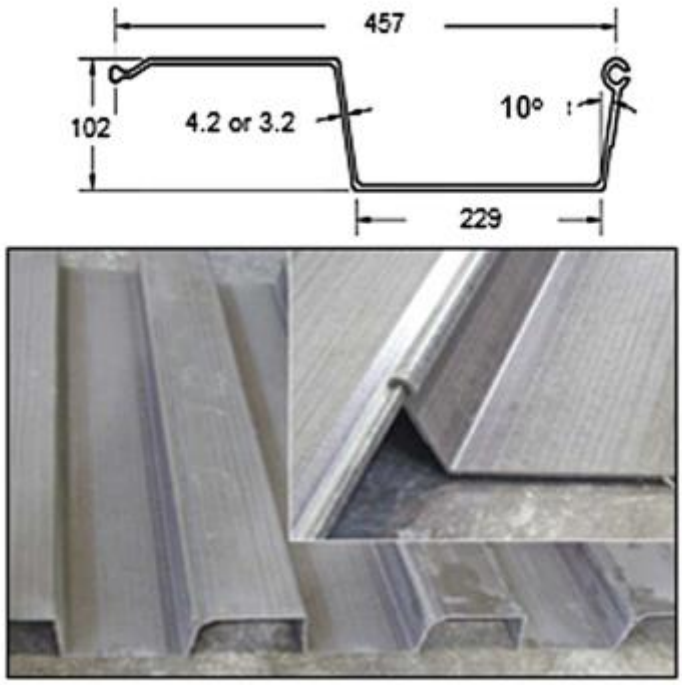

Fig.2.15 Corrugated GFRP Panels with Pin-and-Eye Connections ***(Fam et al. (2012))***

Cheng et al. (2005) studied the behavior of FRP-concrete composites which includes hybrid modular deck system and eliminates the use of reinforcement and how the two different material combines and performs together. For this study, a concrete slab is cast without the use of reinforcement over the CFRP plank which was stiffened with CFRP that plays the role of both SIP formwork and also the role of flexural reinforcement (Fig.2.16). To improve the interface connection between concrete casted and the deck panel, the panel surface is made rough by treating it with sand and fitted with shear ribs. The main purpose of performing this study is to fully understand the structural behavior of this composite FRP-concrete deck system through the incorporation of analytical simulation and investigation involving experiments on the static flexural-shear behaviour and the fatigue responses under cyclic loads. Test specimens includes five 610 mm wide concrete slab (SF1–SF5) which were made without the use of reinforcement and installed with stiffeners and shear ribs having different spacing. All the testing specimens were casted using concrete blocks with reinforcement at both ends so as to generate the fixity condition at the supporting girders. Fig. 2.17 shows that at one end the test specimen was simply supported by a roller along with a pin at the other end and loaded from the top using a double rod hydraulic actuator at a very slow rate. The load was transferred through an elastomeric loading bearing pad at different service loads as per the AASHTO wheel load (98 kN), including the impact factor of 33%. A load factor of 1.75 was used for STRENGTH I design level according to AASHTO (2004).

The structural behavior of first three specimens having stiffeners at the spacing of 305 mm at center was very much similar. As soon as the load reaches 98 kN, vertical Flexural cracks were noticed at the mid span near the bottom slab. As the load increased further, some more cracks were found at the sites of the interfacial shear ribs and further moved diagonally up to the load point, as shown in Fig.2.18, due to the effect of principal tensile stresses. As per the investigations of this particular paper, the designing of rectangular stiffener for carrying construction load only was not recommended, but it is also required that FRP-concrete deck system composites flexural strength should be taken into account.

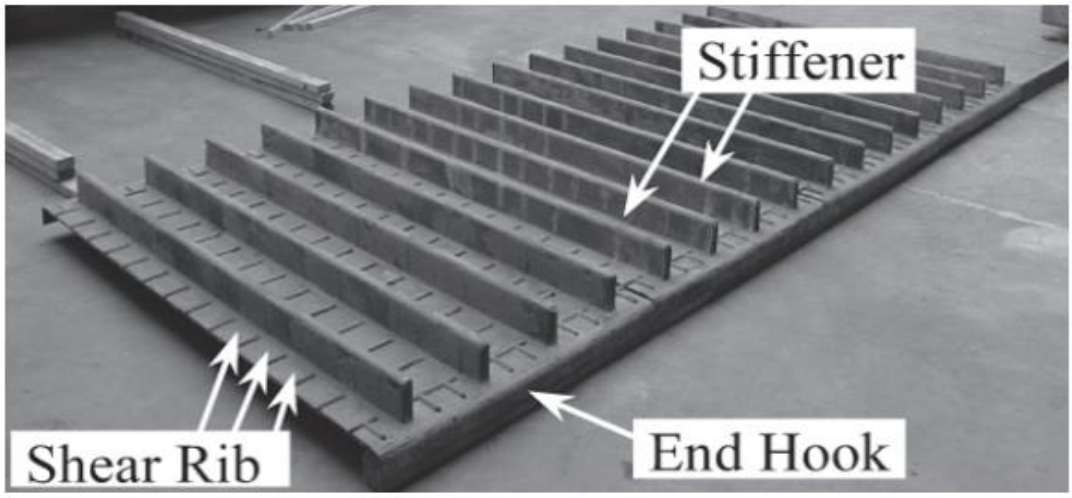

Fig.2.16 Geometry of FRP Composite Deck Panel ***(Cheng et al. (2005))***

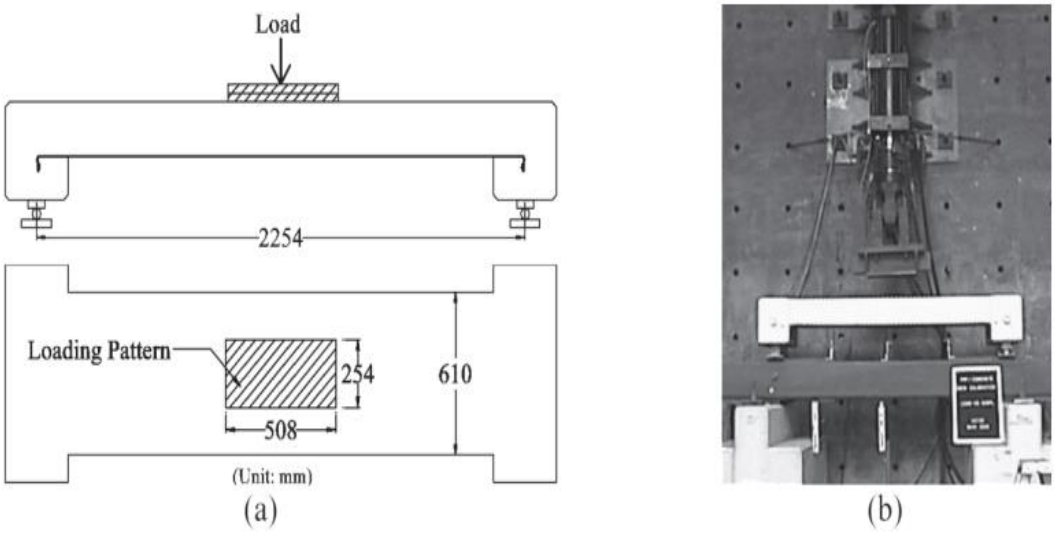

Fig.2.17 (a) Geometry and (b) Configuration of Test Setup ***(Cheng et al. (2005))***

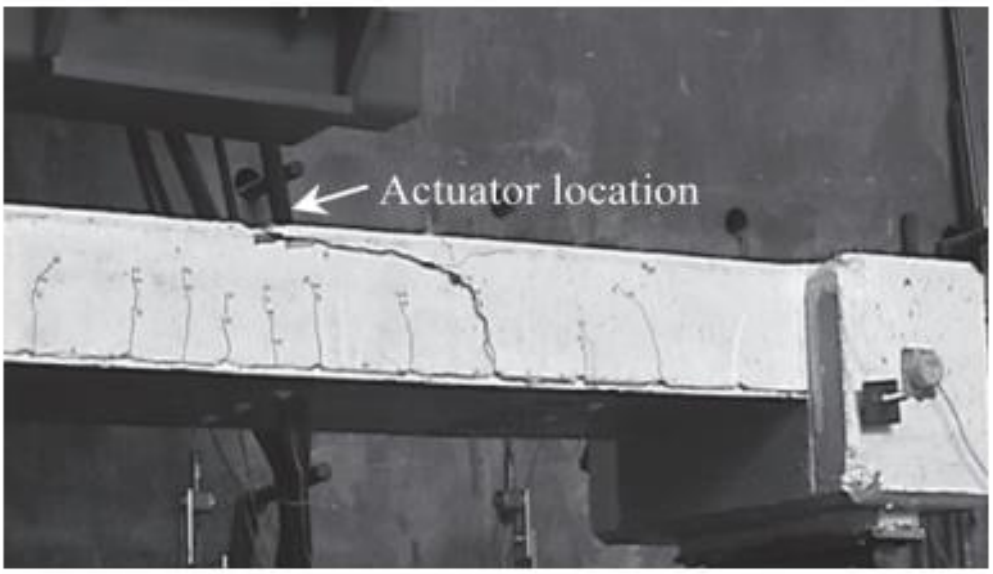

Fig.2.18 Load vs. Displacement Response for SF1, SF2 and SF3 ***(Cheng et al. (2005))***

Honickman et al. (2009) studied the behaviour of the bond between the concrete and GFRP formwork. Testing specimens includes eight concrete slabs casted using GFRP SIP formwork and tested in flexural bending to understand and compare the different bonding systems and GFRP reinforcement ratios. This study gives the experimental and analytical analysis of concrete slabs casted using GFRP planks as SIP formwork and also playing the role of tension reinforcement. In this paper different bond mechanism were studied like mechanical and adhesive bond system. Concrete slab thickness was varied to study the effect of GFRP plate reinforcement ratios. In order to study different bond mechanisms, test specimen are casted out of which first 4 having the size of 1,220 × 400 × 160 mm. The different bond mechanisms to be study includes: (*a*) adhesive bonding, (*b*) aggregate bonding, (*c*) GFRP shear connectors, and (*d*) steel shear connectors. Other test specimens to be casted were slabs of size 2,440 × 400 mm (96 × 15.7 in.), numbered as 5 to 8 and having different thickness of 110 to 210 mm, having different GFRP reinforcement ratio varying from of 8.5 to 4.3%, respectively. Adhesive bonding was applied in slabs 5 to 7 on the other hand aggregate bonding was applied in Slab 8. Four-point bending was performed on the specimen (Fig.2.19). Testing of specimens 1 to 4 having a span of 1,000 mm and a constant moment zone of 250 mm and specimens 5 to 8 having a span of 2,200 mm with a constant moment zone of 250 mm were performed. Load rate applied was 1 mm per minute. In order to measure the deflection at mid span between concrete and GFRP plate linear potentiometer, 100 mm strain transducers and strain gauges were used.

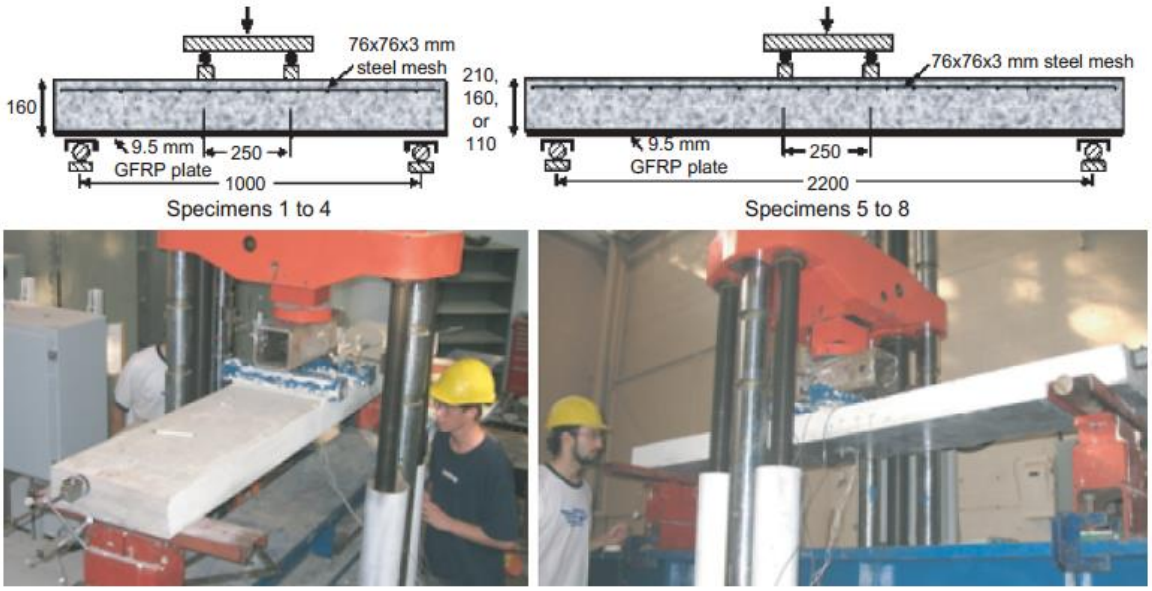

Fig.2.19 Test specimens and experimental setup**. *(Honickman et al. (2009))***

By critically investigating the interfacial surfaces after failure of Specimens 1 and 2, it was inferred that there was no failure occurred at the adhesive bond line whereas bond failure occurred within a very thin layer of the cement mortar. Fig.2.21 and Fig.2.22 depicts the failure modes of the different specimens. This was proved in (Fig.2.23) by a layer of cement paste that remained in contact with the GFRP plate. Specimen 4 shows lower stiffness post cracking than Specimens 1 and 2 due to the occurrence of some slip, on the other hand it shows higher stiffness than Specimen 3 (Fig.2.20(*a*)). This was because of the steel studs which were having higher modulus of elasticity as compared to the GFRP studs, which inturns reduces slip (Fig. 2.20(*c*)). Fig.2.20(f) shows that specimen 5 to 7 have flexural stiffness proportional to the reinforcement ratio which shows that using readily available GFRP planks as formwork for concrete slabs is very much convenient and very much effective when adhesive bonding was used as it led to a significant increase in stiffness of the slabs as compared to that of mechanically bonded slabs casted with shear connectors. The major reason for failure was due to debonding of the GFRP plate, for both flexural or shear cracking criteria. The longitudinal strains that were measured at midspan gives an idea that there are very less chances of tension failure in GFRP plate. Compression failure of concrete was imminent in some of the slabs. Since with the increase in reinforcement ratio flexural strength also increases, but its effect on ultimate moment could not be assessed as there was no flexural failure but there was consistent bond failure.

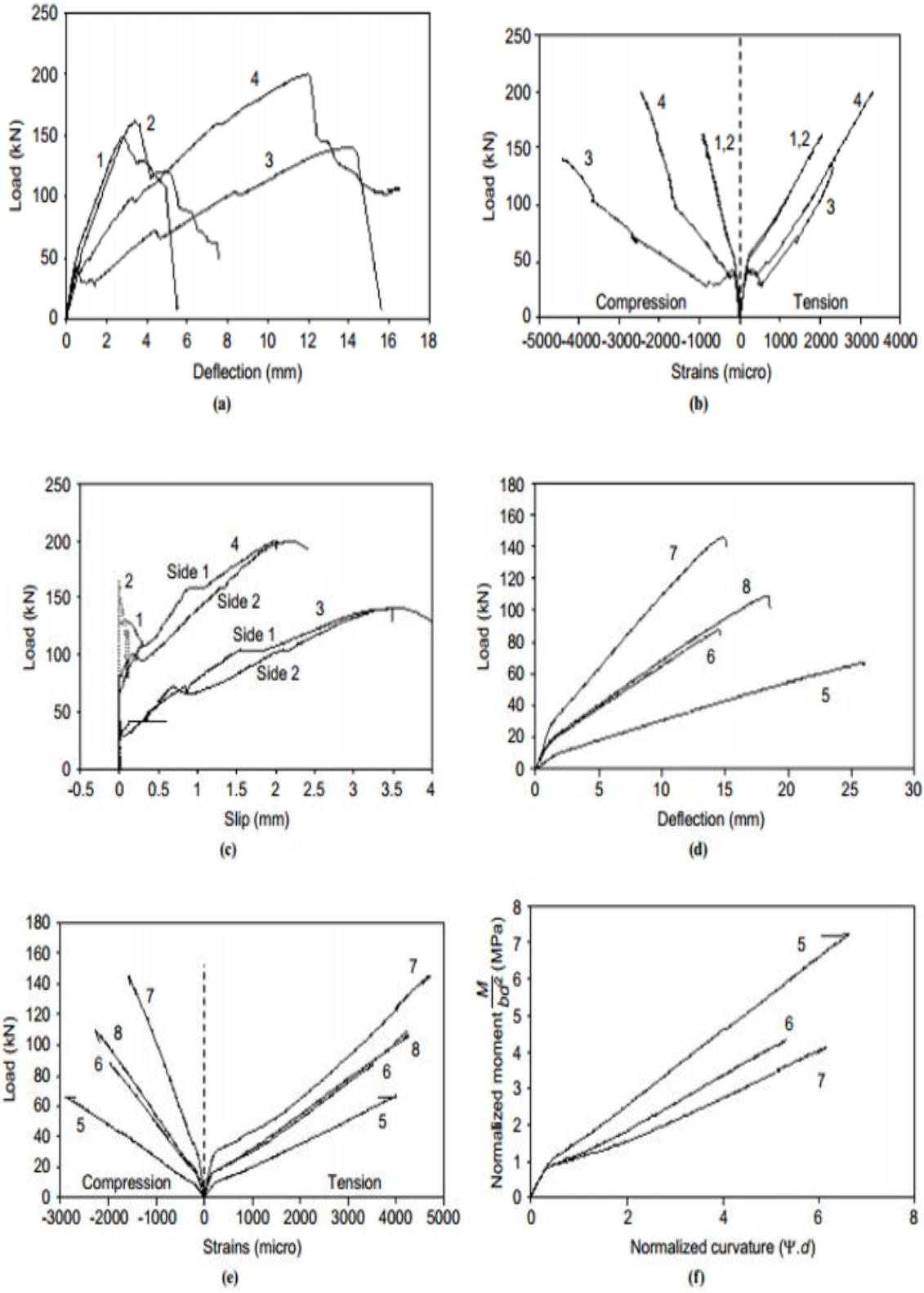

Fig.2.20 Summary of test Results for Specimens 1 to 4: (*a*) Load–Deflection Responses, (*b*) Load–Strain Responses, and (*c*) Load–Slip Responses; for Specimens 5 to 8: (*d*) Load–Deflection Responses, (*e*) Load–Strain Responses, and (*f*) Load–Slip Responses**.**
(Honickman et al. (2009))

Fig.2.21 Failure Modes Specimens 1 to 4 ***(Honickman et al. (2009))***

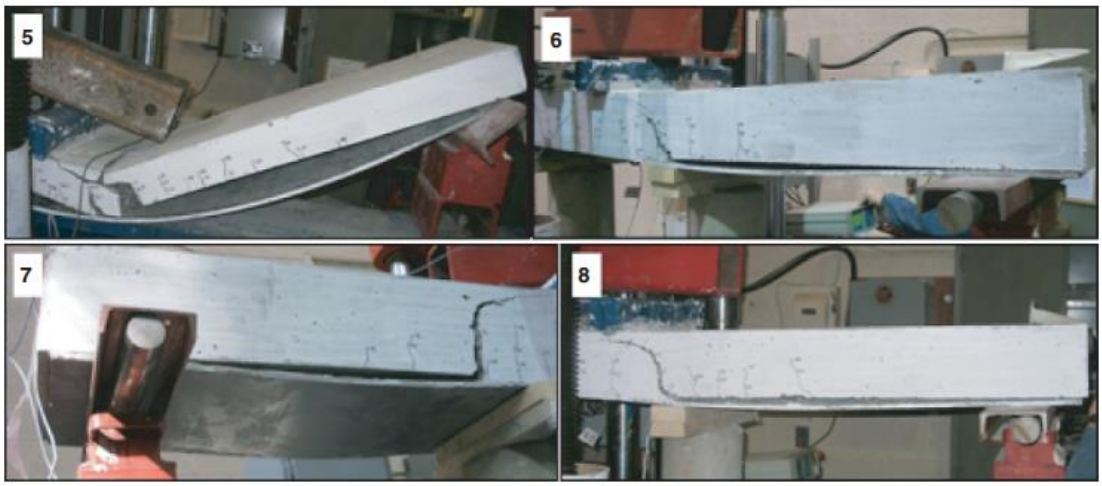

Fig 2.22 Failure Modes of Specimens 5 to 8 ***(Honickman et. al. (2009))***

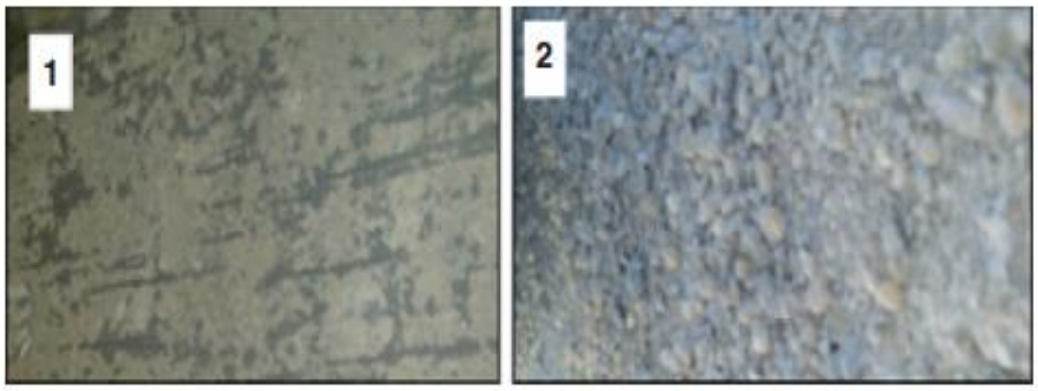

Fig 2.23 Surface Texture after Failure (Specimens 1 and 2) ***(Honickman et al. (2009))***

Orretal et al. (2013) studied the iterative methods for the design of simply supported, flexibly formed, concrete beams. This design and construction methods using flexible formwork has resulted in the saving of the material up to 40%. This paper also discusses the different methods for geometrical control in construction of beams using different methods. Different methods for anchorage of fabric formed beams is also mentioned in this paper. This paper also provides method required for the construction of concrete beams using fabric formwork. The process mentioned in this paper is for a simple beam, proceeding from the calculation of moment and shear envelopes, through capacity prediction, to the design detailing of the steel reinforced concrete beams element.

Goyal et al. (2017) studied the practicability of FRP profile as stay-in-place (SIP) formwork and also as reinforcement. There were three stages of experimental investigation regarding the practicability of FRP profile as stay-in-place (SIP) formwork and also as reinforcement. To use FRP profile as SIP formwork at the time of casting of concrete its deflection should be within permissible limits, therefore sand loading test was performed as shown in Fg.2.24. In the second stage, to check the efficiency of adhesive in making bond with concrete and GFRP plank through aggregate and adhesive bonding, different type of adhesive were used that were commercially available as mentioned in Table 2.3. In the third stage, flexural test was performed to study the role of the GFRP plank as reinforcement. Fig.2.25 shows the load–deflection plot and load–strain plot of the tested specimens. To study the role of FRP as reinforcement and the requirement of proper bond mechanism for the FRP-concrete composite action three criteria were studied, i.e. initial cracking load, crack pattern and ultimate load. This was concluded that using GFRP planks as SIP forms for concrete slabs and beams is very much convenient if proper bonding between concrete and GFRP is endured using appropriate bond system. Choice of adhesive greatly varries the FRP–concrete interface bond strength. Both aggregate and adhesive bonding provided better bond between FRP and concrete whereas, adhesive bonding gives better results than aggregate bonding when it comes to ultimate load and failure mode. It can also be concluded that use of the FRP plank as SIP formwork and tensile reinforcement without using any adhesive for bond treatment resulted in notable slip between concrete and correspondingly less capacity during testing. The plank with proper bond treatment with adhesive bonding using particular adhesive shows better results as tensile reinforcement. Therefore, it is suitable to be used as SIP formwork.

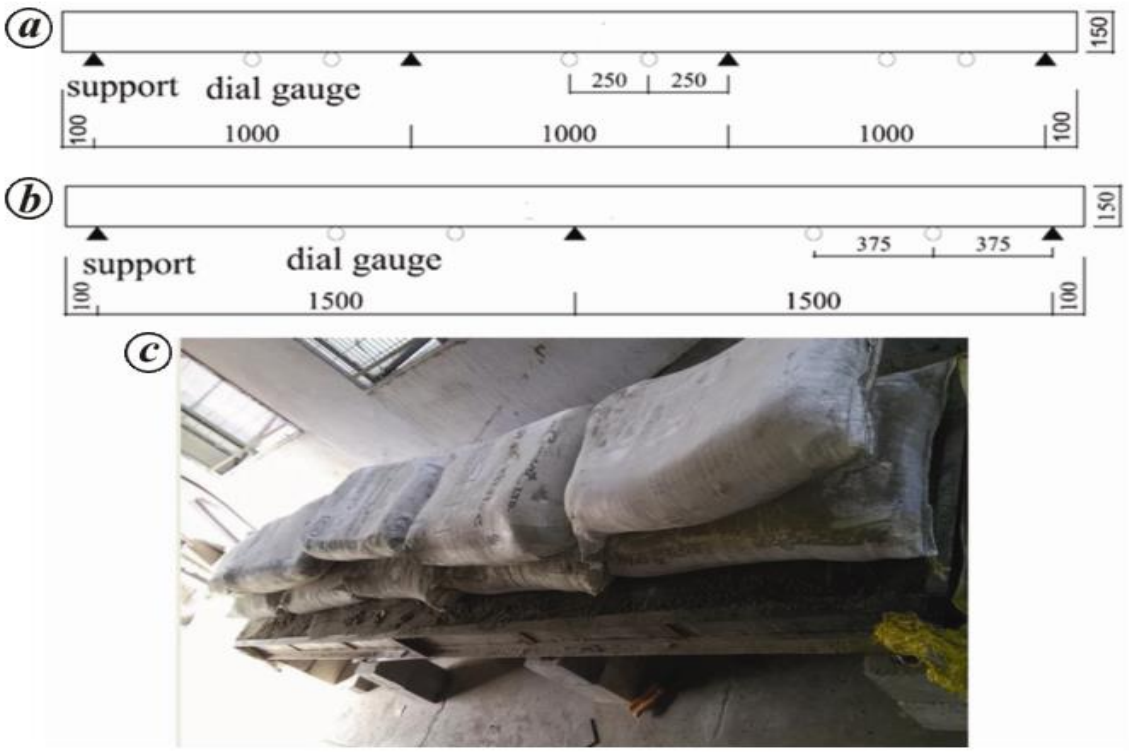

Fig 2.24 Sand-loading test. ***a***, Three-span testing; ***b***, Two-span testing; ***c***, Experimental set-up for three-span testing ***(Goyal et al. (2017))***

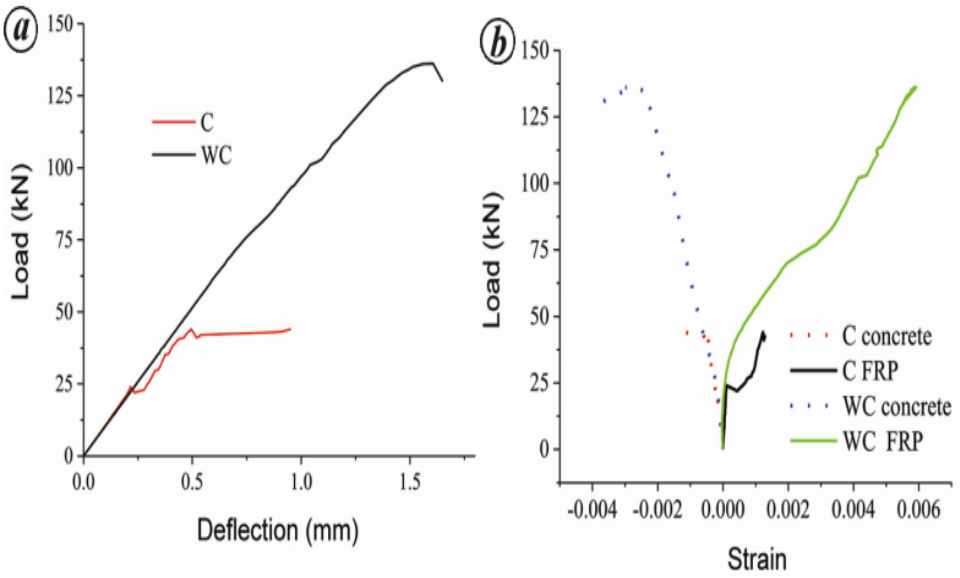

Fig 2.25 Comparison between Bond Treated and Untreated Specimens. ***a***, Load–Deflection Plot; ***b***, Load–Strain Plot. ***(Goyal et al. (2017))***

Table 2.3 Specimen Summary and Load Capacity ***(Goyal et al. (2017))***

Specimen ID	Bond mechanism	Adhesive bond	Ultimate load (kN)	Deflection (mm)	Failure mode
C1	-----	-----	5.25	0.50	FRP-concrete interface failure
C2			5.3	0.45	
DA1	Aggregate bonding	-----	23.91	1.19	FRP-adhesive interface failure
DA2			23.08	1.08	
WA1	Adhesive bonding	-----	41.19	1.52	FRP-adhesive interface failure
WA2			44.07	1.54	
DB1	Aggregate bonding	-----	62.3	1.04	Mixed mode interface failure
DB2			63.59	1.05	
WB1	Adhesive bonding	-----	69.91	1.30	Adhesive -concrete interface failure
WB2			72.53	1.26	
DC1	Aggregate bonding	-----	72.56	1.23	Adhesive -concrete interface failure
DC2			75	1.18	
WC1	Adhesive bonding	-----	89	1.27	Concrete failure
WC2			79.32	1.53	

2.4 REVIEW OF ACOUSTIC EMISSION TECHNIQUE FOR DAMAGE DIAGNOSIS

Acoustic emission (A.E) technique is one of the most favourable technique of monitoring of the structure at different stages of degradation. AE technique can be adopted to give pre warnings to the maintenance team and to execute retrofitting work as required, thus saving a great deal of time and improves life span of the structure.

AE in simple words is defined as a transitory elastic wave generated as a result of material malformation. This stress wave travels along the solid because of the energy liberated during

the deformation process. The amount of acoustic energy which is released depends majorly on the speed and size of the deformation procedure ***(Nair, (2006))***.

Acoustic emissions can be dedined as the class of phenomena whereby transient elastic waves are generated by rapid release of energy from localized sources within the material, or the transient elastic waves so generated. AE waves can be generated as a result of various sources dislocations, microcracking and other changes due to increase in strain. The method is very senstive which enables it to detect damage long before its visible. AE sensors record the vibrations created by waves when they reach the materials surface. The peizoelectric crystal the detected wave to electric signal, amplify it (internally or using the external pre-amplifier), and send it to the data acquisition system. The passive ability of AE, external excitation or stimulus for data collection once sensors are placed, makes it a suitable candidate for real time monotoring and structural health monitoring of in-service structures. The method has also shown promise in assessment of damage during load tests of different structures and material including fibre reinforced polymer(FRP), steel, reinforced concrete(RC) and prestressed concrete(PC).

2.4.1 Instruments used for AE testing

There are different components required for proper AE monitoring and each component plays an important role. These components involves couplants, sensors and data acquisition system are described below.

1. Couplants: In order to affix the AE sensors on the surface of the slab couplants are required. They help in providing the proper conduction of the acoustic waves generated from the source. Commonly used couplants are oil, glue, high vacuum grease etc.
2. AE sensors: These are the most important instruments which sense the waves generated from the cracks or any deformation produced in the specimen tested and convert these waves into electrical signals. In AE testing generally piezoelectric resonant sensors are used. These sensors can be used in environments where very low level AE signals as well as high level AE signals needs to be processed.
3. Data Acquisition System: Most of the modern AE systems use computer operated in which software is installed for parameter input and system control. All the signals received are procured and saved in the data acquisition system.

2.4.2 Waveform Parameters

A typical AE signal (or wave) is shown in Fig.2.26, in which different parameters are defined below:

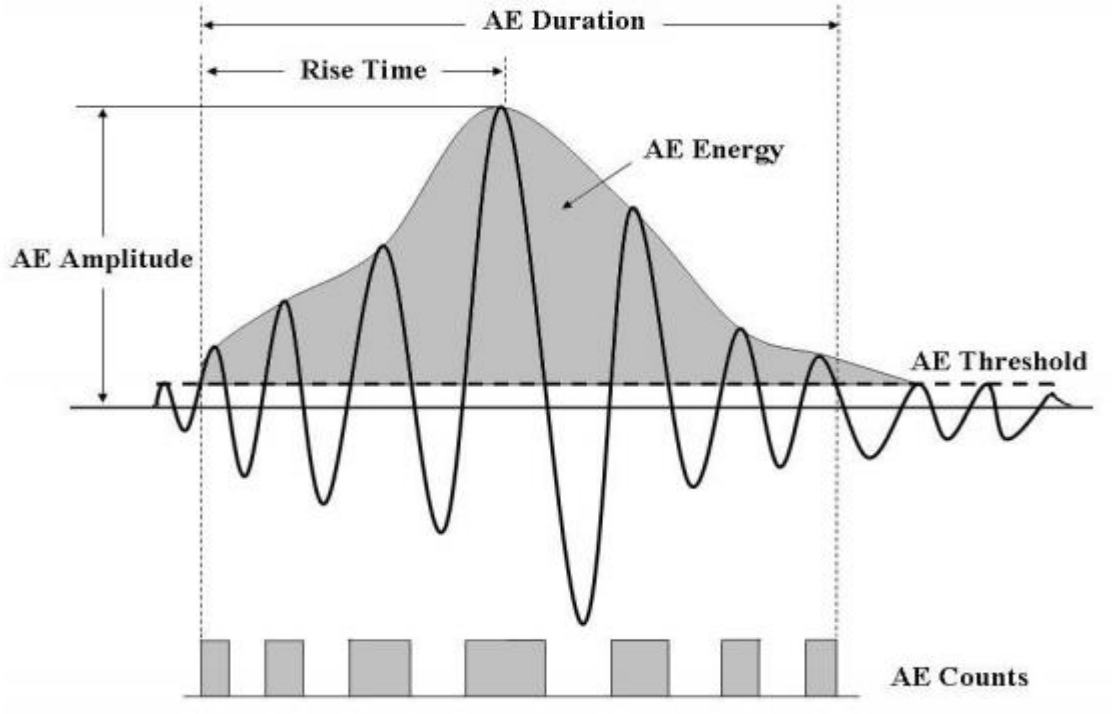

Fig.2.26 AE Signal

1. Threshold: It is amplitude value in decibels (dB), generally decided and set based on background noise, such that AE-signal which have amplitude value above the threshold value would only be considered for analysis.
2. Amplitude: It is the maximum rise in the AE waves generated during the testing of the specimen. Its unit is decibels.
3. AE hits: Whenever there is a change in the material, waves are generated which are detected by the individual sensors and are measured as hits.
4. AE event: It is the change in material locally which is detected by the multiple sensors giving rise to acoustic emission.
5. Rise time: It is the time between the wave crossing very first threshold value and the maximum rise of the wave.
6. AE duration: It is the time between the first threshold and the last threshold value crossing.
7. AE energy: The are under the plot of amplitude vs time above the threshold value is termed as AE energy.

Mostafa and Razaqpur. (2017) proposed a non linear analytical model in order to determine the normal stresses and shear at the interface of CFRP strengthened RC beams. This paper mainly focused on the intermediate crack debonding It was found out that at the section of maximum moment where the debonding occurs due to cracks can be easily predicted with the help of stresses computed. The model presented in this paper is based on composite beam theory with partial slip at the FRP-concrete interface permitted. The results generated from the experiments were in good agreement with the theoretical predicted delamination load.

Colombo et al. (2005) have used acoustic emissions (AE) technique for performing experiments on RC beams which are prototype of the beams in bridges. Cyclic loading was applied on the beams during testing and AE signals were recorded. A new parameter called relaxation ratio was used in this paper in order to analyse the AE signals. This parameter quantifies the AE energy that is recorded during the unloading phase and loading phase of a cyclic loading test. When the load reaches the value which is approximately 45% of the ultimate bending load applied a change in trend is noted by the author. Factors such as the loading rate and concrete strength were found to influence the results and recommended further work required to extend the results to full scale testing of bridge beams.

Wu et al. (2000) have analysed the acoustic emission (AE) signals from mortar, concrete and steel fiber RC beams during the complete fracture process. Based on the amplitude distribution characteristics different filters were set on the AE signal duration. As per the value of AE signal amplitude that correlates with the occurrence of the peak for AE hits, the author have bifurcated the AE signals from mortar, concrete and steel reinforced concrete into five, seven and nine sections, respectively. The relationship between the failure mechanism and AE signal of these materials at meso-structure level were determined.

Sharma et al. (2017) have estimated the strength of corrosion effected reinforcement in concrete with the use of two non-destructive techniques based on wave propagation. During the corrosion process the specimens were continuously monitored with acoustic emission (passive) and ultrasonic guided wave (active) techniques. The main focus in this paper is on investigating the applicability and effectiveness of monitoring different stages of initiation, progression and concrete cracking due to chloride induced corrosion in RC structures involving both active and passive techniques. It has been found out that AE parameters like cumulative AE hits and their amplitudes clearly predicts the cracks that are produced due to corrosion and also distinguishes between the various stages of mechanism of chloride induced corrosion in RC structures.

Sharma et al. (2018) presents the monitoring of corrosion in concrete before it is visible using two non-destructive techniques. This research reports simultaneous monitoring of corrosion in RC structures with HCP, UGW and AE and correlation among these different technologies have been presented. In order to record the AE events inside the concrete occurring due to corrosion activity the beam specimen is required to be mounted with AE sensors over its surface. Ultrasonic Guided Waves (UGW) technique was also used to monitor the corrosion in the beam by passing an ultrasonic pulse through the bar. It was found out that results obtained from the observation of all the three specimens were in close agreement.

CHAPTER 3

EXPERIMENTAL PROGRAM

3.1 GENERAL

In this chapter details of all the preliminary testing conducted, casting procedure, and all the experimental procedure for testing of one-way concrete slabs casted using GFRP SIP stay-in-place formwork which performs the role of permanent formwork and tensile reinforcement. The details of two different bond mechanism aggregate bonding and adhesive bonding is presented along with details of experimental set-ups during casting and flexural testing stage has been presented.

3.2 PRELIMINARY TESTING

In order to check whether the GFRP plank that will be used for casting of the curved slabs can be used as a flexible formwork or not sand loading test was conducted.

3.2.1 Sand Loading Test

This test was done to check deflection that may occur in the proposed pultruded section of GFRP plank while using it as formwork. Since, main requirement was to achieve flexibility in the formwork for the casting of the curved slabs, therefore basic aim of this test was to find out whether GFRP plank could serve the purpose of base formwork or not. Suitability of a material as a formwork will depend upon how much deflection may occur when concrete is poured on the formwork during the initial stage i.e. casting stage. Concrete that will be casted was simulated as the weight of sand that is required to be filled during the test.

For the test, a pultruded GFRP plank of length 3.2 m was used. The plank along with the steel side formwork was placed on cubes at a height of 300 mm from the ground, moreover steel rods were placed to provide condition of simple supports.

First 200 kg of sand was poured on the plank and was spread evenly to cover the whole surface of the plank. After pouring of sand, further 10 cement bags weighing 50 kg each were placed on the plank and deflection was measured to be 65mm. Test set up for sand load test is shown in Fig.3.1

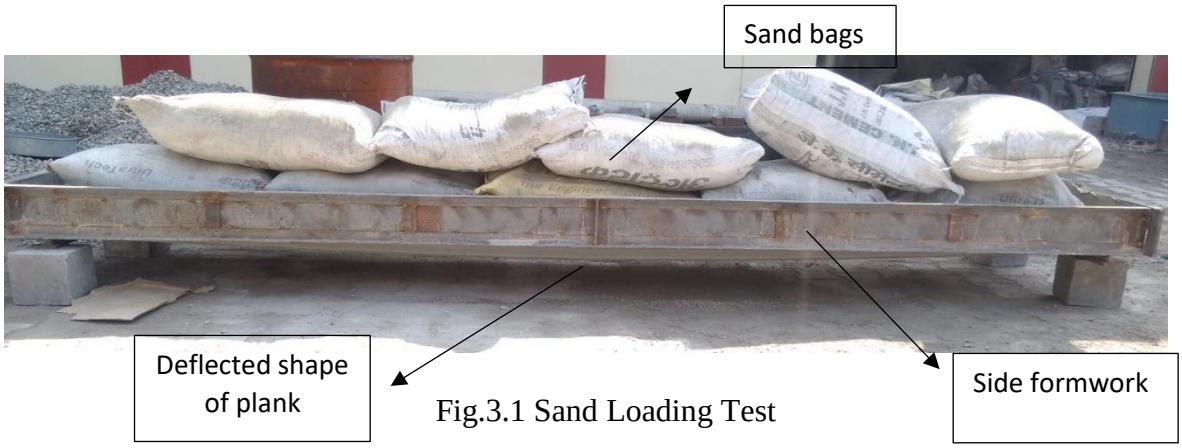

Fig.3.1 Sand Loading Test

3.3 CURVED SLAB CASTING

After the sand loading test, it was confirmed that the GFRP plank can be used a permanent flexible formwork and slab can be casted with a deflection from the bottom. Therefore, the materials required, different type of bond and all the set-up required for casting is mentioned below.

3.3.1 Materials Used

The major materials used in FRP SIP formwork construction are GFRP planks, adhesive and concrete. The properties of all these materials have been discussed in the following section.

- **GFRP Plank** - GFRP formwork was used as a permanent formwork for casting of concrete. Actual width of the plank available was 600mm as shown in Fig.3.2(a). Total length of the formwork used was 3.2m and width of around 0.375m. There were three T stiffners running along the length of the plank that plays the of reinforcement. Other specifications of the plank are mentioned in Fig.3.2(b). Properties of GFRP plank are mentioned in Table 3.1.

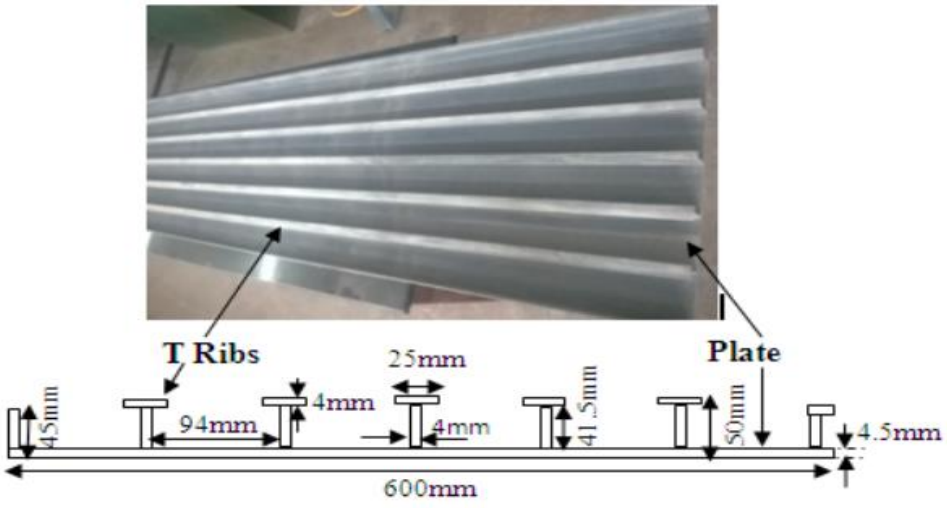

(a)

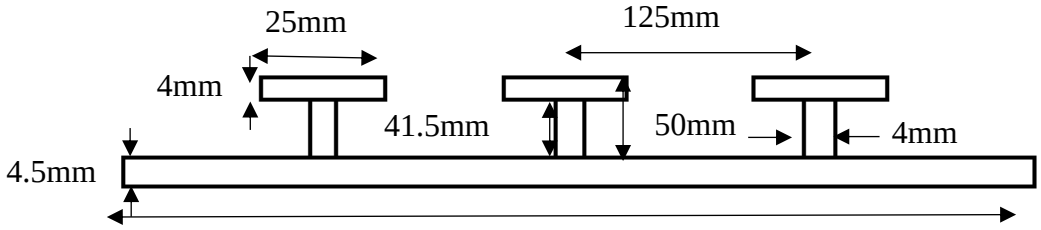

(b)

Fig 3.2 (a) GFRP Plank Available (b)Dimensions of the Used GFRP Plank

Table 3.1 Properties of GFRP Profile ***(Goyal et al. (2016))***

	Thickness(mm)	Young's modulus (GPa)		Tensile strength (MPa)		Volume fraction
		Average	Std. Dev.	Average	Std. Dev.	
Plate	4.5	27.9	2.55	375.5	5.86	0.35
Stiffeners	4	23.8	2.2	352.3	5.45	0.3

- **Concrete**- For casting of slabs concrete of grade M-40 was used as per the IS codal provisions. The design mix proportions that was followed in preparation of M-40 was 1:1.73:2.13 and the w/c ratio used was 0.41. Pozzolonic Portland cement is used for preparing concrete. Two type of aggregates were used i.e. 10mm and 20mm with specific gravity of about 2.62 and 2.69 respectively. specific gravity of the sand which was used 2.65 and it belonged to zone II. Also super plasticizer called Auramix 200 was used with a dosage of 0.2%.
- **Type of adhesive used**- Adhesive used was Sikadur 31 for bonding between concrete and GFRP. The mechanical properties specified by the manufacturer are presented in Table 3.2.

Table 3.2 Mechanical Properties of the Adhesive Specified by Manufacturer

Properties	Adhesive (Sikadur 31)
Pot life	45 minutes at 25°C
Viscosity	Viscous thixotropic
E modulus	5 GPa
Elongation at break	0.4%
Tensile strength	15 MPa
Flexural strength	30 MPa
Bond strength	8-10Pa

- **Steel side forms** - For the casting of the slabs steel side forms were used as shown in Fig.3.3 These side forms were placed around the GFRP plank for casting of concrete.

Fig.3.3 Steel Side Form

3.3.2 Bond Treated Curved Slabs

Prior to casting of concrete, it is required to prepare the formwork for casting which means that while pouring of concrete the plank is required to form a strong interfacial bond with the concrete. From the previous studies ***(Goyal et al. (2016), (2017))*** it has been clear that surface treatment is required for composite action between GFRP plank and concrete, also the choice of adhesive influence the bond characters.

Therefore, the two type of bonding were adopted

(a) Aggregate bonding:

Starting with the preparation of formwork for different type of bonding. In case of aggregate bonding, firstly we clean the formwork properly and then place it on a flat surface, further adhesive coating was applied on it. Adhesive used was **Sikadur 31**.

After the application of adhesive over the surface of plank and also on the flanges of T- ribs, that run along the length of the plank. Then aggregates which were retained amidst of 2.36 mm sieve and 1.18 mm sieve were sprinkled on the plank and was tapped properly.

After sprinkling of aggregates, plank was left for drying for 2 days. Then all the aggregates which are not properly bonded to planks surface are removed with the help of brush. Then the plank is ready for pouring of concrete. Aggregate bonding is shown in Fig.3.4.

Fig.3.4 Aggregate Bonding on GFRP Plank

(b) Adhesive bonding:

While preparing the formwork for adhesive bonding, we clean the formwork properly and then place it on a flat surface, further adhesive coating was applied on it. Adhesive used was **Sikadur 31**. Within 30 minutes of application of adhesive concrete is poured over the plank. Adhesive bonding is shown in Fig.3.5.

Fig.3.5 Adhesive Bonding on GFRP Plank

3.3.3 Casting Set-up

For the casting of the curved slabs it was required to put the plank along with the steel side formwork on a raised platform. Therefore, a platform of cubes was created to achieve the height of 300mm from the ground after which the steel rods were placed over the cubes at a distance of 100 mm from the ends over which the plank was placed. The steel formwork was placed around the plank in such a way that bottom of the steel form is 75mm below the plank so as to facilitate the curved shape without concrete leakage. The front view of the test set-up is shown in the Fig.3.6.

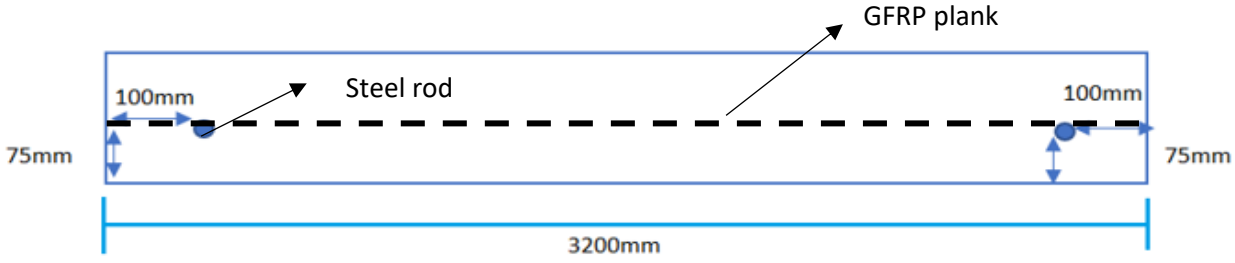

Fig.3.6 Position of Rods for Support (front view)

3.3.4 Slab Fabrication

There were 3 types of slabs to be casted out of which two were casted with curved profile and one with straight. The curved slabs were casted with two different type of bonding i.e. aggregate bonding and adhesive bonding. The straight slab was casted with adhesive bonding. The test matrix for the casted specimen is shown in Table 3.3.

Table3.3 Test Matrix

Test matrix		
1	CG	Curved slab with aggregate bonding
2	CA	Curved slab with adhesive bonding
3	SA	Straight slab with adhesive bonding

3.3.4.1 Casting of Curved Slab with Aggregate Bonding (CG)

For the casting of curved slabs, the very first step was to cut the plank as per the dimension of the slab. The required dimension of the plank was 3.2 m in length and 375mm in width. The required section of the plank consists of three T-ribs running along the length of the plank. After the plank has been cut adhesive is applied over the base plate and also on the top flanges of the T- section of the plank. There was no adhesive applied on the vertical ribs of the T-section. After the application of the adhesive aggregates which retain on 2.36 mm sieve and pass through 1.18 mm sieve were sprinkled on the plank and was tapped properly. The plank was then allowed to cure for almost 2-3 days. After the drying of the plank extra aggregates which are not bonded with the adhesive are removed with the help of a brush as shown in the Fig.3.7.

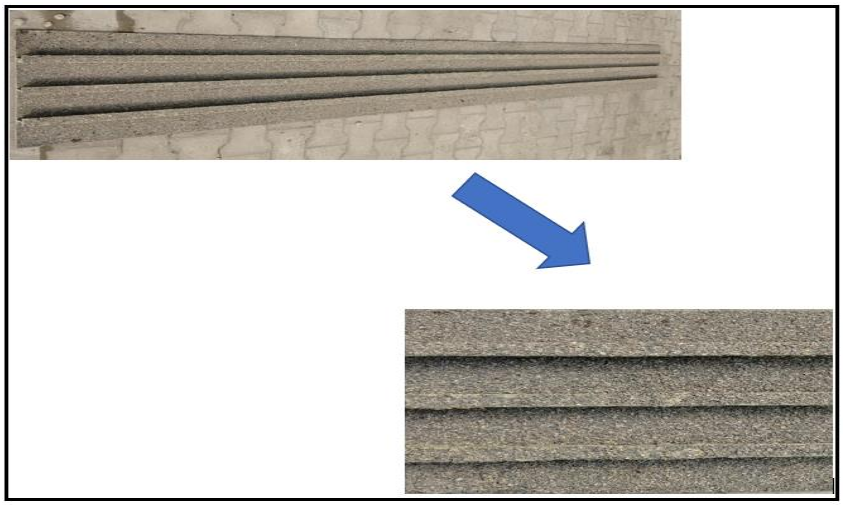

Fig.3.7 Aggregate Bonded GFRP Plank

Now the plank was placed over the raised platform of height around 300 mm with rods acting as a support at the ends. After this the side forms of height 150 mm were put around the GFRP plank as shown in Fig.3.8. To measure the deflection in the slab 3 dial gauges were placed below the slab out of which one was placed at the centre and other two were placed at a distance of 500 mm to the right of the centre and 1000 mm to the left of the center as shown in Fig.3.9

.

(a)

(b)

Fig.3.8. (a) Position of Side Form (b) Position of Rods Below Plank for Support

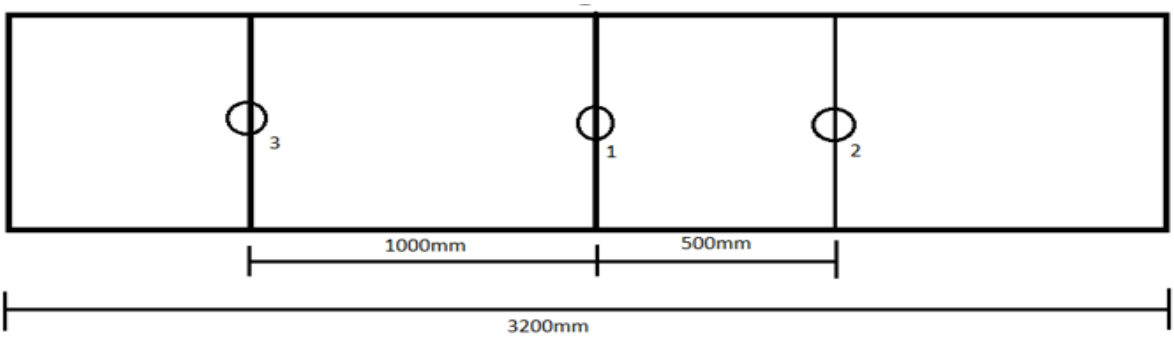

Fig.3.9 The Position of the Dial Gauges

Casting of the slab was done using the concrete of 28 days compressive strength of 40 MPa. During pouring of concrete the weight of concrete in one container was measured which comes out to be 25 kg and after pouring of every 4 container of concrete that is around 100 kg, concrete was spread evenly as shown in Fig.3.10 and reading in the dial gauge were taken. After taking

the dial gauge reading they were again set to zero and the same procedure was repeated till the concrete fills up to the height of the side form.

Fig.3.10 Casting of Specimen CG

3.3.4.2 Casting of Curved Slab with Adhesive Bonding (CA)

For the casting of curved slab using adhesive bonding, the very first step was to cut the plank as per the dimension of the slab to be casted. The required dimension of the plank was 3.2 m in length and 375mm in width. The required section of the plank consists of 3 T ribs running along the length of the plank. After the plank has been cut adhesive is applied over the base plate and also on the top flanges of the T- section of the plank as shown in the Fig.3.11. There was no adhesive applied on the vertical ribs of the T- section. Now the plank was placed over the raised platform of height around 300 mm with rods acting as a support at the ends. After this the side forms of height 150 mm were put around the GFRP plank.

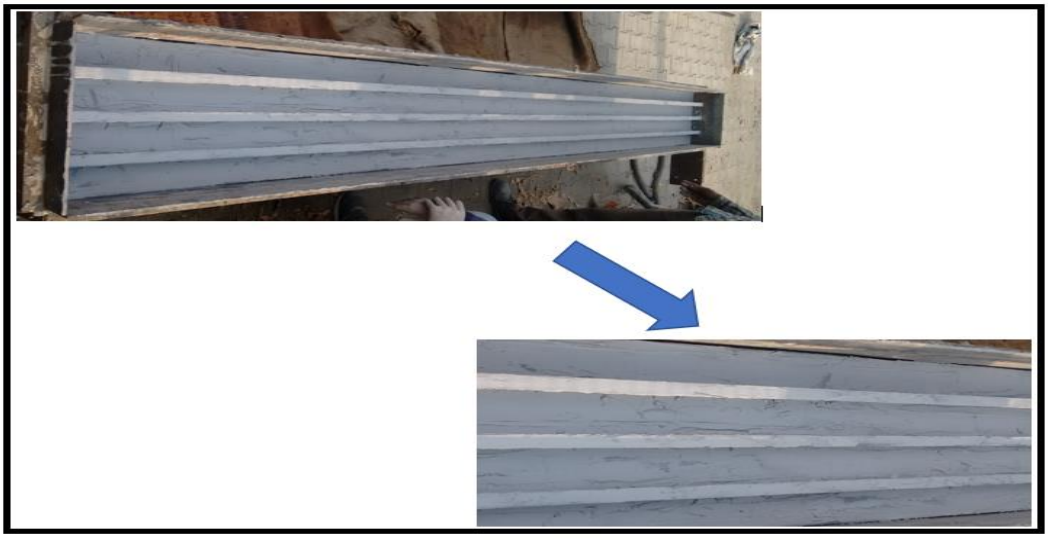

Fig.3.11 Adhesive Bonded GFRP Plank

After the application of the adhesive the concrete was poured within 30 minutes. To measure the deflection in the slab 3 dial gauges were placed below the slab out of which 1 was placed

at the center and other two were placed at a distance of 500 mm to the right of the center and 1000 mm to the left of the center respectively. Casting of the slab was done using concrete of 28 days compressive strength of 40 MPa. During pouring of concrete the weight of one concrete in one container was measured which comes out to be 25 kg and after pouring of every 4 container of concrete that is around 100 kg, concrete was spread evenly and reading in the dial gauge were noted. After taking the dial gauge reading they were again set to zero and the same procedure was repeated till the concrete fills up to the height of the side form. Casted specimen CA is shown in Fig.3.12

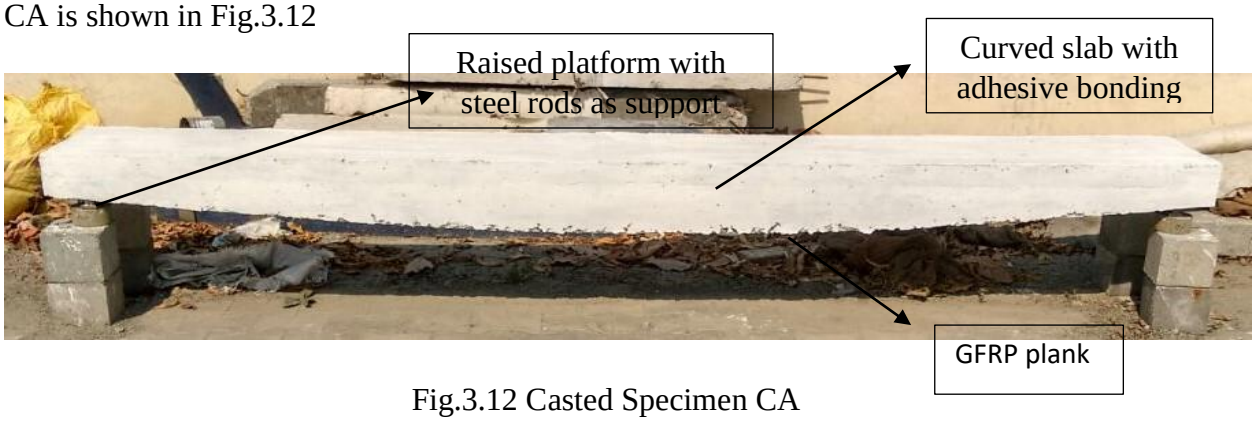

Fig.3.12 Casted Specimen CA

3.3.4.3 Casting of Straight Slab with Adhesive Bonding (SA)

For the casting of the straight slab with adhesive bonding, the very first procedure was to cut the plank as per the required dimension. The length of the plank required was about 3.2 m and width was about 0.375m. The plank was placed over raised platform with 4 supports at a distance of 1000mm. The steel formwork was then placed around the plank and the concrete was poured as shown in Fig.3.13. Adhesive was applied over the base of the plank and over the flanges of the T-ribs. There was no adhesive applied on the vertical portion of the T-ribs. To measure the deflection during the casting, dial gauges were placed at the center of each support. The deflection was measured after every set of 100 kg of concrete poured. Needle vibrator was used after every 3 sets of concrete poured.

Fig.3.13 Straight Slab with Adhesive Bonding

3.4 FLEXURAL TESTING OF THE CURVED SLABS

Two point loading cyclic flexural test with load cycle of 30kN was conducted. The parameters that were studied are deflection at mid span and at quarter span. Strain gauges were used to measure strains in both concrete and GFRP. Acoustic emission sensors were also used to monitor the cracks.

3.4.1 Test Set-up and Instrumentation

To perform the flexural test on the slab it was tested under two point cyclic loading. The slab was placed over the two I sections which were at a distance of 3m apart. Two-point loading frame was used to transfer the load. The slab was tested under cyclic loading with the increment of 30 kN in each cycle. Three LVDTs were used to measure the deflection occurred during the flexure testing of the slab. One LVDT was placed at the centre and other two were placed at a distance of 750mm from the ends. There were two type of strain gauges used. For measuring strain in GFRP plank 5mm strain gauges were used and for measuring strains in concrete 60mm strain gauge was used. Load vs deflection curves were plotted for different points where LVDT were placed i.e. at center and at quarter span and load vs strains curve were plotted for different points where the strain gauges were placed as shown in Fig.3.14. Fig.3.15 shows the test set up for flexural testing.

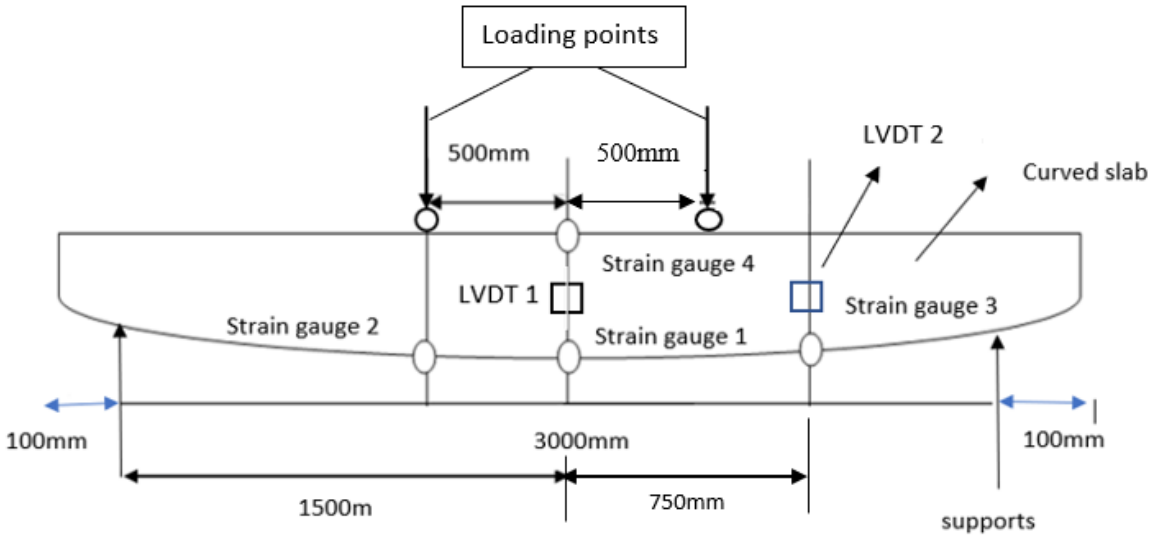

Fig.3.14 Position of Strain Gauges

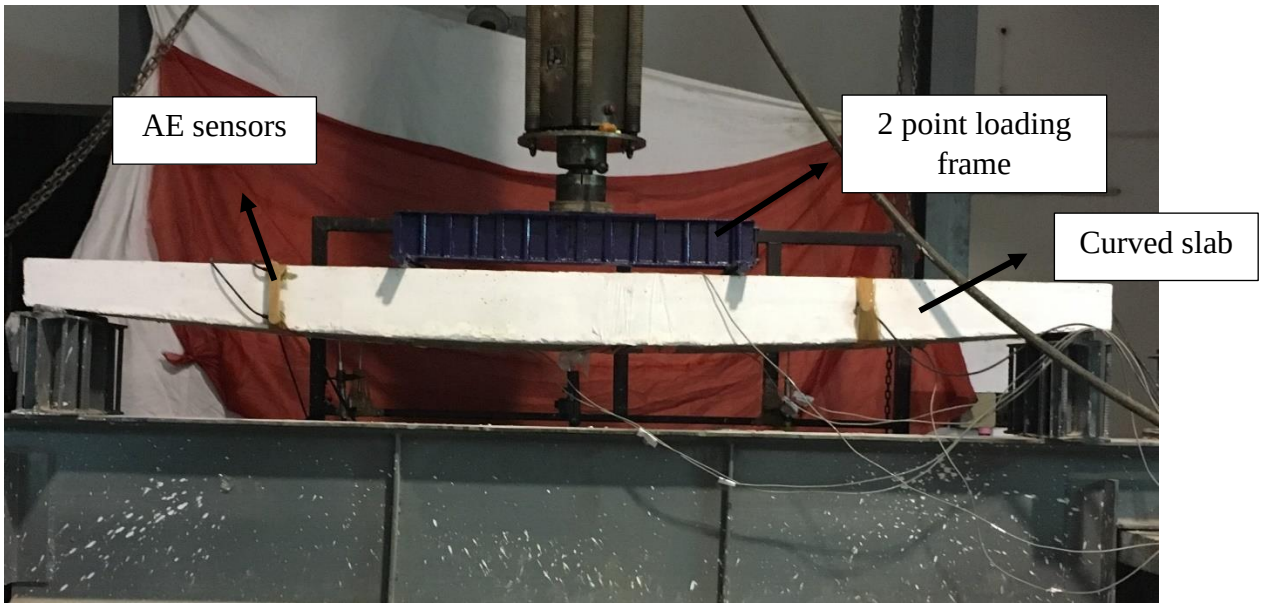

Fig.3.15 Test Set-Up for Flexural Testing

For Acoustic Emission (AE) monitoring of the slabs, a Micro-II digital AE data acquisition system along with 8 AE channels, filters and AE sensors were used. All the signals and waveforms that are generated due to micro cracks produced are detected by the AE sensors. During testing 6 AE sensors were affix to the slab with the help of coupling gel and were held in position using tape. Three sensors were put on front face and remaining three on the back face as shown in Fig.3.16. In order to obtain the AE data having different attributes of AE signals, AE win software was used. AE parameters used for damage detection are AE hits, AE signal strength and AE events.

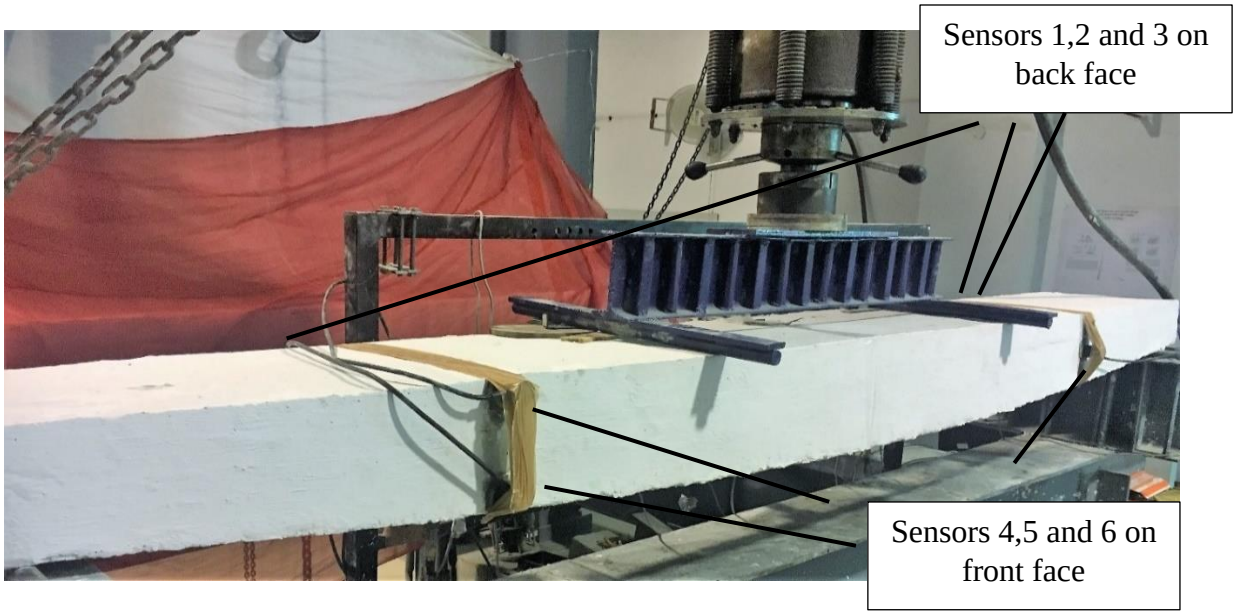

Fig.3.16 AE Sensors Placement

CHAPTER 4
RESULTS AND DISCUSSION

4.1 GENERAL

This chapter presents the results and outcomes of the testing that has been performed on the different slab specimens. GFRP planks were tested for deflection during the concrete casting and prepared curved hybrid GFRP-concrete slabs were tested for flexure behavior The comparison was made between the straight and curved slabs and between adhesive bonding and aggregate bonding bond mechanisms.

4.2 CASTING STAGE DEFLECTIONS

In order to know about the flexible nature of the GFRP plank during the casting stage dial gauges were used to measure the deflection that occurred during the casting stage. During casting of straight adhesive bonded slab, curved aggregate bonded slab and curved adhesive bonded slab deflection was measured at different load interval during pouring of concrete.

4.2.1 Straight Adhesive Bonded Slab (SA)

Straight slab with three spans was casted using adhesive bonding and deflection for each span was measured using dial gauges at center of each span. The deflection was measured after every set of 100 kg of concrete poured. Needle vibrator was used after every 3 sets of concrete poured.

- Fig 4.1, Fig 4.2 and Fig 4.3 shows the load deflection plot for three spans dial gauge 1 (center), dial gauge 2(left span) and dial gauge 3 (right span) respectively of straight adhesive bonded slab.
- It was observed that the maximum deflection that occurred in the slab was around 1.2 mm in the left span which is almost negligible due to the supports provided. The maximum deflection occurred is within the limits for the GFRP formwork to be used as permanent formwork.

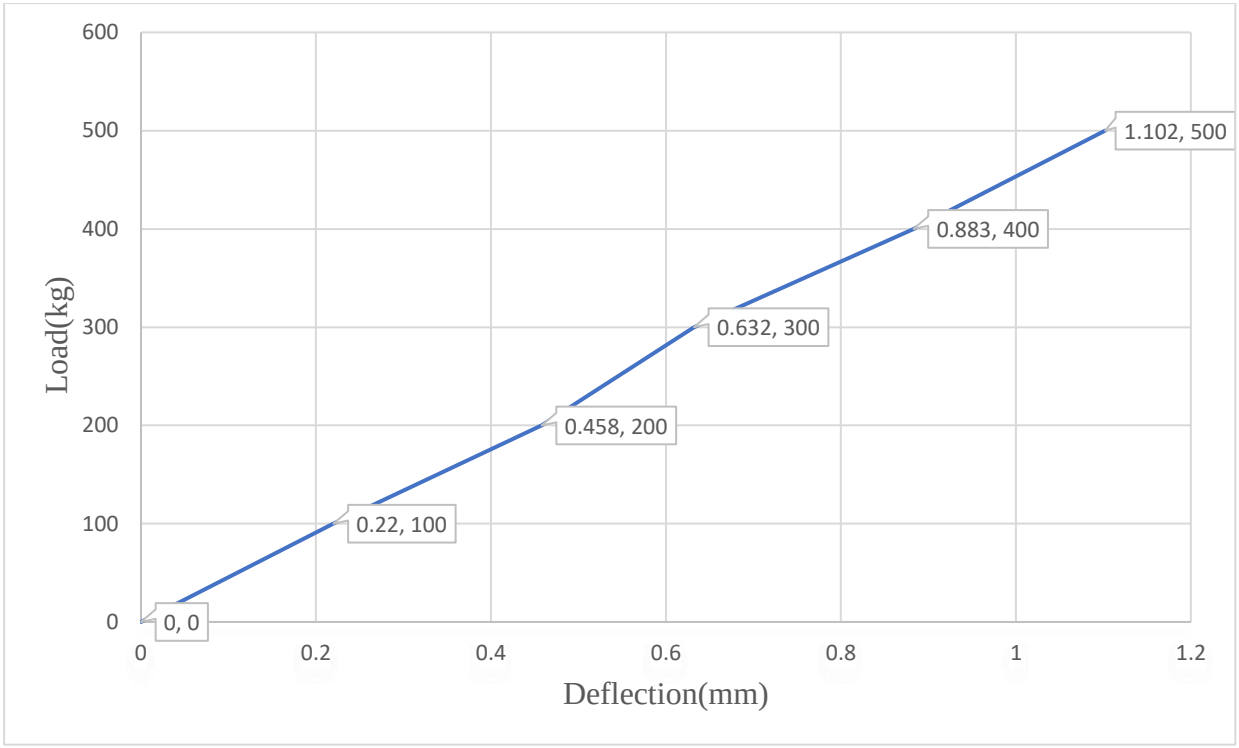

Fig. 4.1 Load Deflection Plot for SA (Dial gauge 1)

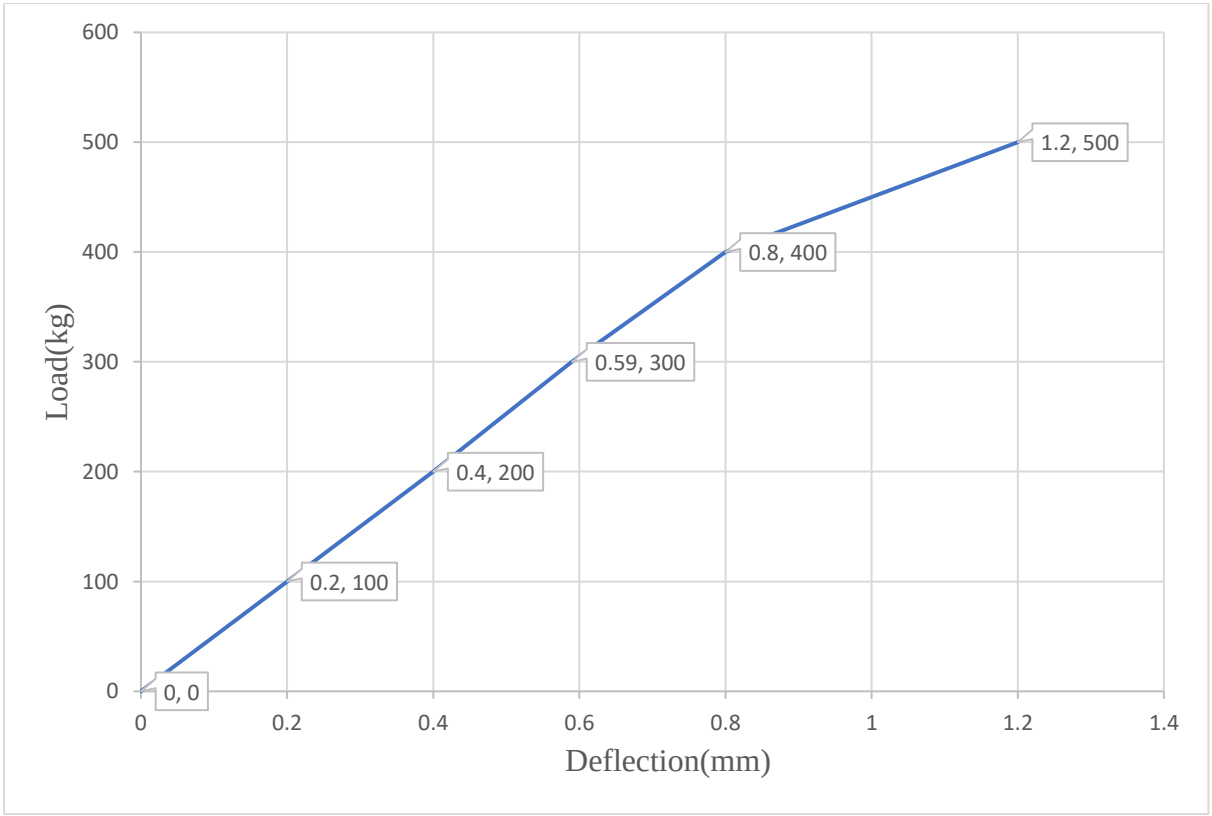

Fig.4.2 Load Deflection Plot for SA (Dial gauge 2)

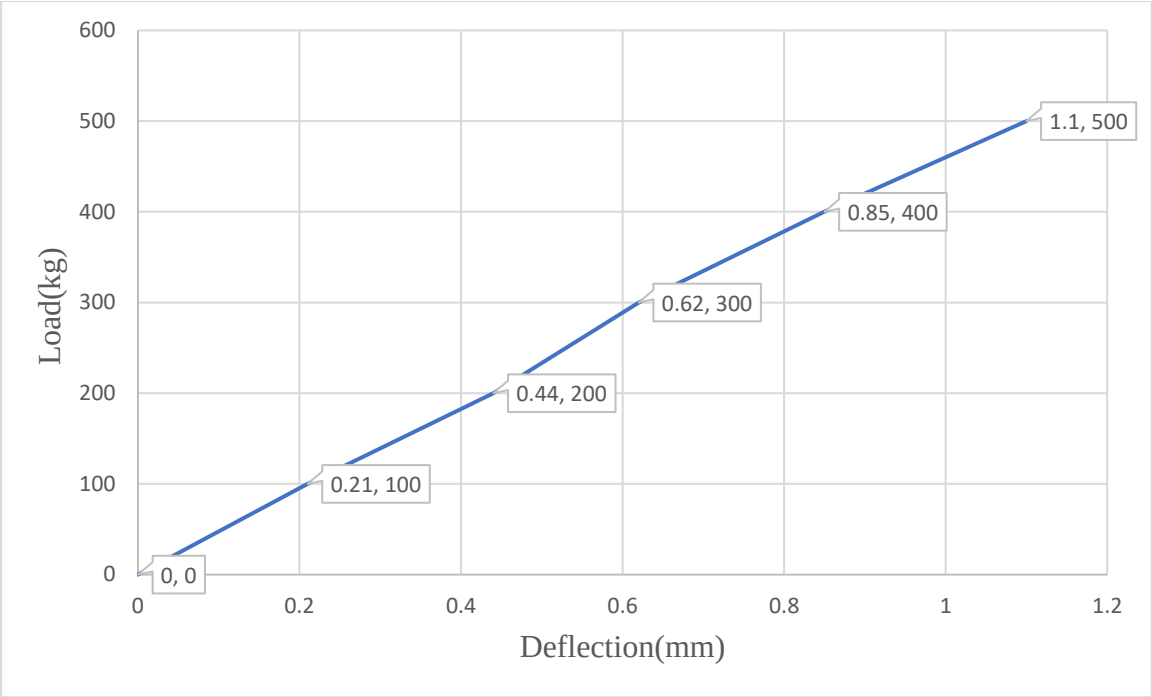

Fig.4.3 Load Deflection Plot for SA (Dial gauge 3)

4.2.2 Curved Aggregate Bonded Slab(CG)

- From Fig.4.4 it is observed that the maximum deflection occurred at the center (dial gauge 1) during the casting was 68.48mm with the total thickness of the slab to be around 218mm at the center.
- Fig.4.5, Fig.4.6 and Fig.4.7 shows the load deflection plot at center (dial gauge 1), at a distance of 500mm from center to the right (dial gauge 2) and at a distance of 1000mm from center to the left (dial gauge 3) respectively.
- From Fig.4.5 it is observed that the deflection occurred in the slab (dial gauge 2) is around 58.05mm with the total thickness of the slab at that point to be around 208mm.
- From Fig.4.6 it is observed that the deflection occurred in the slab (dial gauge 3) is around 50.27 with the total thickness of the slab at that point to be around 200mm. Deflection at different points at a distance of 250mm apart is shown in Fig.4.4.

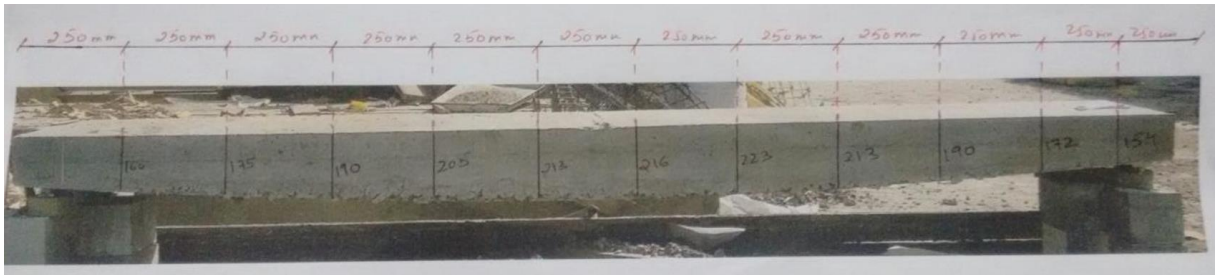

Fig.4.4 Deflection at Different Points for CG

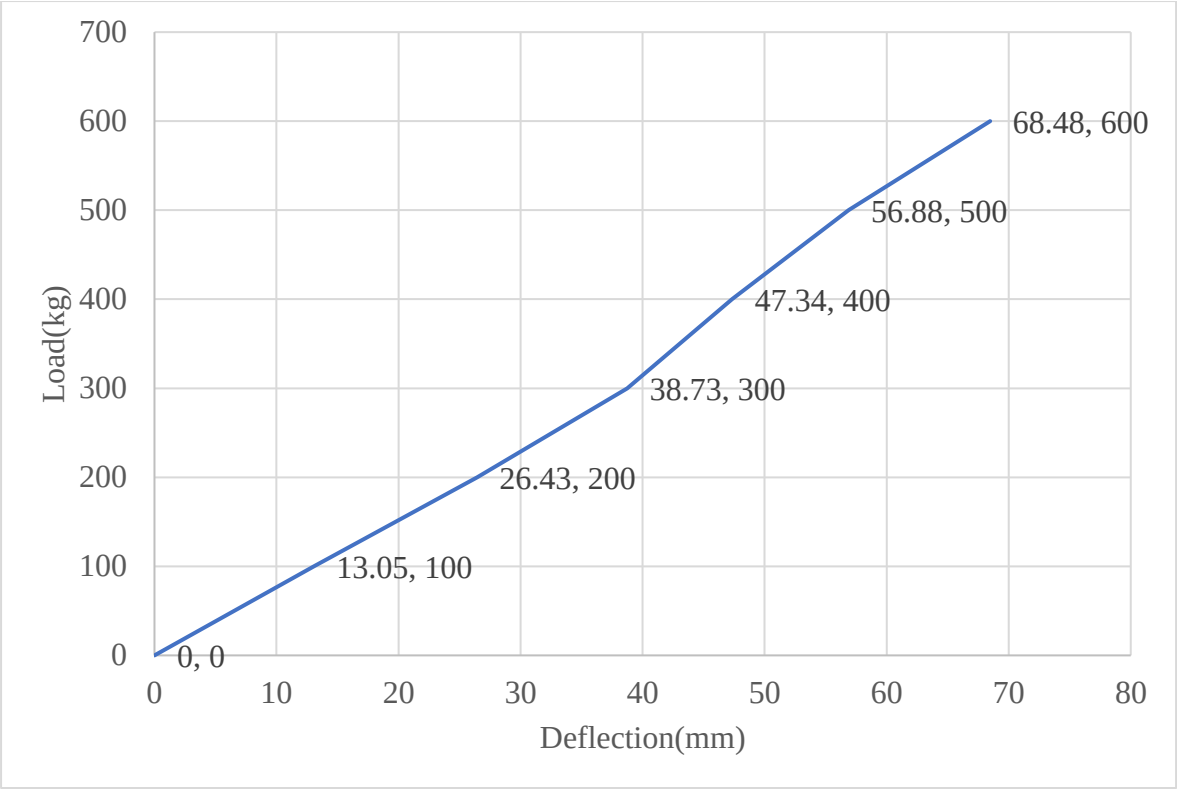

Fig.4.5 Load Deflection Curve for CG (dial gauge 1)

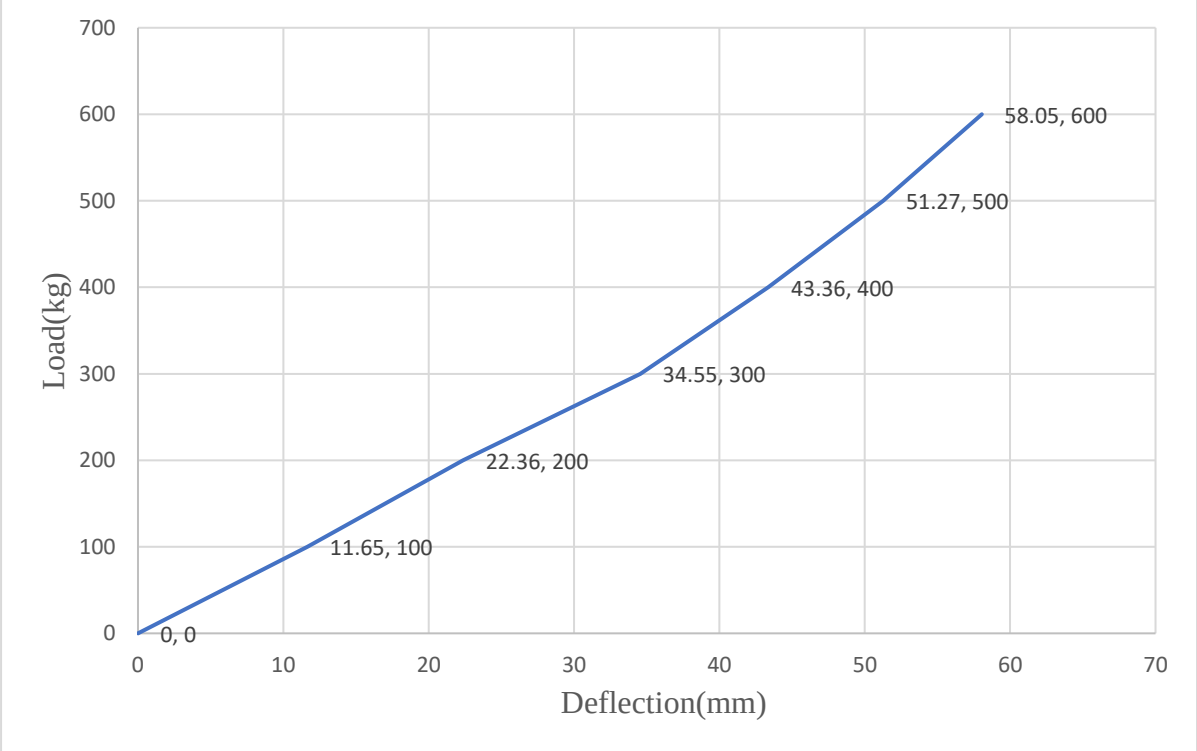

Fig.4.6 Load Deflection Curve for CG (dial gauge 2)

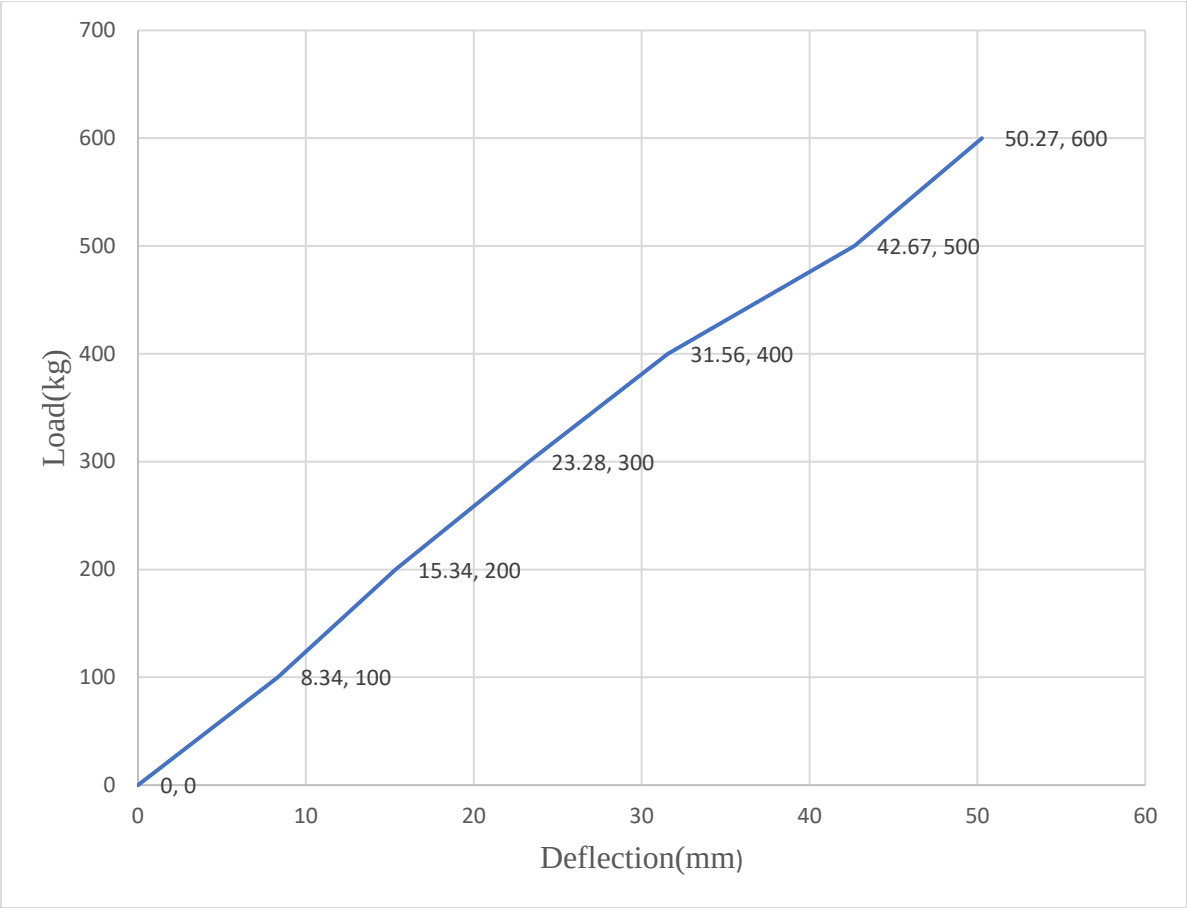

Fig.4.7 Load deflection curve (dial gauge 3)

4.2.3 Curved Adhesive Bonded Slab (CA)

Fig.4.8, Fig.4.9 and Fig.4.10 shows the load deflection plot at center (dial gauge 1), at a distance of 500mm from center to the right (dial gauge 2) and at a distance of 1000mm from center to the left (dial gauge 3) respectively.

- From Fig.4.8 it is observed that the maximum deflection occurred at the center (dial gauge 1) during the casting was 74.88mm with the total thickness of the slab to be around 225mm at the center.
- From Fig.4.9 it is observed that the deflection occurred in the slab (dial gauge 2) is around 64.05mm with the total thickness of the slab at that point to be around 214mm.
- From Fig.4.10 it is observed that the deflection occurred in the slab during casting (dial gauge 3) is around 56.83mm with the total thickness of the slab at that point to be around 206mm.

The results show that the deflection in case of adhesive bonded slab is more than the deflection occurred in case of aggregate bonded slab. This is because of the reason that there was more

stiffness due to aggregates that were bonded to the plank with the adhesive in case of curved aggregate bonded slab.

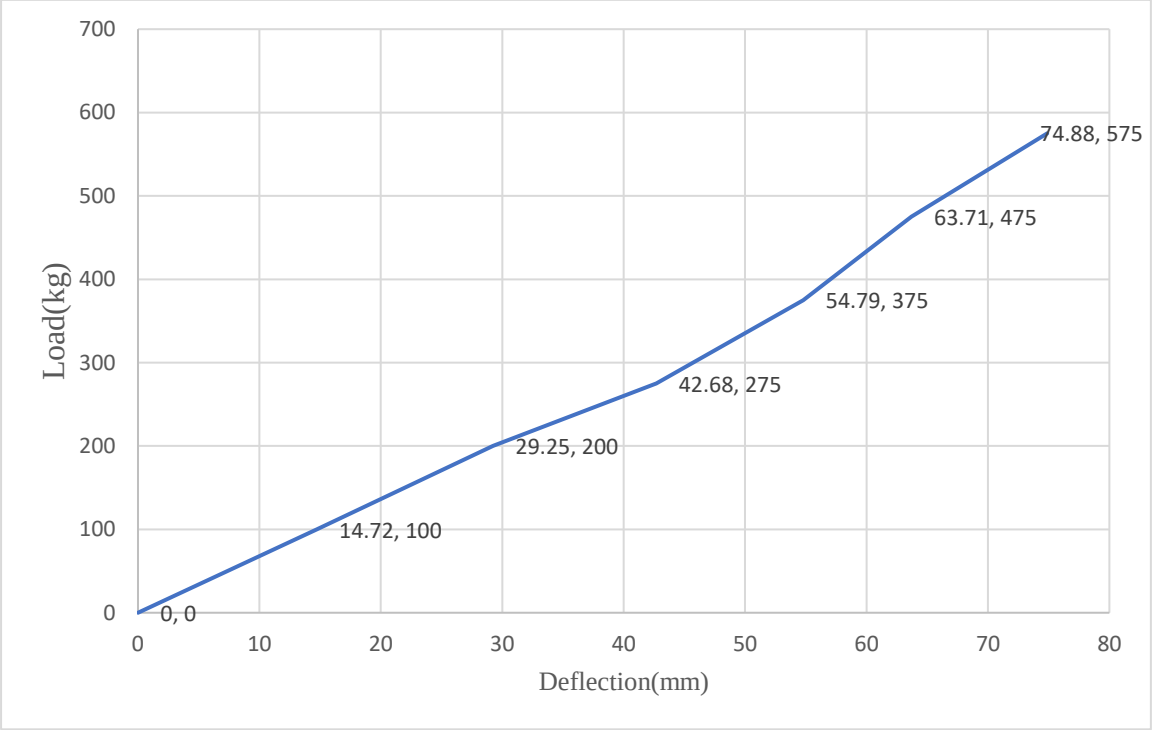

Fig.4.8 Load Deflection Curve for CA (dial gauge 1)

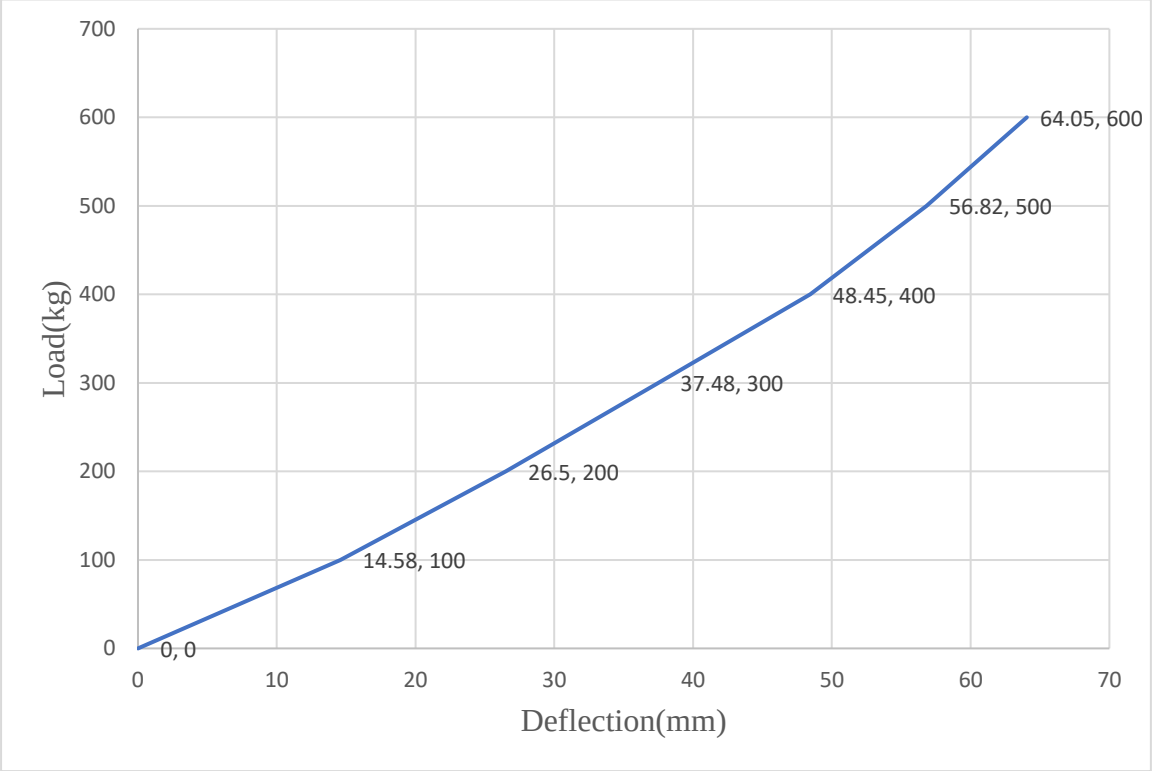

Fig.4.9 Load Deflection Curve for CA (dial gauge 2)

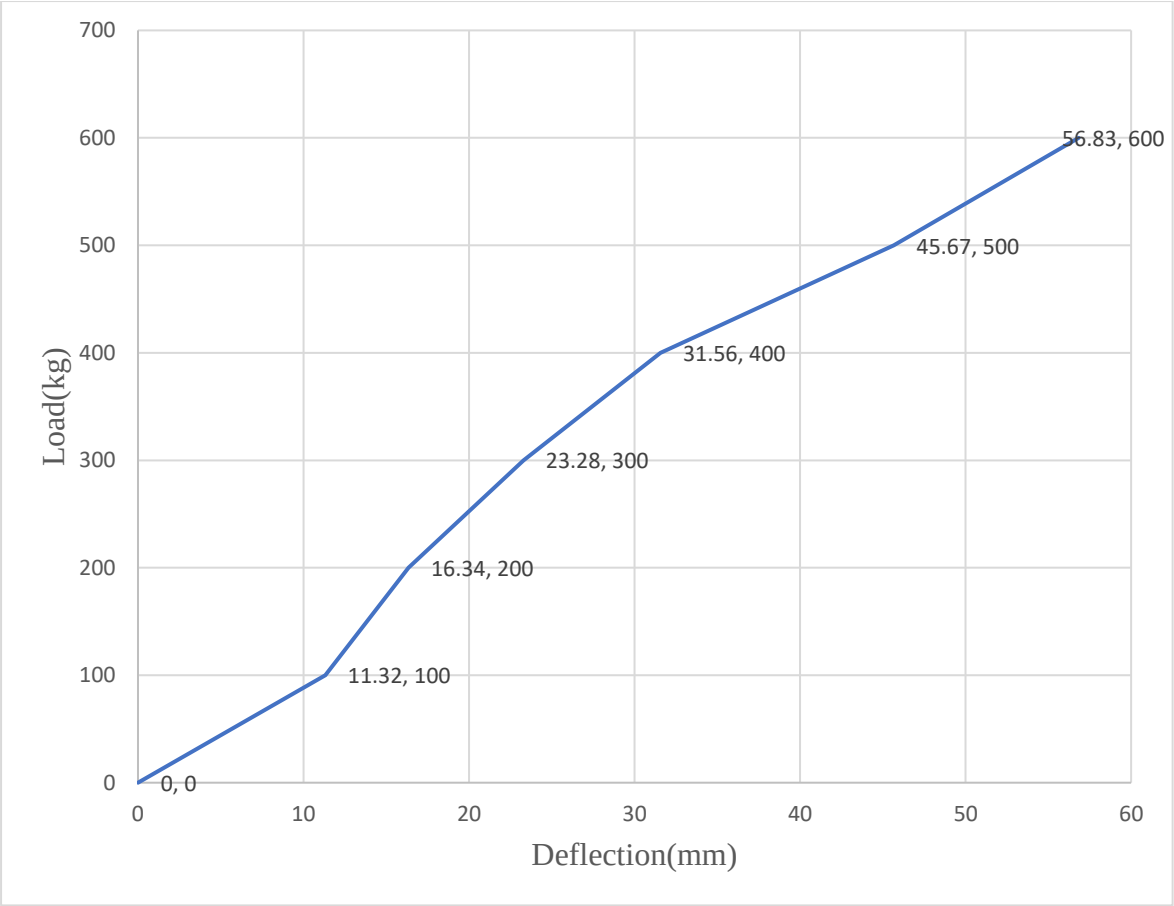

Fig.4.10 Load Deflection Curve for CA (dial gauge 3)

4.3 CYCLIC LOADING RESULTS

4.3.1 Straight Adhesive Bonded Slabs (SA)

The specimen SA was tested under two-point loading test on loading frame on which cyclic loading was applied. As the load increased cracks started to appear on the surface of the slab. The crack pattern of the straight slab that occurred during flexural testing and also the final failure of the slab that occurred when the load reached its ultimate value is shown below.

- Fig.4.11 shows the initial flexural cracks that occurred in the slab after the completion of the 2nd load cycle when load reached 42 kN which further propagated. Large number of flexural cracks were observed and very minute shear crack was observed at load of 130 kN and then failed suddenly by debonding of GFRP plank at an ultimate load of 144 kN as shown in Fig 4.12.
- The total deflection achieved at ultimate load was of about 58mm at center as shown in Fig.4.13. In this slab the failure mode was shear failure of concrete which resulted due to debonding of GFRP plank in one of the shear spans.

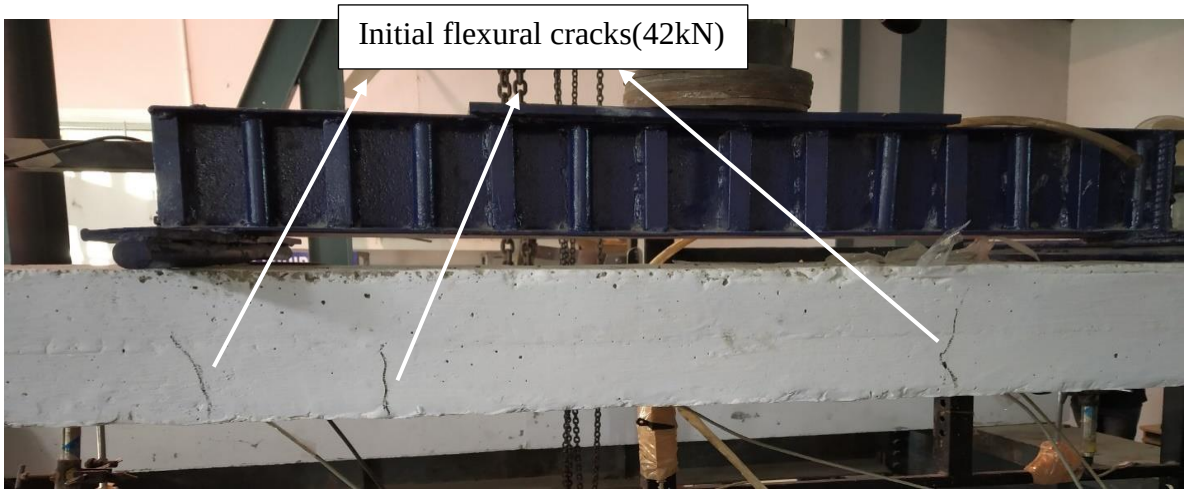

(a)

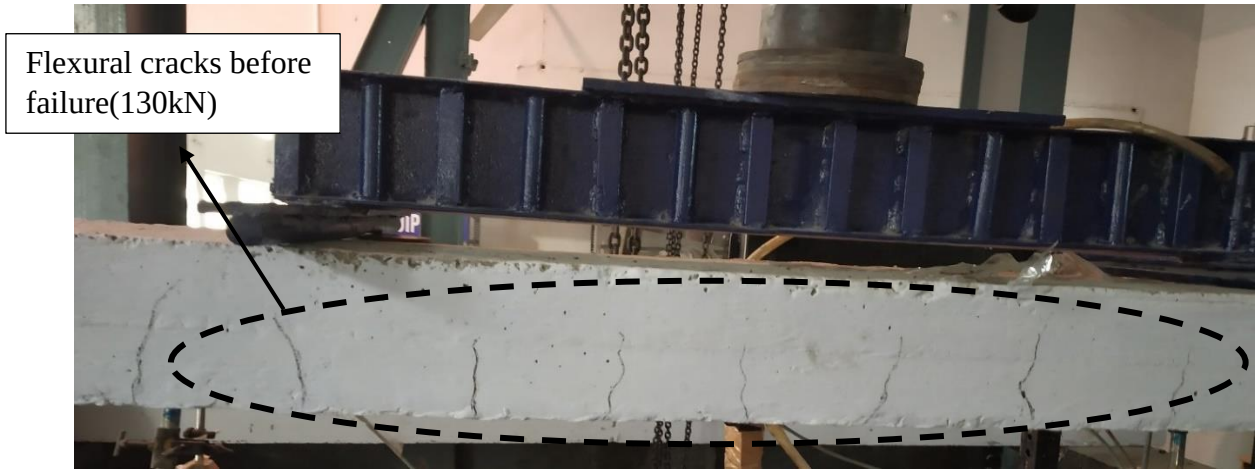

(b)

Fig.4.11 (a) Initial Cracking (b) Cracks Before Failure

Fig 4.12 Failure of the Slab SA

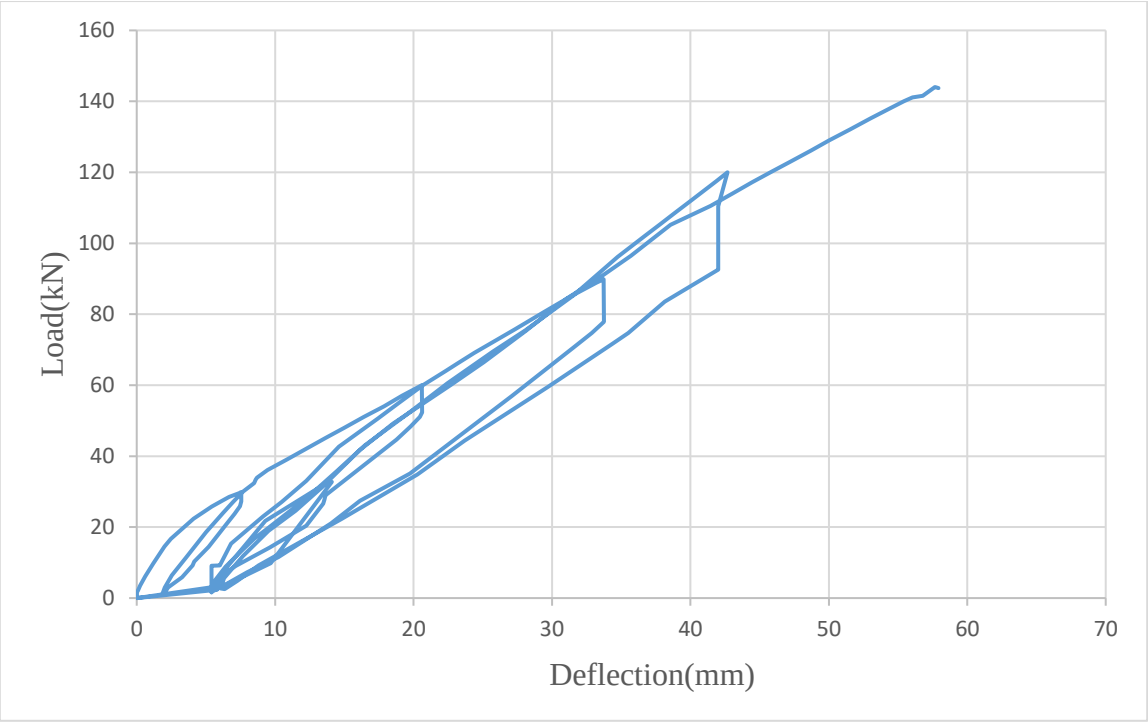

Fig.4.13 Load Deflection Plot at Center for SA

4.3.2 Curved Aggregate Bonded Slabs (CG)

The specimen CG was tested under two-point loading test on loading frame on which cyclic loading was applied. As the load increased Initial flexure crack was observed were observed on the surface of the CG slab.

- The crack pattern of the specimen CG at the initial stages and at the final stage is shown in Fig.4.14. Specimen CG shows considerable increase in the ultimate load carrying capacity by 25% as compared to the specimen SA. The ultimate load at which the failure took place is 183.24 kN. Moreover, the occurrence of the first crack took place at higher load as compared to the specimen SA.
- The initial cracks occurred in the slab after the completion of the 4^{th} load cycle at a load of 96 kN as shown in Fig.4.14 which further propogates and leads to the sudden failure of the slab at an ultimate load of 183.24 kN.
- Maximum deflection was observed to be 44mm at center in AG specimens which was much lower than the maximum deflection in case of specimen SA as shown in Fig.4.17. The quarter span deflection at ultimate load achieved was 27 mm as shown in Fig.4.18. Final failure mode of the slab is shown in Fig.4.17. The failure mode in specimen CG was shear failure of the concrete.

- In Fig.4.16(a) it is observed that failure was initially due to delamination of the plank as concrete is still bonded to the plank at some places which further leads to debonding of the plank from the concrete and the T-ribs that were running along the length of the plank gets embedded into the shattered part as shown in Fig.4.16(b). The flexural cracks were less in comparison to specimen SA.

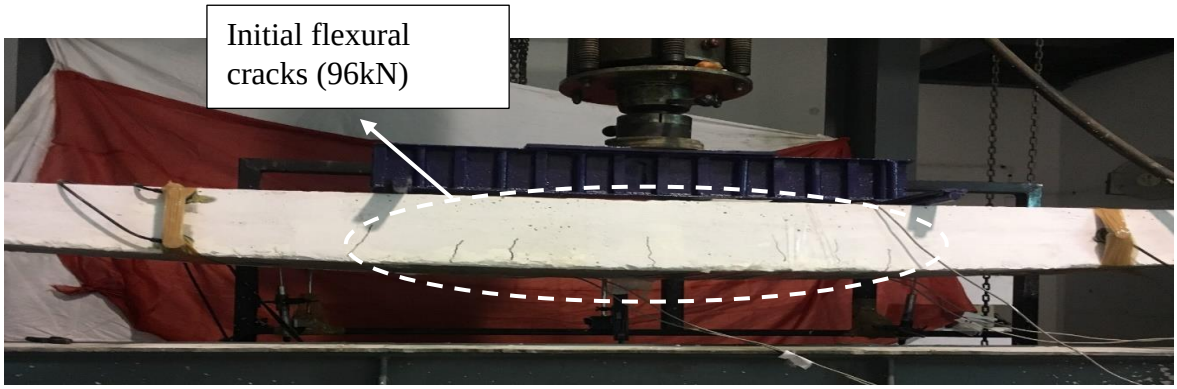

Fig.4.14 Cracks Appeared in CG

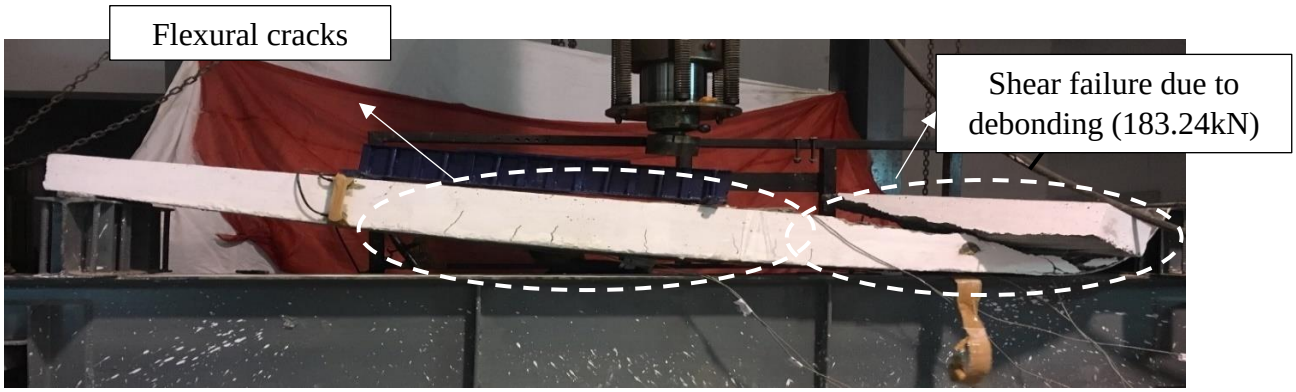

Fig.4.15 Failure Mode of CG Slab

(a) (b)

Fig.4.16 (a) Plank After Failure (b) Seperated concrete Part After Failure

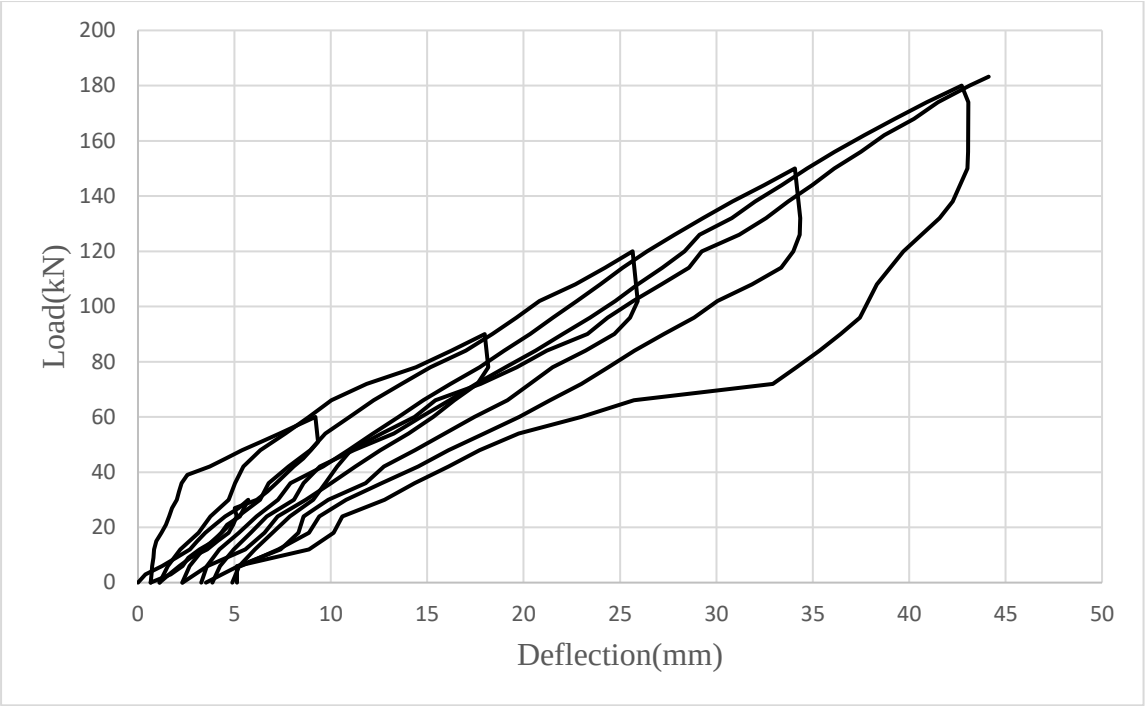

Fig.4.17 Load Deflection Plot for CG at Central Span for CG

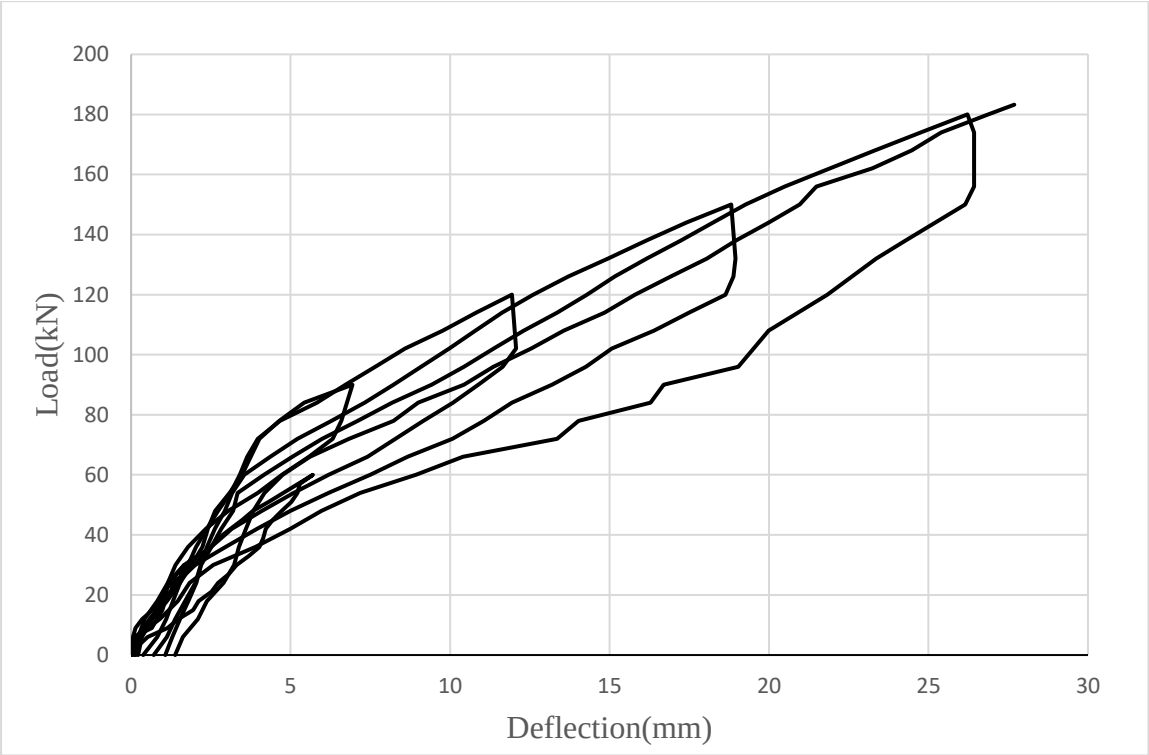

Fig.4.18 Load Deflection Plot for CG at Quarter Span for CG

4.3.3 Curved Adhesive Bonded Slabs (CA)

The specimen CA was tested under two-point loading test on loading frame on which cyclic loading was applied. As the load increased cracks started to appear on the surface of the CA

slab. The crack pattern of the specimen CA that occurred during flexural testing and also the final failure of the slab that occurred when the load reached its ultimate value is shown below.

- There is a remarkable increase in the ultimate load carrying capacity of Specimen CA as compared to both specimen CG and SA. The ultimate load at which the failure took place in specimen CA is 201.36 kN. Moreover, the occurrence of the first crack took place at higher load as compared to the specimen CG and SA.
- The initial cracks occurred in the slab CA after the completion of the 4^{th} load cycle at a load of 106 kN which is more than in case of specimen CG as shown in Fig.4.19 which further propogates and leads to the sudden failure of the slab at an ultimate load of 201.36 kN.
- There was negligible increase in the deflection in specimen CA when compared with the specimen CG with deflection of about 48 mm at the center as shown in Fig.4.22 The quarter span deflection at ultimate load achieved was 29.15 mm as shown in Fig.4.23.
- The final failure mode of the slab is shown in Fig.4.20. The failure mode in specimen CA and CG was shear failure whereas in case of specimen SA failure mode is flexural failure due to debonding.
- It is also observed that failure was very much similar to that of specimen CG in which initially delamination took place which further leads to debonding and the T-ribs that were running along the length of the plank gets embedded into the shattered part as shown in Fig.4.21.
- The Fig.4.24 shows comparison of load deflection plot at center between straight adhesive bonded slab, aggregate bonded slab and adhesive bonded slab. Therefore, it is evident that at center span specimen SA shows more deflection as compared to both specim CG and CA as the slab thickness in case of SA(150mm) is less than CG(218mm) and CA (225mm)

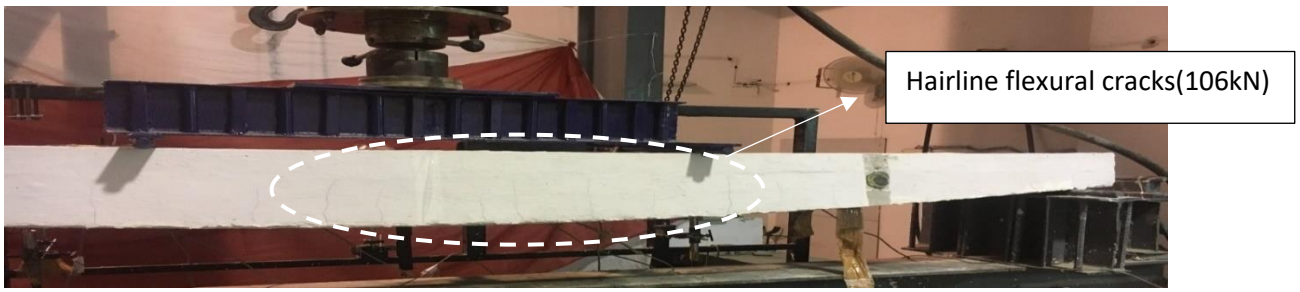

Fig.4.19 Initial Cracking in CA After load Cycle 4

Fig.4.20 Failure Mode of CA Slab at 201.36kN

Fig.4.21 Seperated Concrete Part After Failure

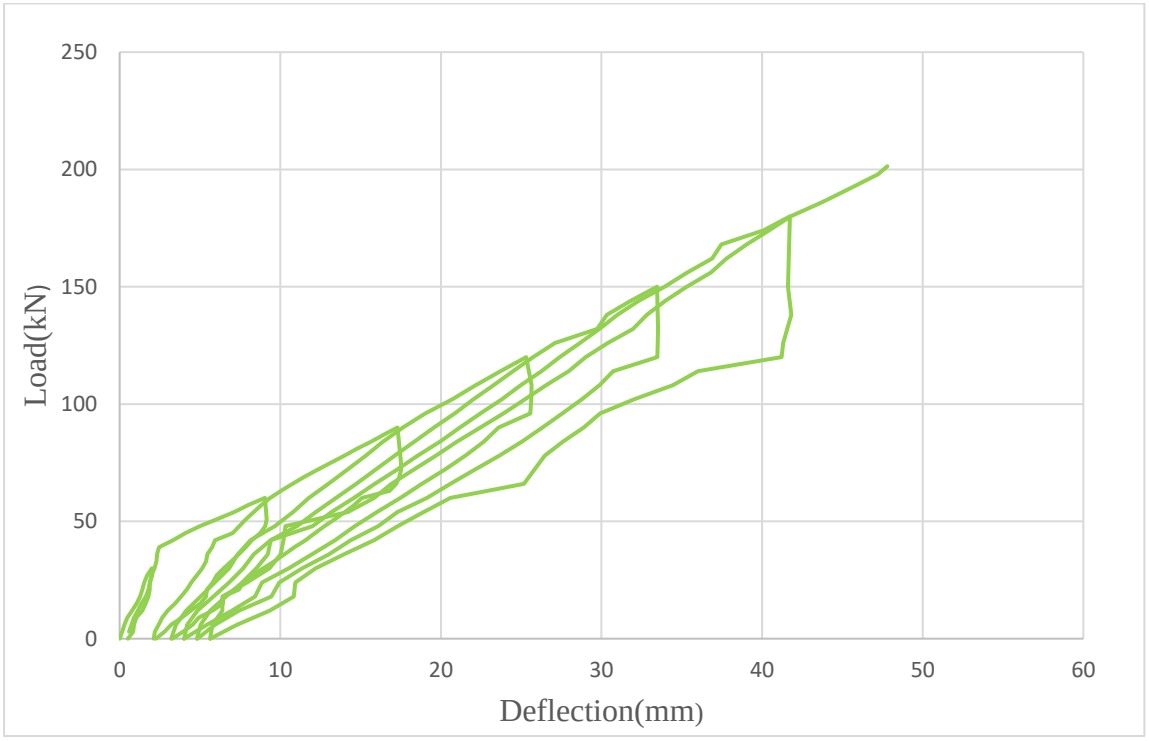

Fig.4.22 Load Deflection Plot for Specimen CA at the Center for CA

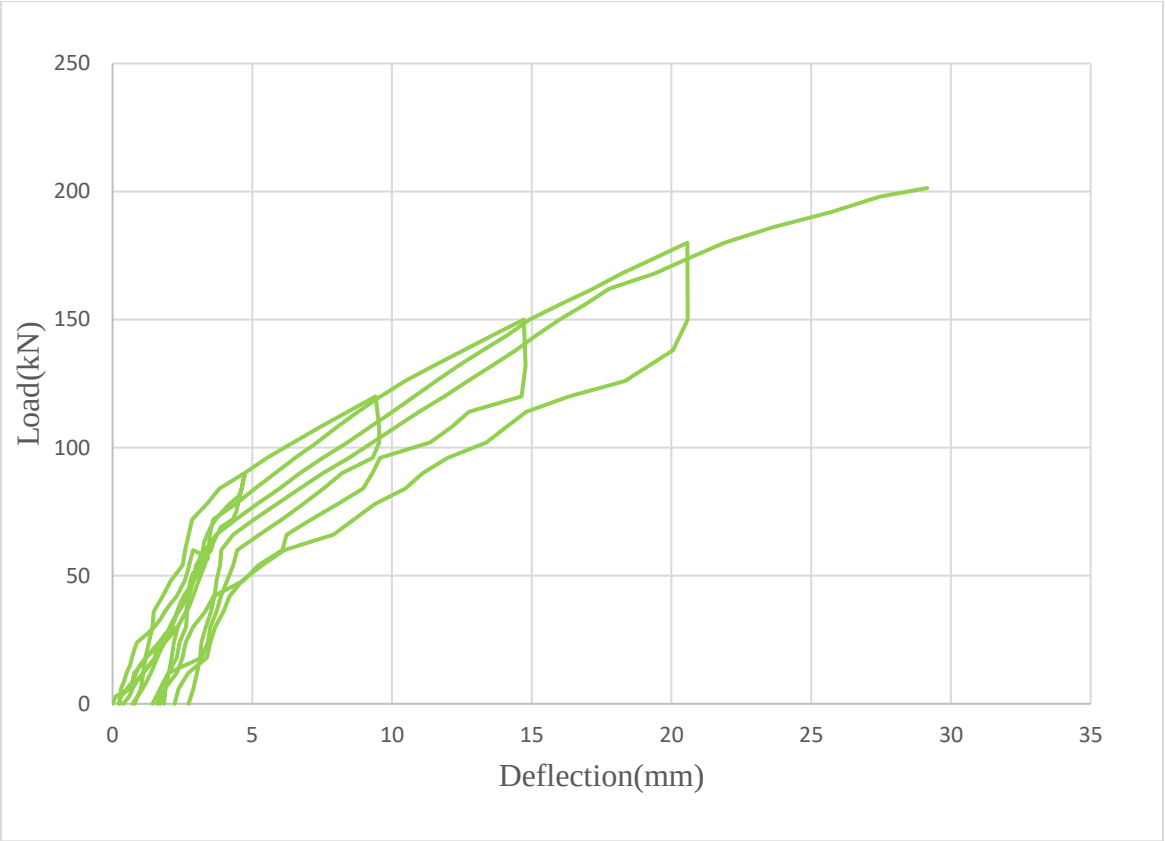

Fig.4.23 Load Deflection Plot for Specimen CA at Quarter Span for CA

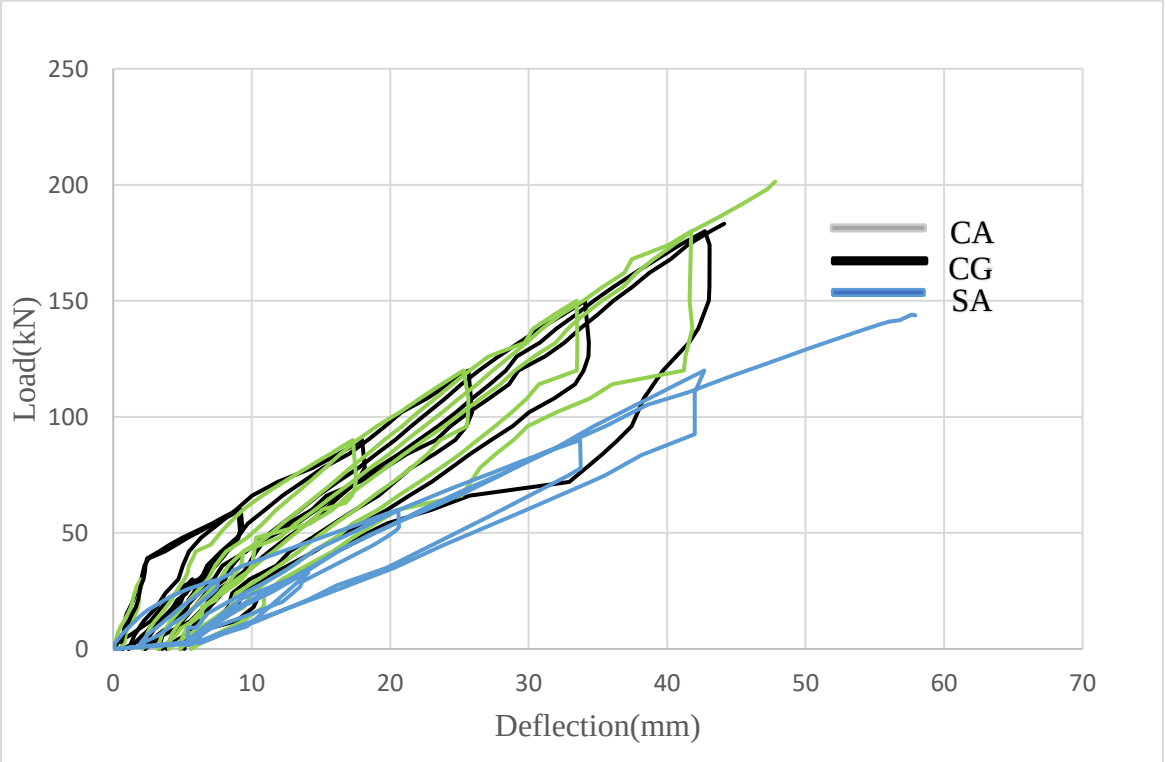

Fig.4.24 Comparison of Load Deflection Plot at Center Between SA, CG and CA

4.4 LOAD STRAIN CHARACTERISTICS

During flexural testing strains were measured using strain gauges for both concrete and the GFRP.

4.4.1 Straight Adhesive Bonded Slab (SA)

Fig.4.25 shows the load vs strain graph for GFRP plank at its center. It is observed that maximum load at which failure took place was around 144 kN and maximum strain achieved at this ultimate load comes out to be 9136 at the center. Fig.4.26 shows the load vs strain plot for GFRP plank at quarter span which comes out to be 7168. Fig.4.27 shows the load vs strain plot for concrete at center which comes out to be -2255. From the concrete strain values it can be seen that the maximum strain value in concrete is less than the failure strain in concrete0.003. Thus, the ultimate failure was not concrete flexure failure.

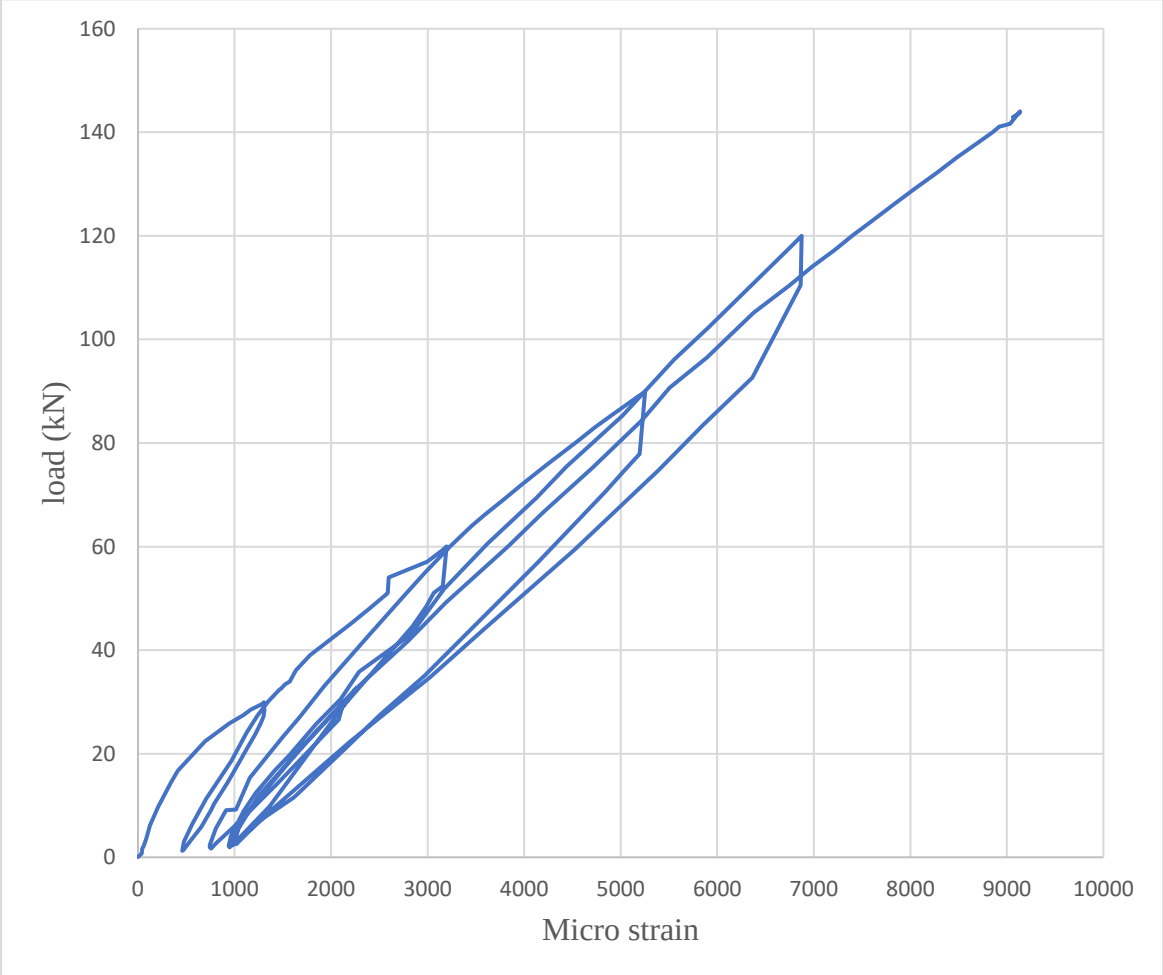

Fig.4.25 GFRP Load vs Strain Plot for SA at Center for SA

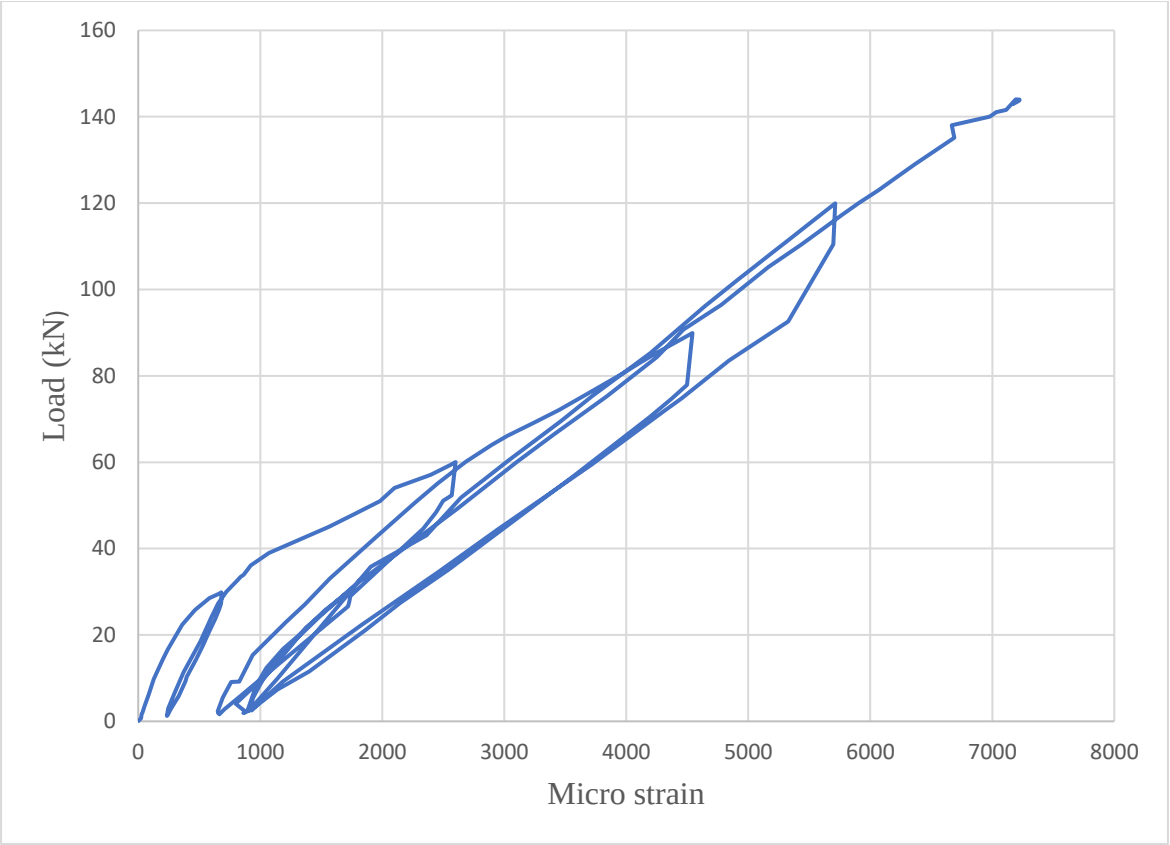

Fig.4.26 GFRP load vs strain plot for specimen SA at quarter span for SA

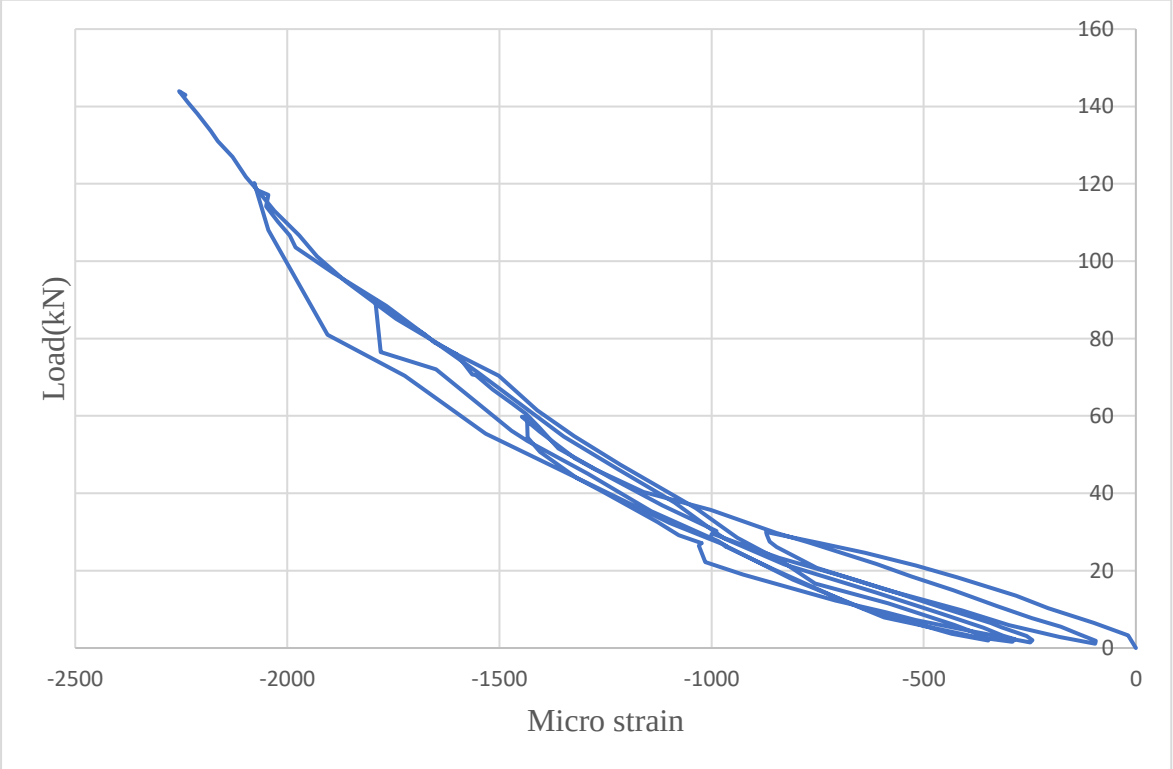

Fig.4.27 Concrete Load vs Strain Plot for Specimen SA at Center for SA

4.4.2 Curved Aggregate Bonded Slab (CG)

There is a notable decrease in the strain level in specimen CG when compared with that of specimen SA. Fig.4.28 shows the load vs strain graph for GFRP plank at its center. It is observed that maximum load at which failure took place was around 183.24 kN and maximum strain achieved at this ultimate load comes out to be 8074 at the center. Fig.4.29 shows the load vs strain plot for GFRP plank at a distance 500mm from the center which comes out to be 5540. Fig.4.30 shows the load vs strain plot for GFRP plank at a distance 750mm from the left support (quarter span) which comes out to be 4895. Fig.4.31 shows the load vs strain plot for concrete at center which comes out to be -1966.

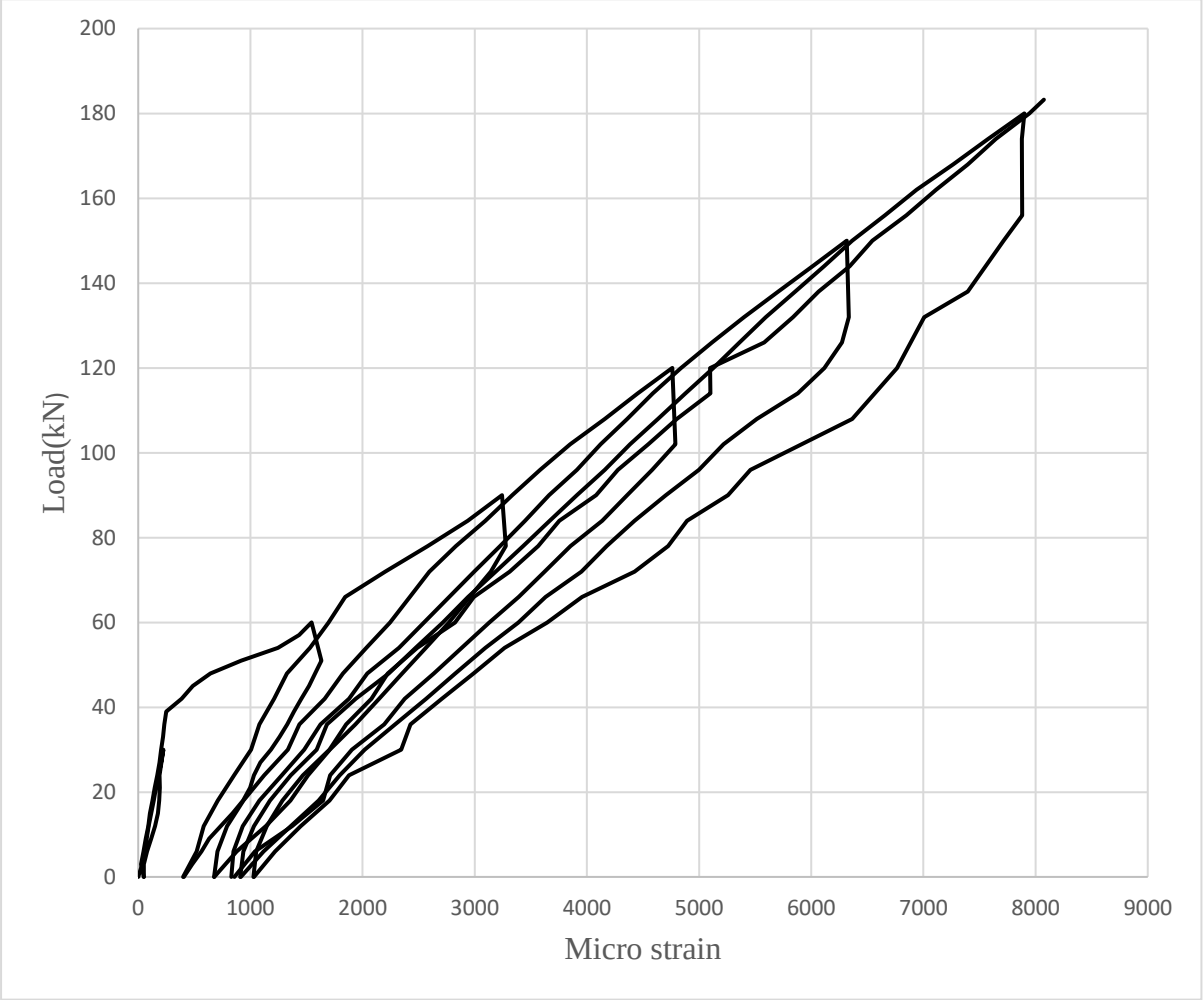

Fig.4.28 GFRP Load vs Strain Graph at Center for CG

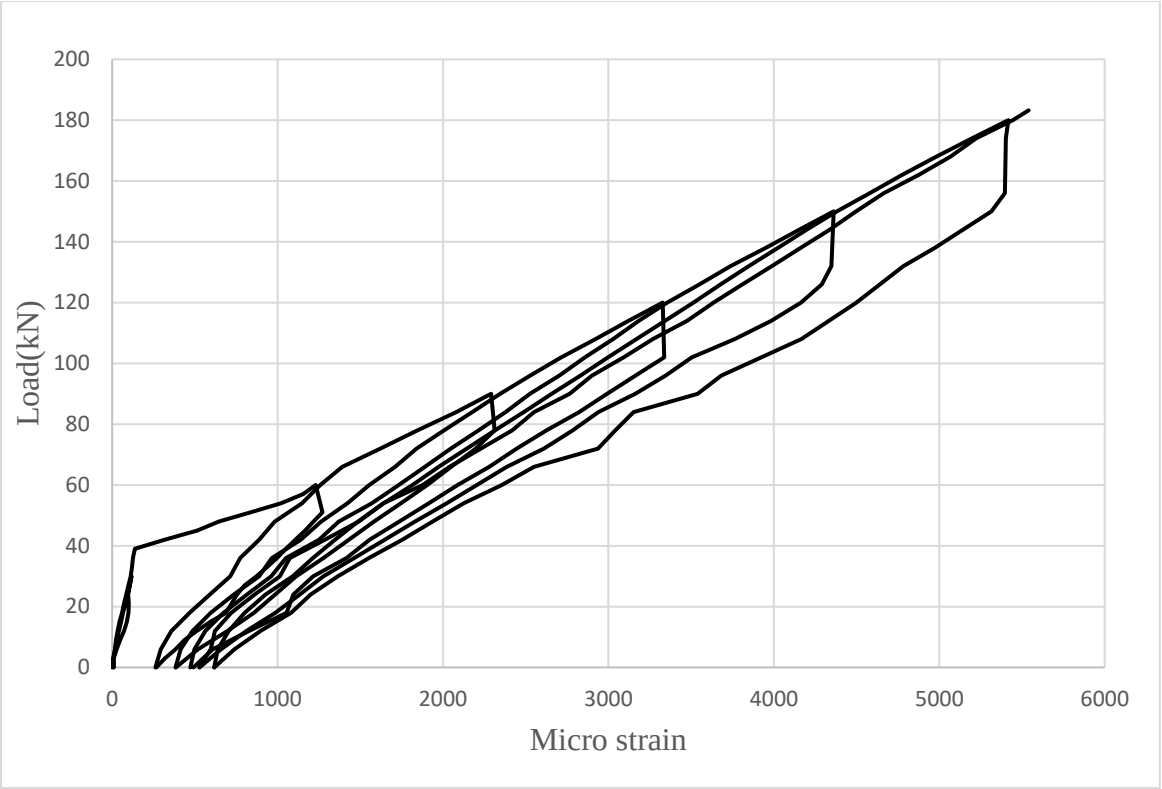

Fig.4.29 GFRP Load vs Strain Plot at a Distance 500mm from the Center for CG

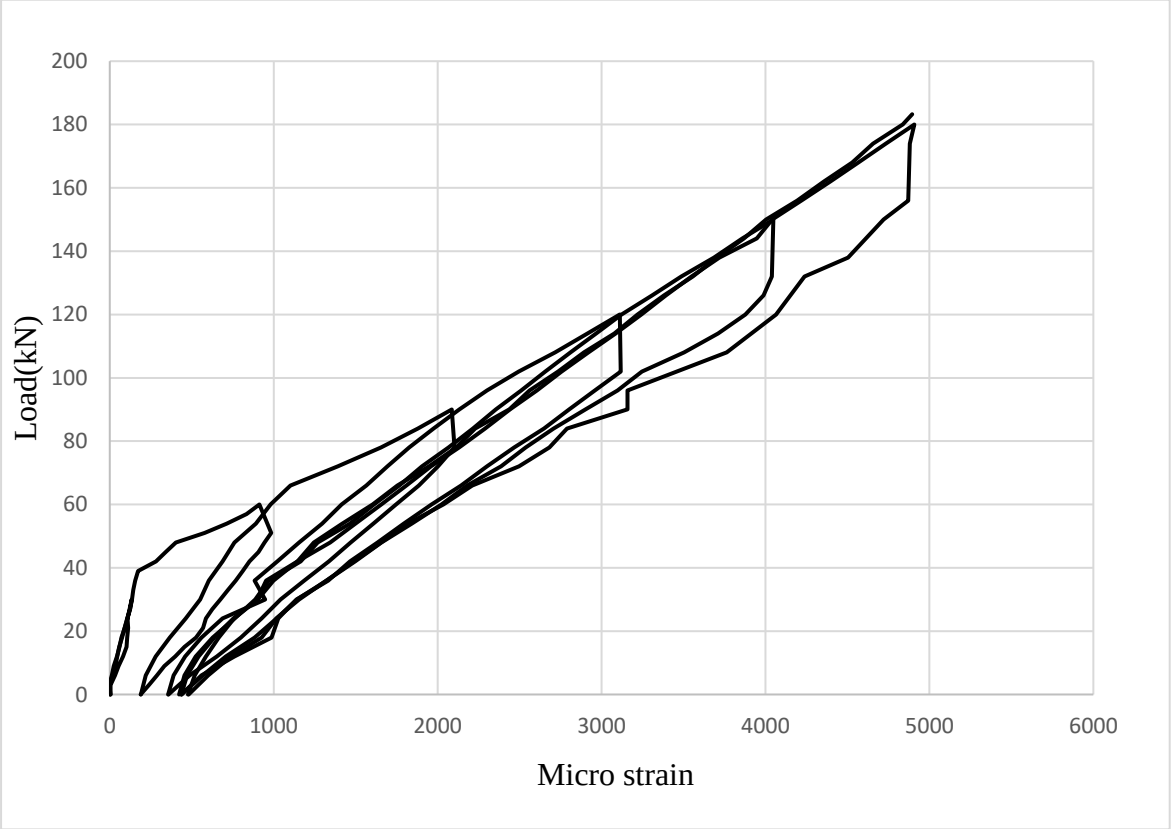

Fig.4.30 GFRP Load vs Strain Plot at Quarter Span for CG

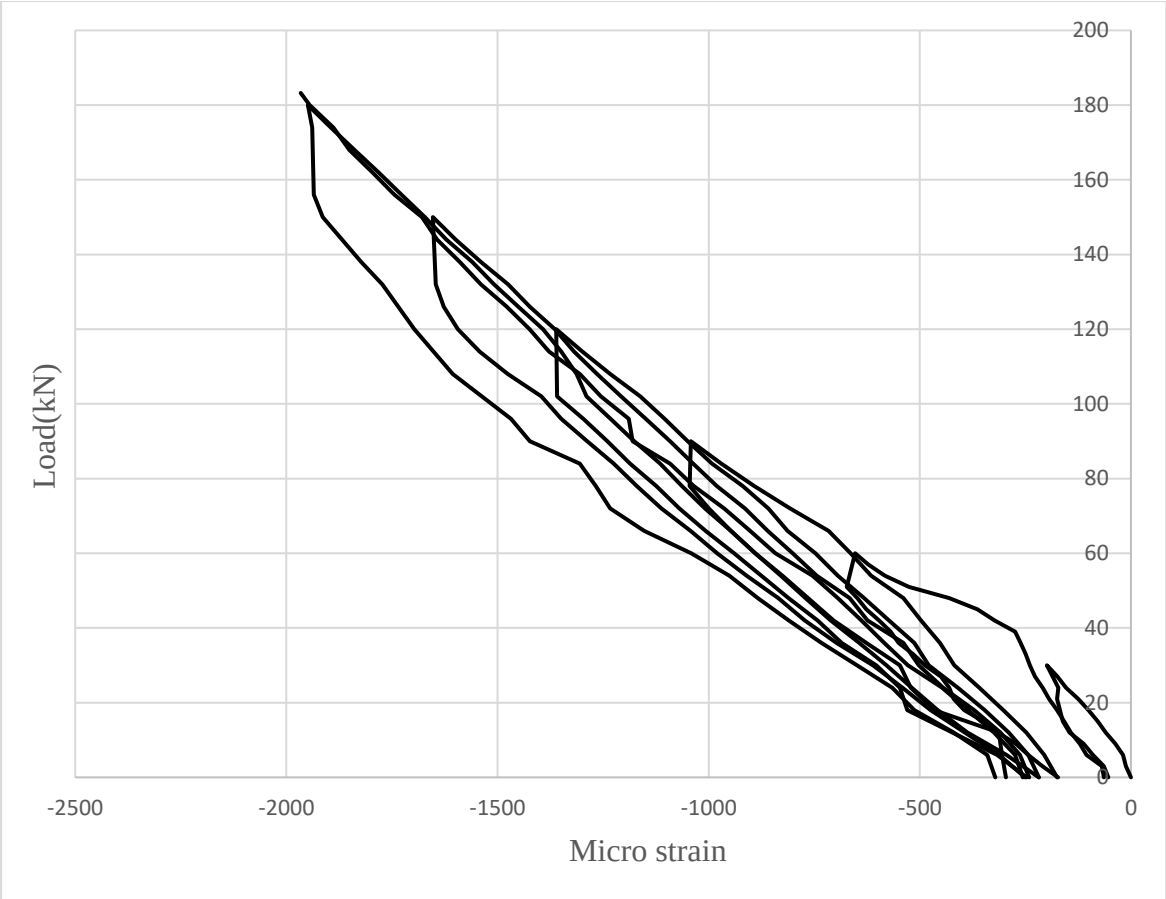

Fig.4.31 Concrete Load vs Strain Plot at Center for CG

4.4.3 Curved Adhesive Bonded Slab (CA)

It is observed that at GFRP level there is an increase in strain level in specimen CA when compared to specimen CG and decreases when compared to specimen SA. Fig.4.32 shows the load vs strain graph for GFRP plank at its center. It is observed that maximum load at which failure took place was around 201.36 kN and maximum strain achieved at this ultimate load comes out to be 8835 at the center. Fig.4.33 shows the load vs strain plot for GFRP plank at a distance 500mm from the center which comes out to be 6487. Fig.4.34 shows the load vs strain plot for GFRP plank at a distance 750mm from the left support (quarter span) which comes out to be 5380. As far as strain in concrete is concerned specimen SA shows more strain as compared to both specimen CA and CG. Fig.4.35 shows the load vs strain plot for concrete at center which comes out to be -2706.

Fig.4.36 shows the comparison of GFRP load vs strain plot of specimen SA, CG and CA at center. Fig.4.37 comparison of concrete load vs strain plot of specimen SA, CA and CG at center. Therefore, it can be seen that at any particular load specimen SA shows more strain as compared to specimen CG and CA in both FRP and concrete although the load carrying

capacity follows reverse order. It might be possible because of the curvature provided in curved beams during casting stage.

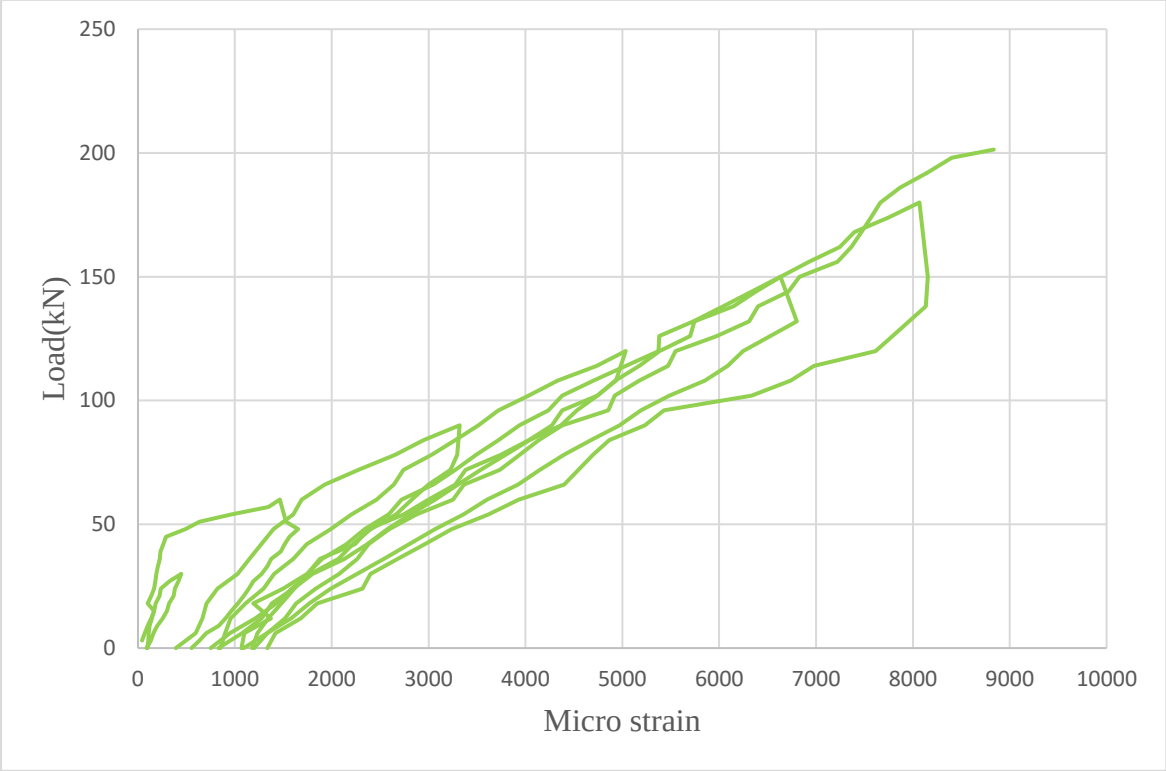

Fig.4.32 GFRP Load vs Strain Plot at Center for CA

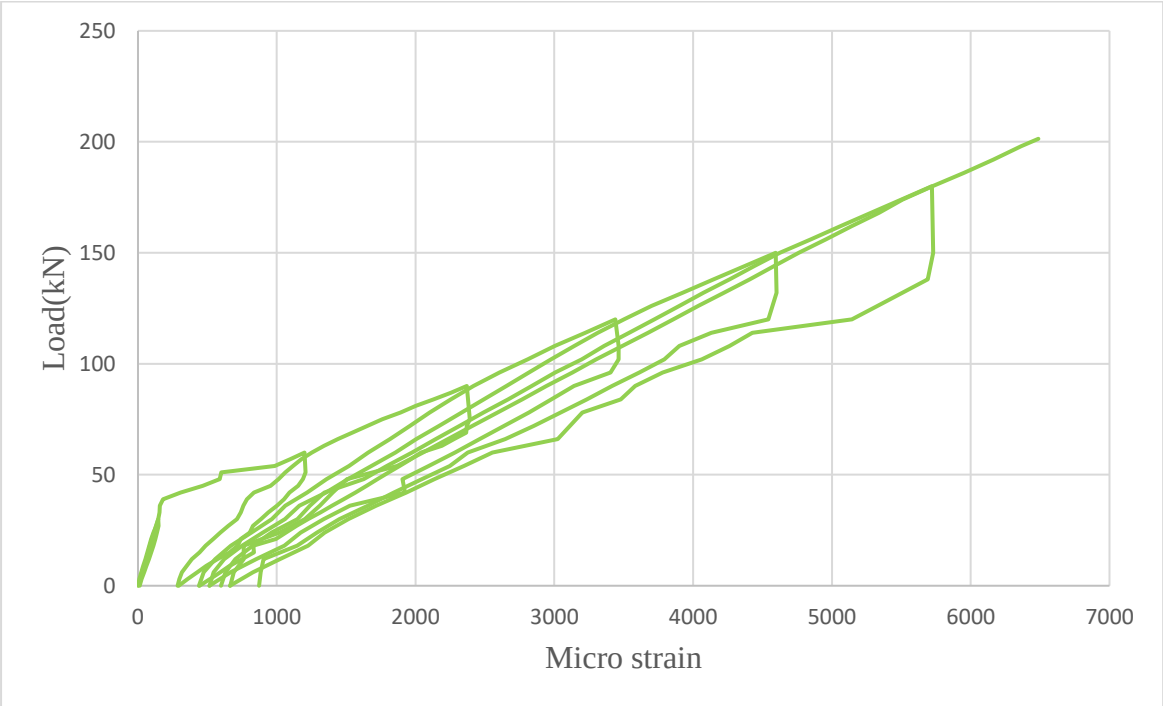

Fig.4.33 GFRP Load vs Strain Plot at a Distance 500mm from the Center for CA

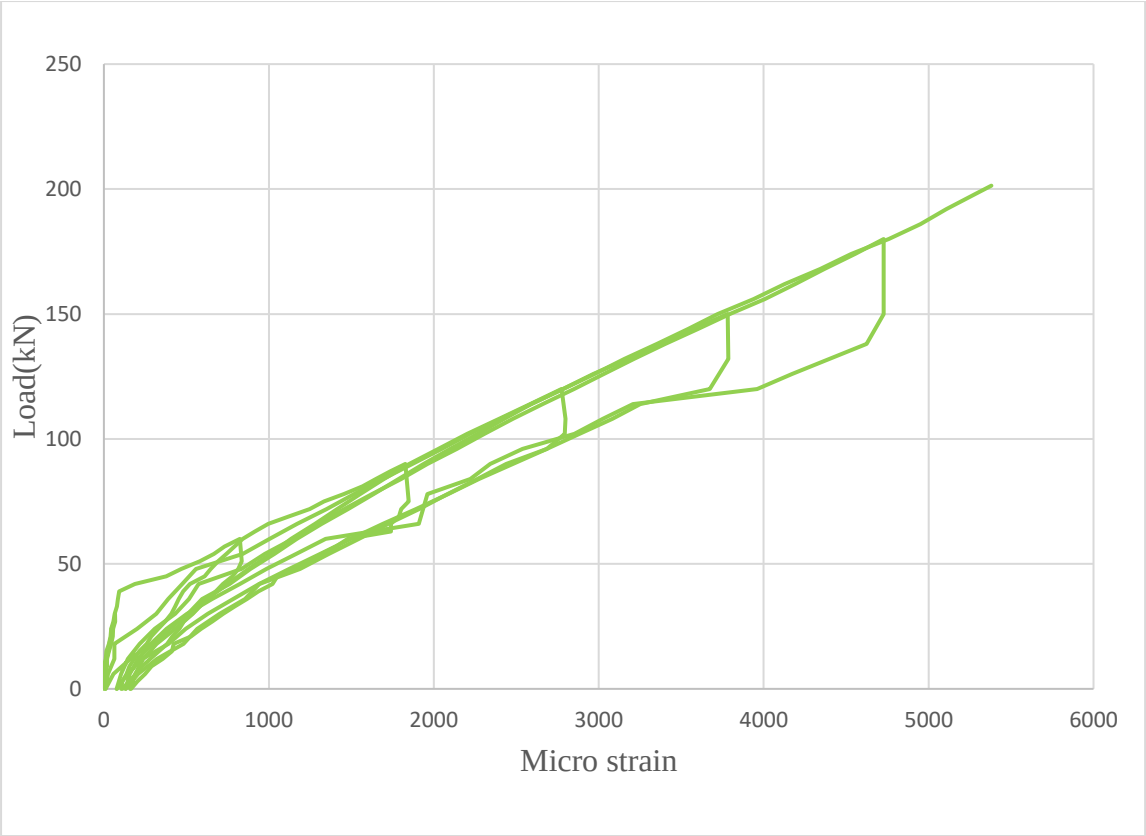

Fig.4.34 GFRP Load vs Strain Plot at Quarter Span for CA

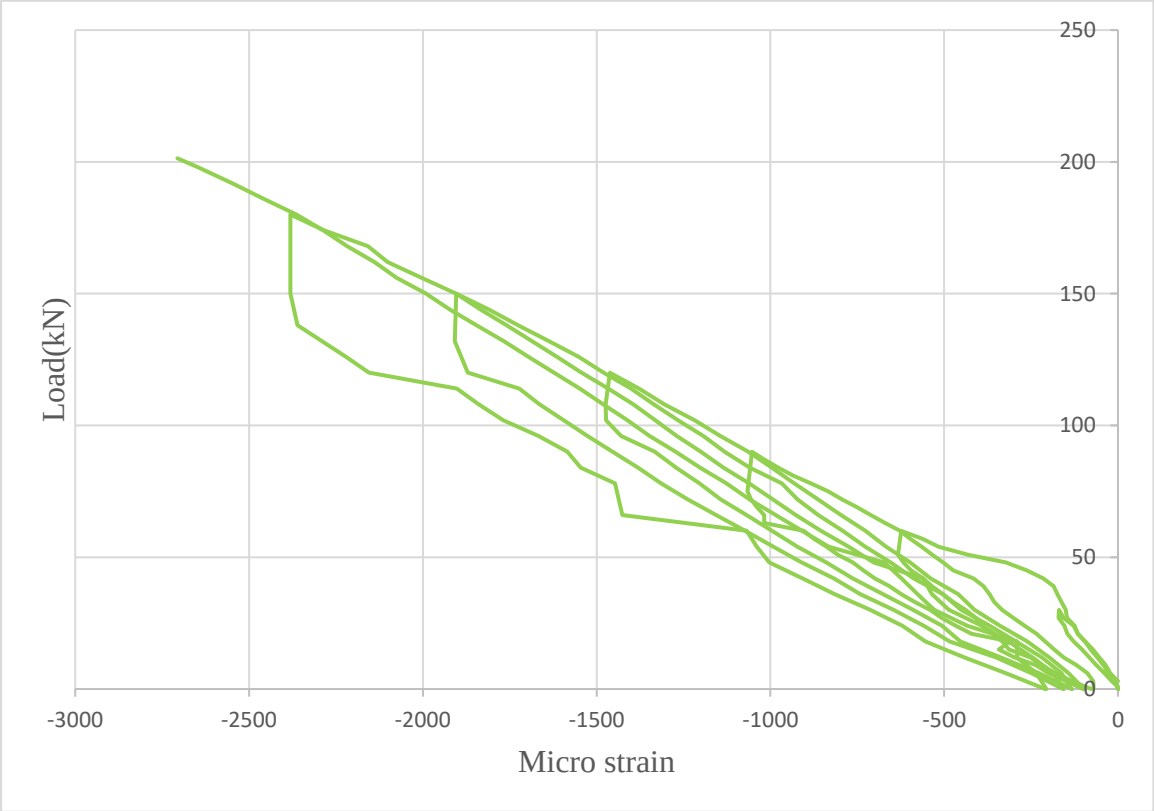

Fig.4.35 Concrete load vs strain plot at center for CA

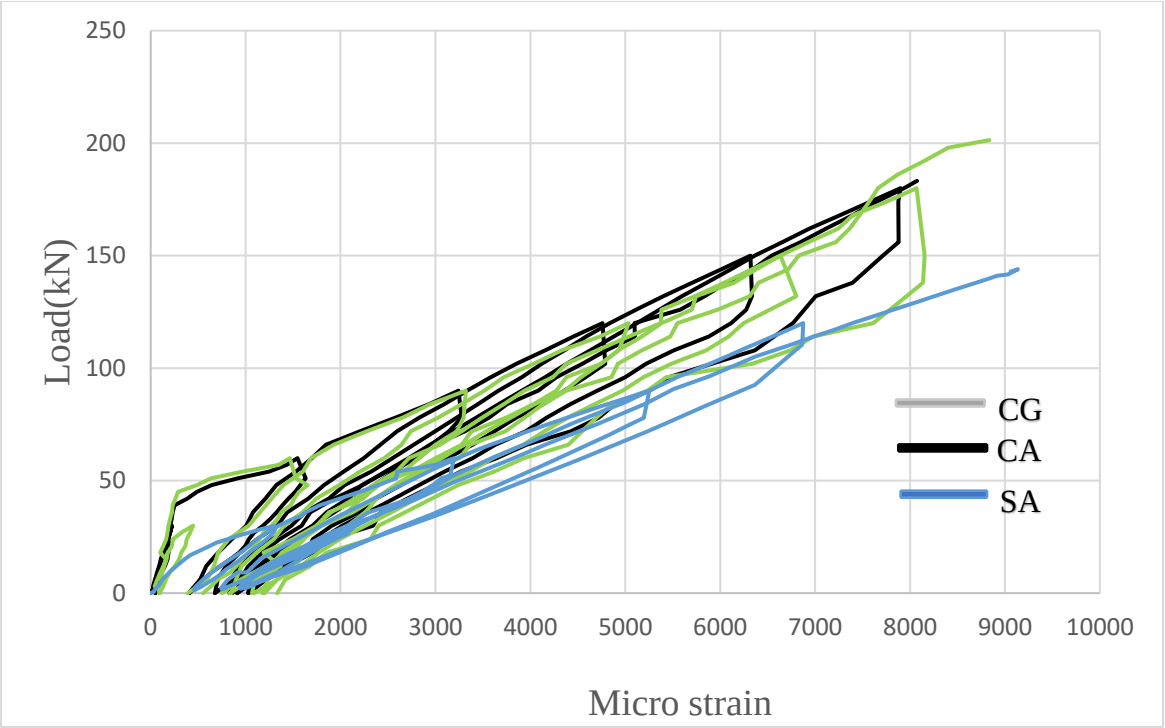

Fig.4.36 Comparison of GFRP Load vs Strain Plot for SA, CG and CA at Center

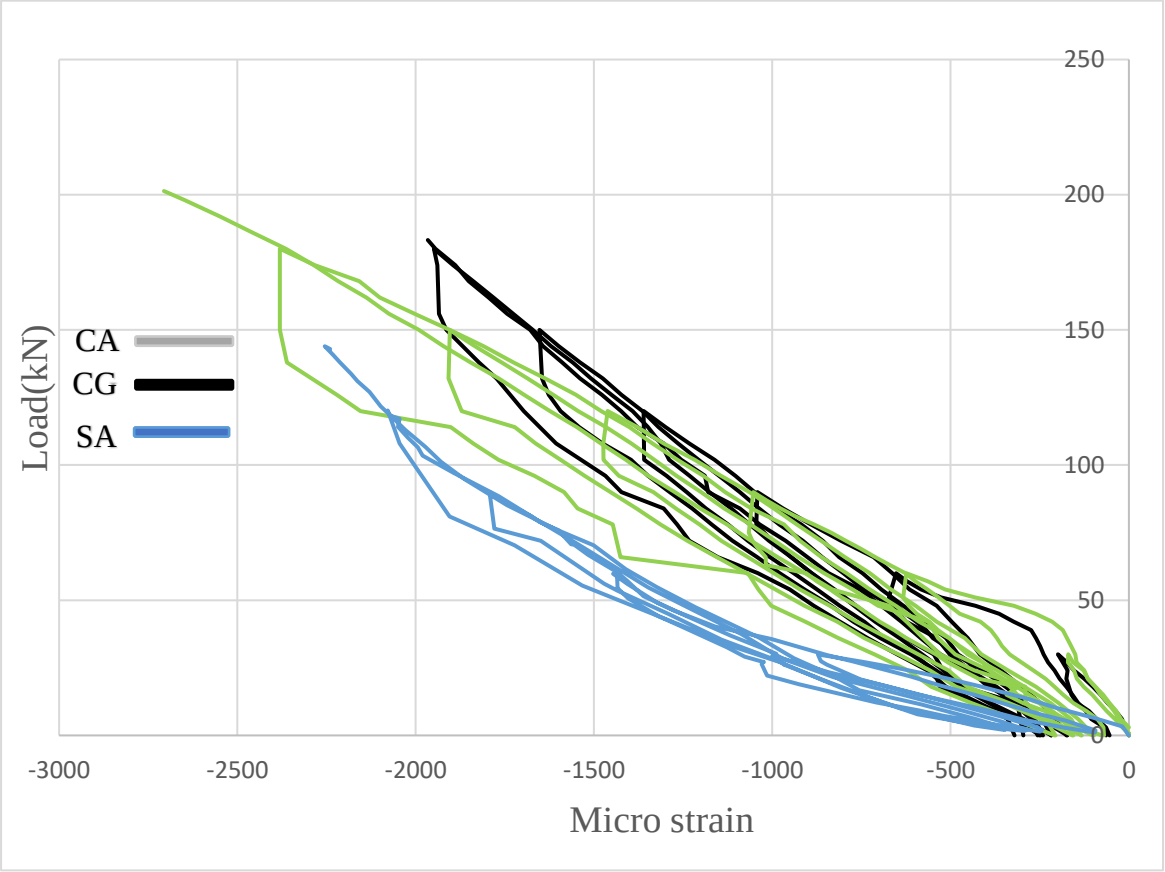

Fig.4.37 Comparison of Concrete Load vs Strain Plot for SA,CA and CG at Center

4.5 ACOUSTIC EMISSION TESTING

4.5.1 Straight Adhesive Bonded Slab (SA)

Cumulative AE Hits

With the increase in cyclic loading cycles on the SA slab, the development of micro and macro-cracking stages can be detected by the six AE sensors surface mounted on the slab. The crack development is related to the plot of recorded cumulative AE hits with time. Fig.4.38 shows the plot of cumulative AE hits with time for which the cyclic loading was applied.

From the plot, it is observed that during the 1st cycle of loading, recorded AE hits slowly increase with time pointing towards minor AE activity and possible initiation of micro- and interfacial cracking. As the loading cycle is increased to 2nd cycle, there is a sharp rise in the AE hits pointing towards joining of micro-cracks to form hairline cracks appearing on the surface of the slab which can be confirmed from visual inspection also Fig.4.39. 3rd cycle of loading represents a 'Calm Phase' where no significant rise in AE activity is observed. But at the end of cycle 3 or the beginning of cycle 4, a sound of delamination and breaking of interfacial bond was noticed which was well established by sudden rise in the AE hits showing sudden debonding and macro-crack formation by coalescing of micro-cracks observed in the 2nd cycle. There is noticeable increase in AE hits recorded in 4th cycle due to progressive delamination and debonding at concrete GFRP interface as shown in Fig.4.40. After 4th cycle AE sensors were removed to ensure their safety as more progressive and sudden delamination and cracking was anticipated.

Cumulative Signal Strength

AE hits is well supported by the plot of Cumulative Signal Strength (CSS) with time in Fig.4.41 which is almost similar to plot of cumulative AE hits with time. 1st peak is observed at the beginning of 1st cycle indicating the initial AE activity due to initiation of micro-cracking in concrete. Micro cracks join to produce huge AE activity in the 2nd cycle shown by 2nd peak at the start of cycle 2. It indicates growing of the micro-cracks to release energy and hence a jump in CSS value. In the 3rd cycle, a calm is observed with no significant AE activity and no CSS value jump or peak was observed as in AE hits record. In the cycle 4, a sudden jump in CSS peak is observed as in AE hits pointing towards macro-cracking and sudden release of huge amount of energy which is well verified by sudden debonding failure of the slab.

AE Event plots

Fig.4.42(b) and Fig.4.43(b) shows AE events with time at two stages of loading (2nd cycle and 4th cycle). It shows the development of AE events at two identified critical stages of loading where a huge and significant AE activity as well as visual changes were observed in the samples as shown in Fig.4.42(a) and Fig.4.43(a). At both the stages, the AE event plot matches with the visual state and location of cracking in the actual slab samples.

AE events accumulated at exact location where the cracks have been produced and ultimately failure took place. AE event plot gives an exact pictorial plot of inside crack development and events which can go a long way in real time monitoring of such slabs.

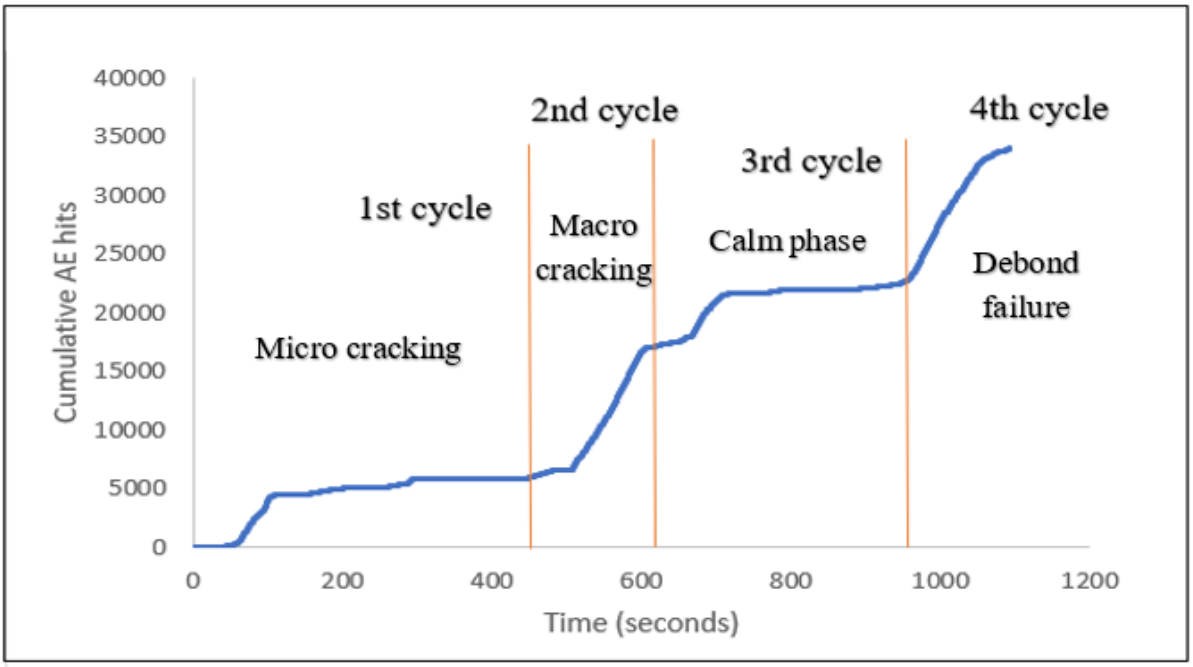

Fig4.38 Cumulative Hits vs Time for SA

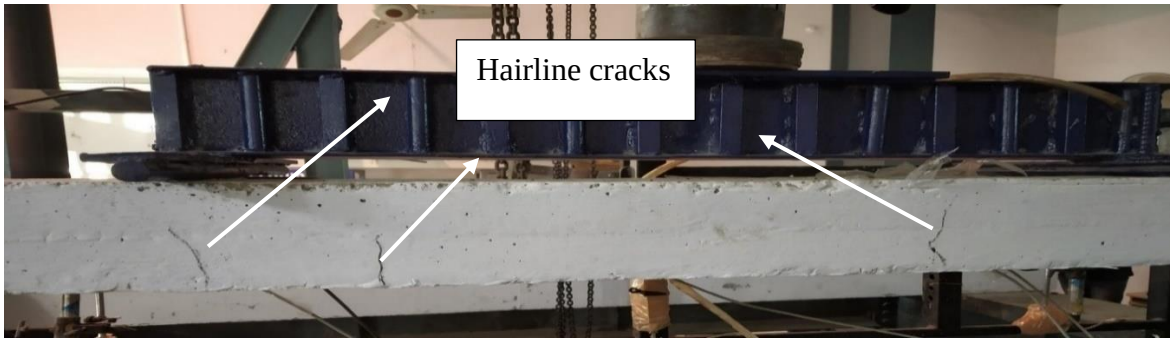

Fig.4.39 Cracks Appeared after 2nd Cycle for Specimen SA

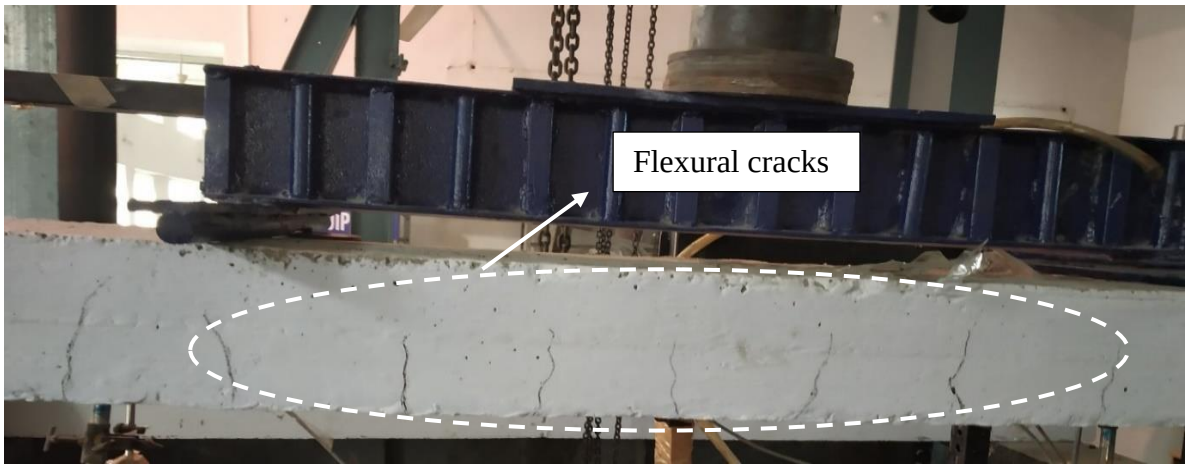

Fig.4.40 Cracks Appeared after 4th Cycle for Specimen SA

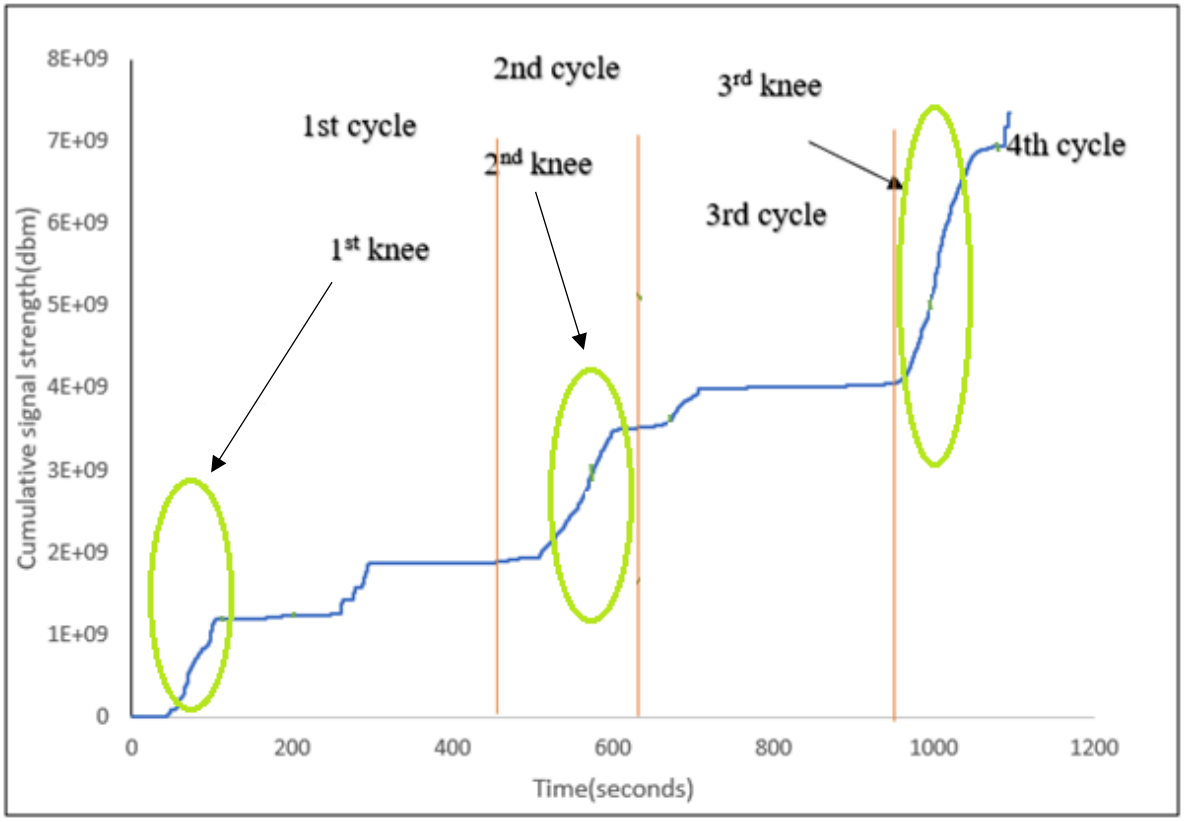

Fig.4.41 Cumulative Signal Strength vs Time for SA

Fig.4.42 (a) Actual cracking at 2nd cycle (SA)

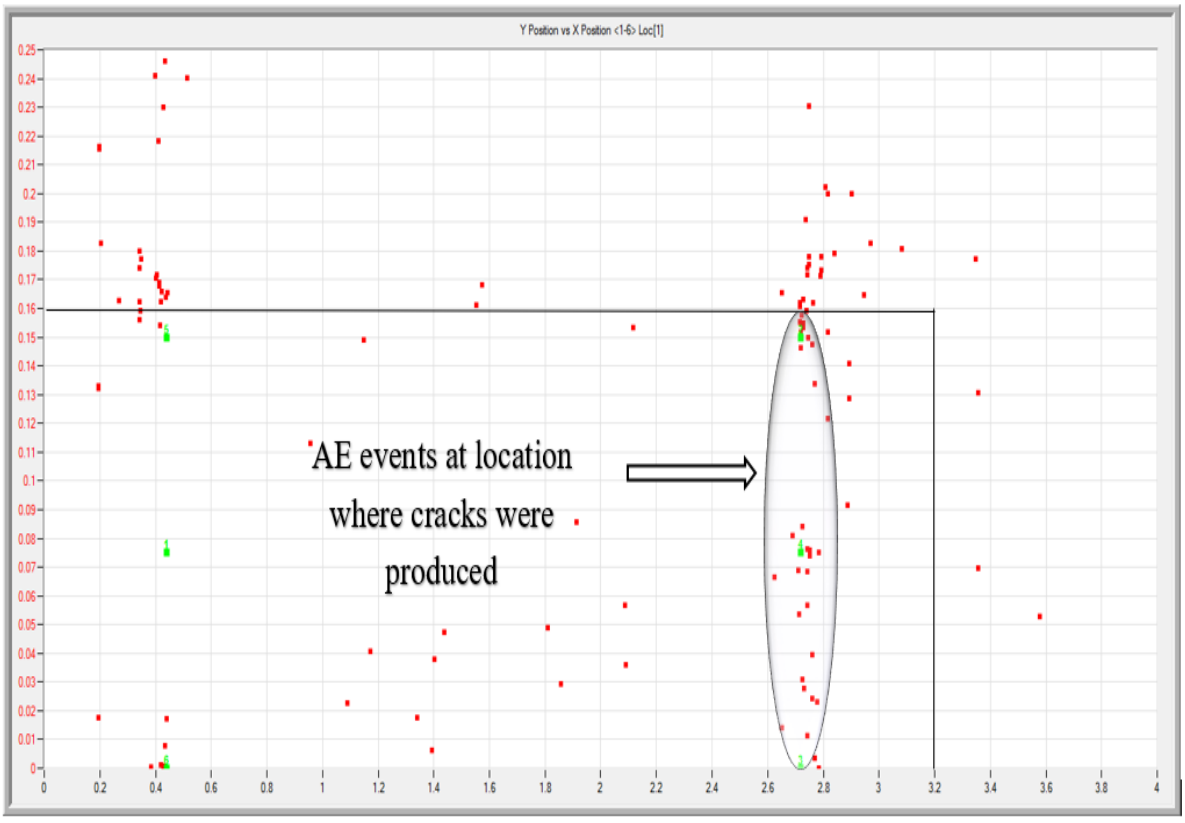

Fig.4.42 (b)AE Events at 2nd Cycle (SA)

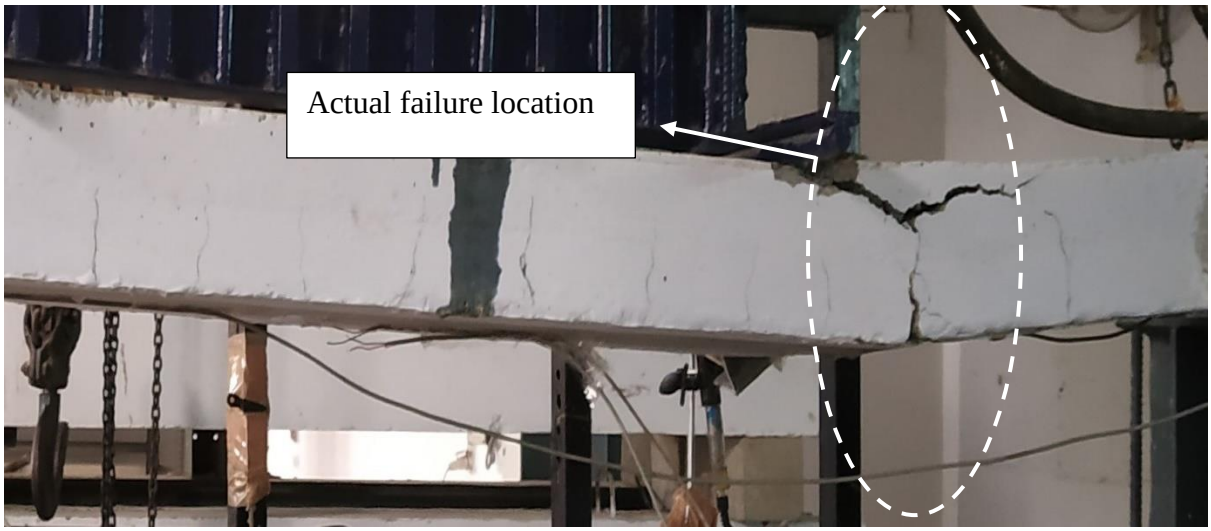

Fig.4.43(a) Actual cracking at Failure (SA)

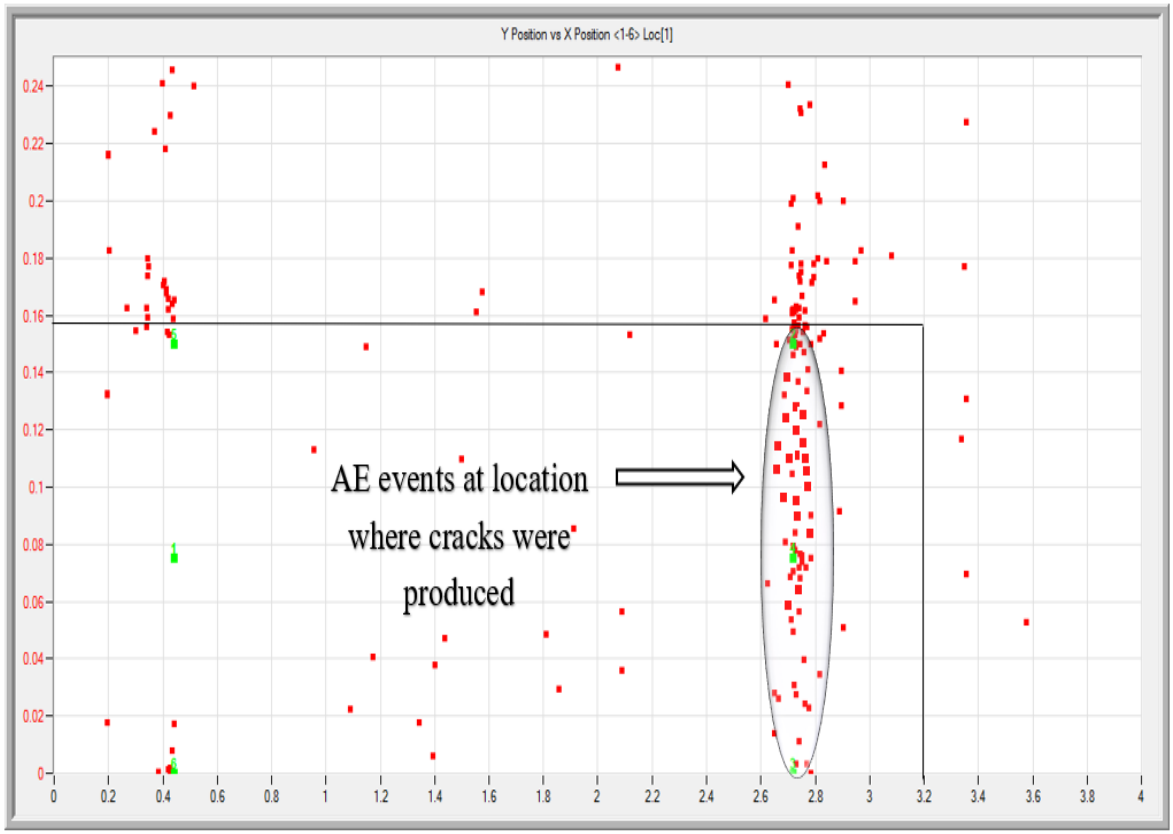

Fig.4.43(b) AE Events at 4th Cycle (SA)

4.5.2 Curved Aggregate Bonded Slab (CG)

Cumulative AE Hits

In order to detect micro cracks and macro cracks in the slabs when it is under cyclic loading test six AE sensors were mounted on the slab. As the cracks are initiated AE hits are produced with the increase in cyclic loading. The plot of cumulative hits vs time is shown in Fig.4.44. From the plot, it is observed that no cracks initiated during the 1st loading cycle since there was no activity recorded.

With the passage of time there is a rise in AE hits recorded which points out the initiation of micro-cracking in the slab during 2nd cycle. With the increase in loading to 3rd cycle there is a sharp rise recorded in AE hits indicating towards the joining of micro cracks and finally combining to form hairline cracks which appeared over the surface of the slab which can be confirmed from visual inspection also Fig.4.45. After 3rd cycle there is no rise in recorded AE hits which shows a calm phase that can be clearly observed in 4th cycle of loading. 5th and 6th cycle of loading shows a large increase in AE hits recorded which confirms the fusion of micro cracks into the formation of macro cracks as there was large sound of delamination and breaking of interfacial bond was noticed as shown in Fig.4.46. There is large amount of increase in AE hits recorded in 6th cycle due to progressive delamination and debonding at concrete GFRP interface which further leads to its failure.

From the comparison of plot with SA slabs the AE activity is observed for a larger duration and AE hits are also larger in number in comparison to SA. This points towards the flexibility and better performance of CG slabs in comparison to SA slab.

Cumulative Signal Strength

Cumulative AE hits is in well agreement with the plot of Cumulative Signal Strength (CSS) with time as shown in Fig.4.47 having very much similar plots. At the end of 2nd cycle, 1st knee is observed which points towards the initiation of the micro cracks in concrete. At the end of the 3rd cycle, 2nd knee is observed which shows some AE activity as there is energy released by the growing of the micro cracks which also shows the jump in CSS graph. Both CSS and cumulative hits plots shows calm phase in the 4th cycle, since there is no CSS value jump or peak and no significant AE activity was observed. 3rd and 4th knee is observed during the 5th and 6th cycle and shows a sudden rise in CSS value pointing towards macro-cracking and sudden release of huge amount of energy which is visually verified by sudden debonding failure of the slab.

AE Event plots

AE events very well verifies the visual changes that are observed in the slab specimen at 3rd stage and at final stage of loading as shown in Fig 4.48(b) and Fig.4.49(b). the points where the actual cracks appeared in the slab (Fig.4.48(a) and Fig.4.49(a)) shows the huge AE activity which is shown in AE events plot at different stages of loading. At both the stages, where the cracks started to appear on the surface of the slab and when the failure took place the AE event plot matches with the visual state.

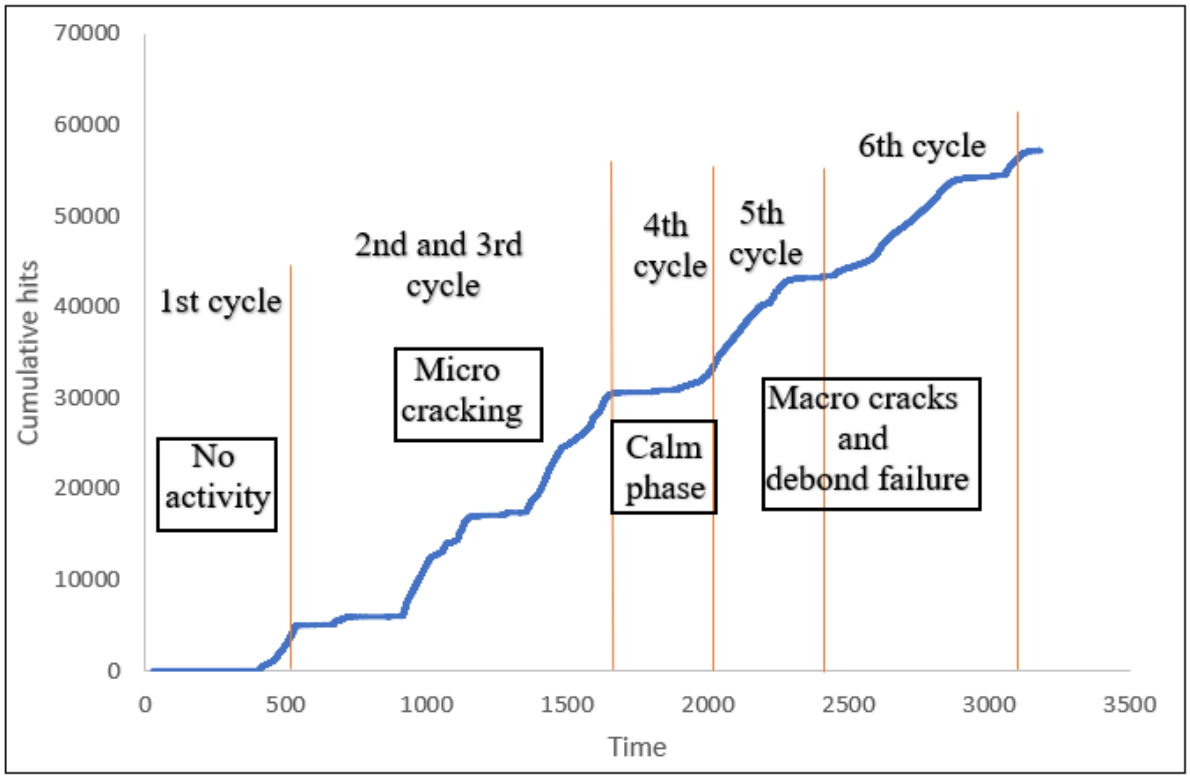

Fig.4.44 Cumulative Hits vs Time for Specimen CG

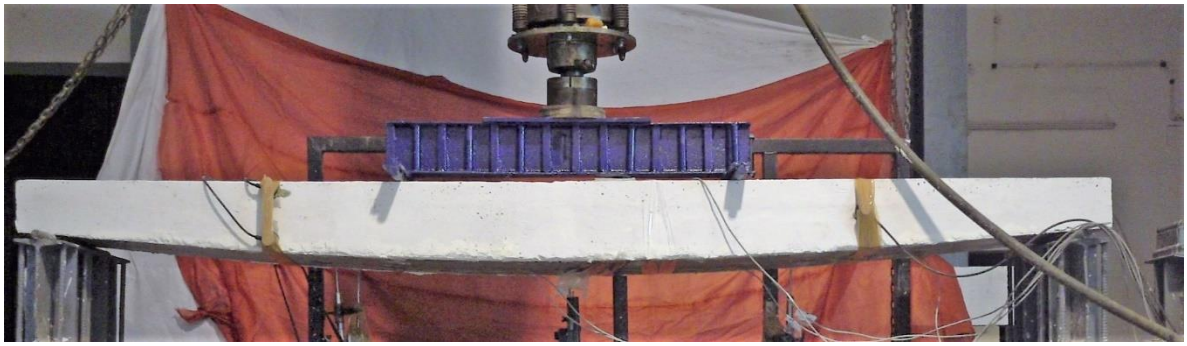

Fig.4.45 Hairline Cracks on the Surface of CG Slab after 3rd Cycle

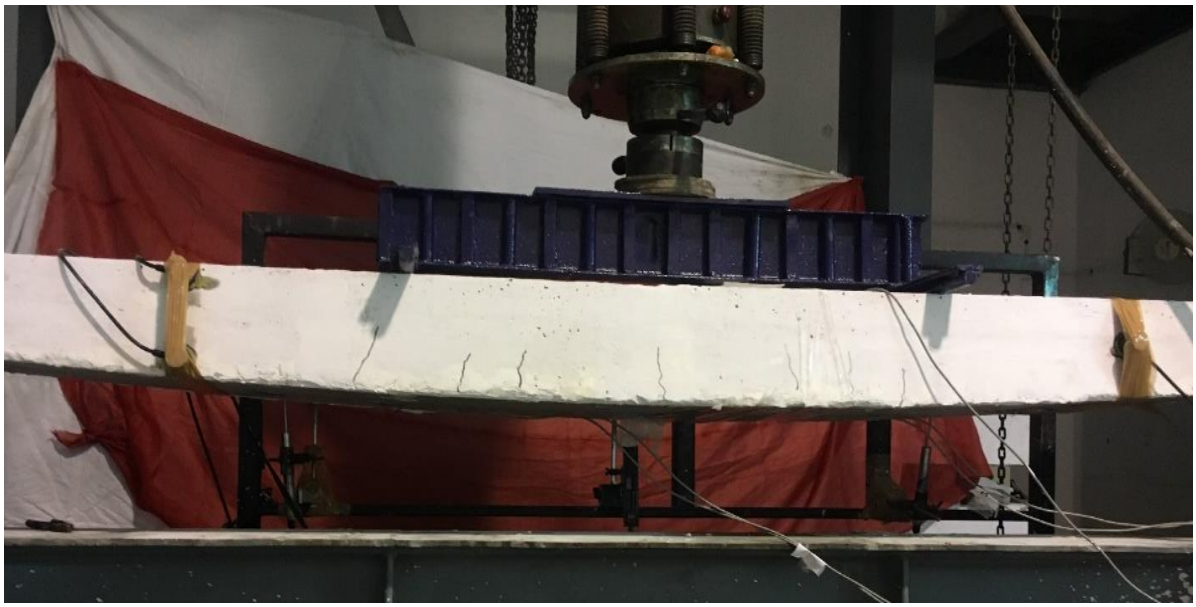

Fig.4.46 Cracks Appeared on the Surface of CG Slab after 6th Cycle

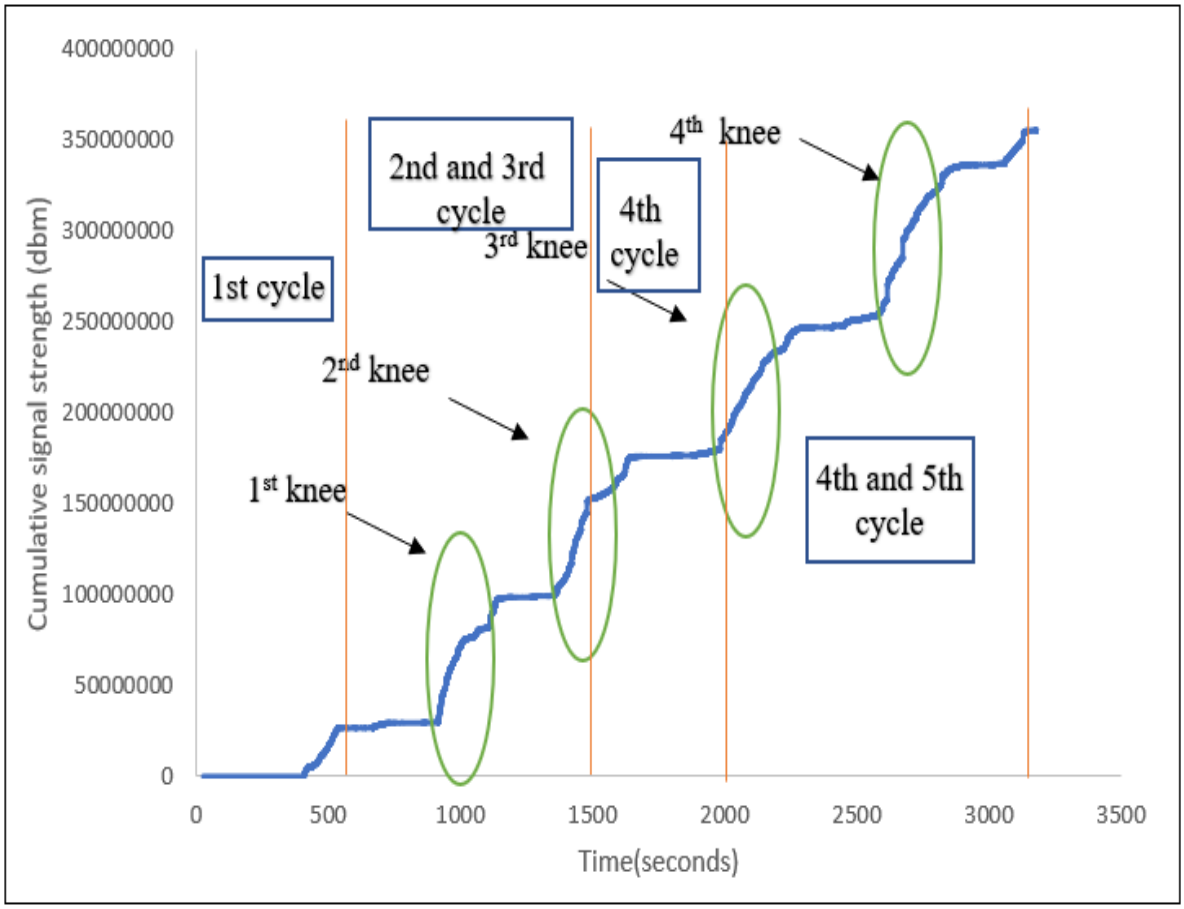

Fig.4.47 Cumulative Signal Strength vs Time for CG

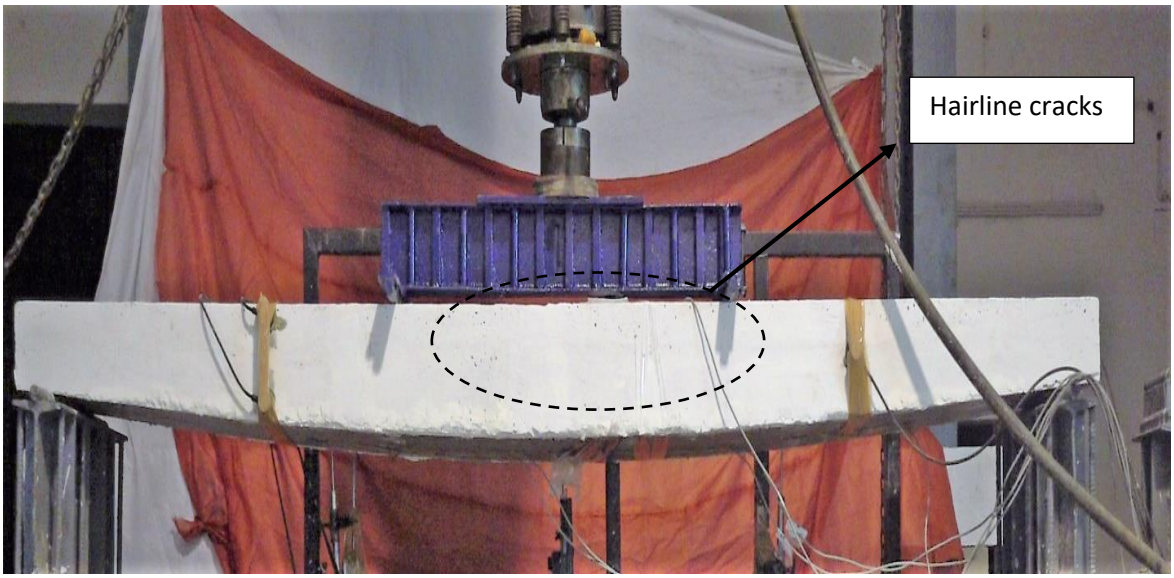

Fig.4.48(a) Hairline Cracks Appeared on the Surface of CG Slab after 3rd Cycle

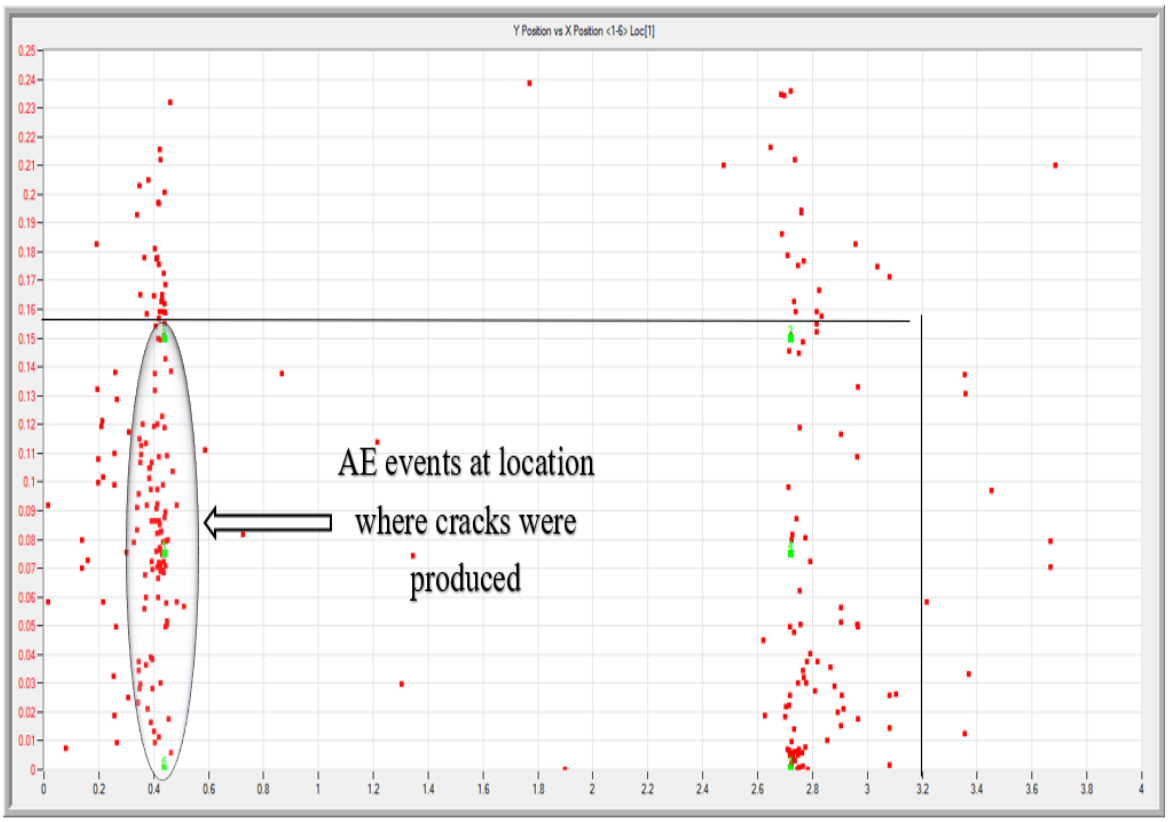

Fig.4.48(b) AE Events at 3rd Cycle for CG

Fig.4.49(a) Actual Cracked Specimen at Failure

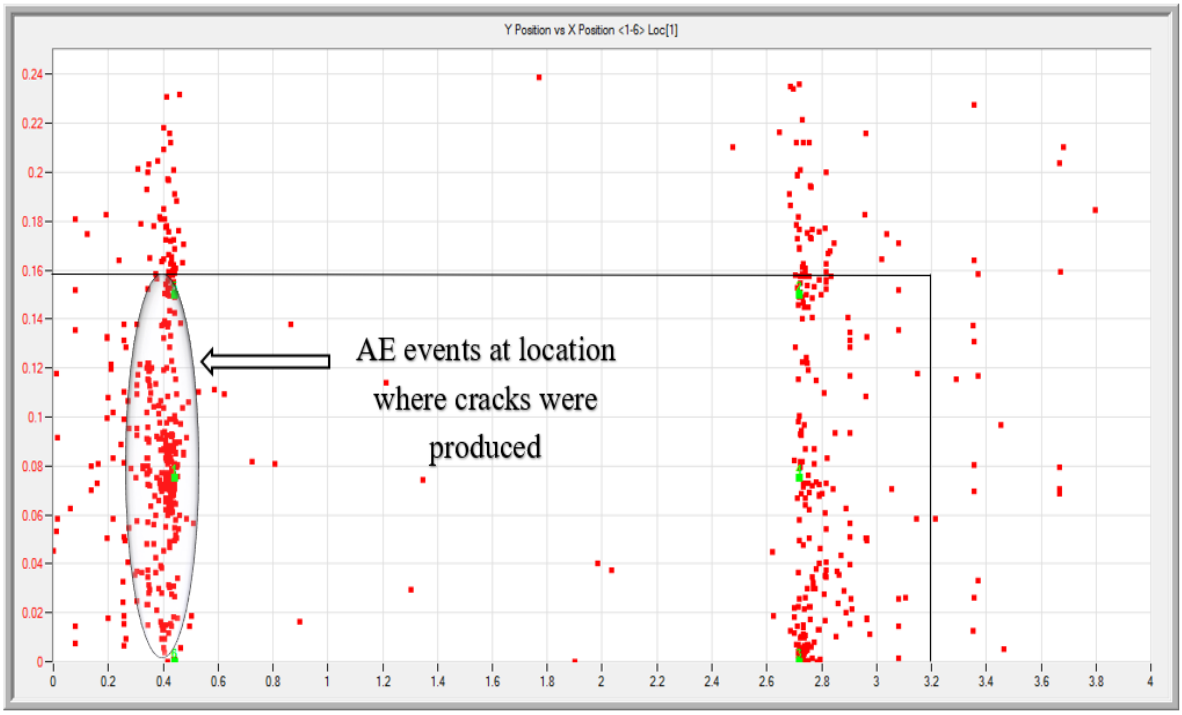

Fig.4.49(b) AE Events at Failure

4.5.3 Curved Adhesive Bonded Slab (CA)

Cumulative AE Hits

Plot of cumulative AE hits with time is shown in Fig.4.50 which depicts the development of micro and macro-cracking stages corresponding to increasing load cycle. From

the plot, it is observed that there is a very small increase in AE hits recorded during the 1st cycle of loading indicating towards minor AE activity and very less possibility of initiation of micro-cracks and interfacial cracking. As the loading cycle is increased, there is a sharp rise in the AE hits during the 2nd cycle which indicated the formation of hairline cracks by joining of the micro cracks, appearing on the surface of the slab which can be confirmed from visual inspection also as shown in Fig.4.51. In 3rd cycle of loading no significant rise in AE activity is observed therefore it is represented as 'Calm Phase'. But at the end of cycle 3or the start of the 4th cycle, there is sudden rise in the AE hits indicating sudden debonding and macro-crack formation by coalescing of micro-cracks observed in the 2nd cycle as shown in Fig.4.52 also a loud sound of delamination and breaking of interfacial bond was noticed. There is noticeable increase in AE hits recorded in 4th cycle due to progressive delamination and debonding at concrete GFRP interface due to which after the 4th cycle AE sensors were removed.

Cumulative Signal Strength

Plot of Cumulative Signal Strength (CSS) with time is shown in Fig.4.53 which is almost similar to plot of cumulative AE hits with time. 1st peak is observed at the beginning of 1st cycle indicating the initial AE activity due to beginning of micro-cracking in concrete. During 2nd cycle the 2nd peak is observed which indicates that micro cracks joins to produce huge AE activity that releases energy and therefore a jump in CSS value is observed. In the 3rd cycle, a calm is observed with no significant AE activity and no CSS value jump or peak was observed as in AE hits record. In the cycle 4, a sudden jump in CSS peak is observed as in AE hits pointing towards macro-cracking and sudden release of huge amount of energy which is well verified by sudden debonding failure of the slab.

AE Event plots

Fig4.54(b) and Fig.4.55(b) shows AE events with time at 2nd cycle and at 4th cycle. It is observed that at these two cycles of loading there is a huge change in AE activity as well as visual changes in slab is observed as shown in Fig.4.54(a) and Fig.4.55(a). The AE event plot can be correlated with the visual state and location of cracking in the actual slab samples for both loading cycles. AE events accumulated at exact location where the cracks have been produced and ultimately failure took place.

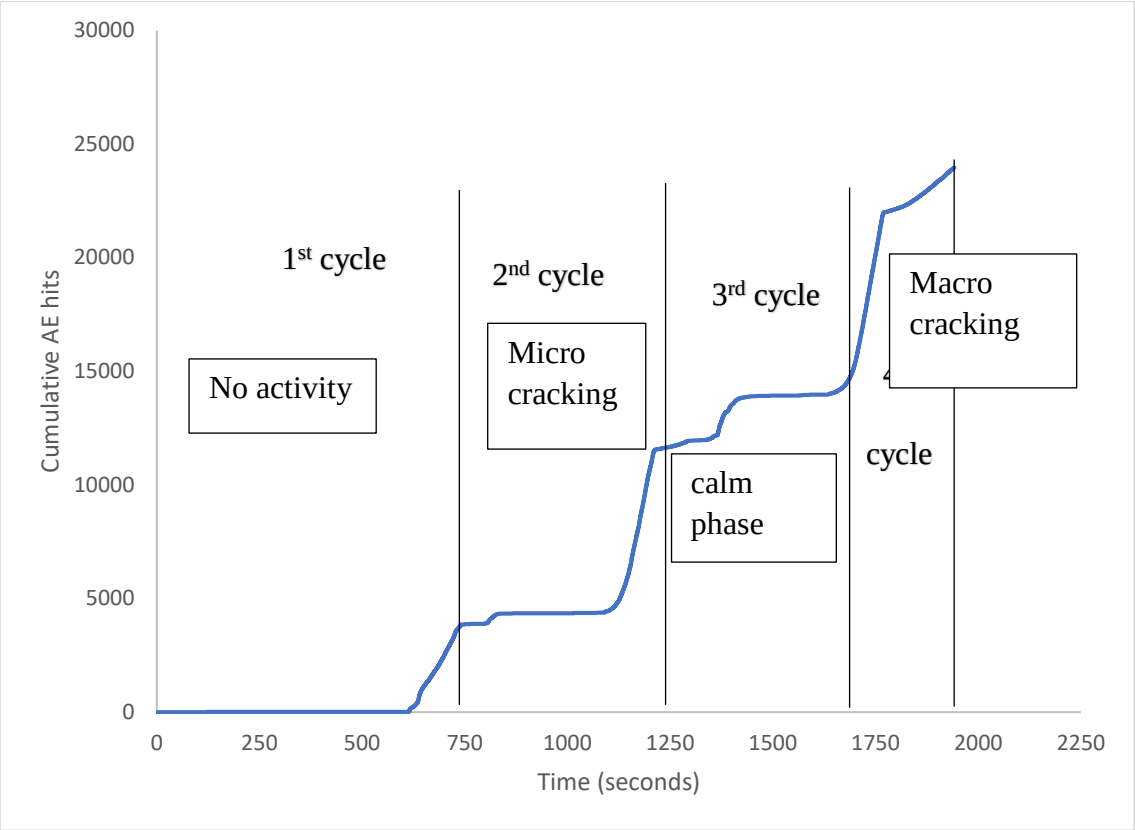

Fig.4.50 Cumulative Hits vs Time for CA

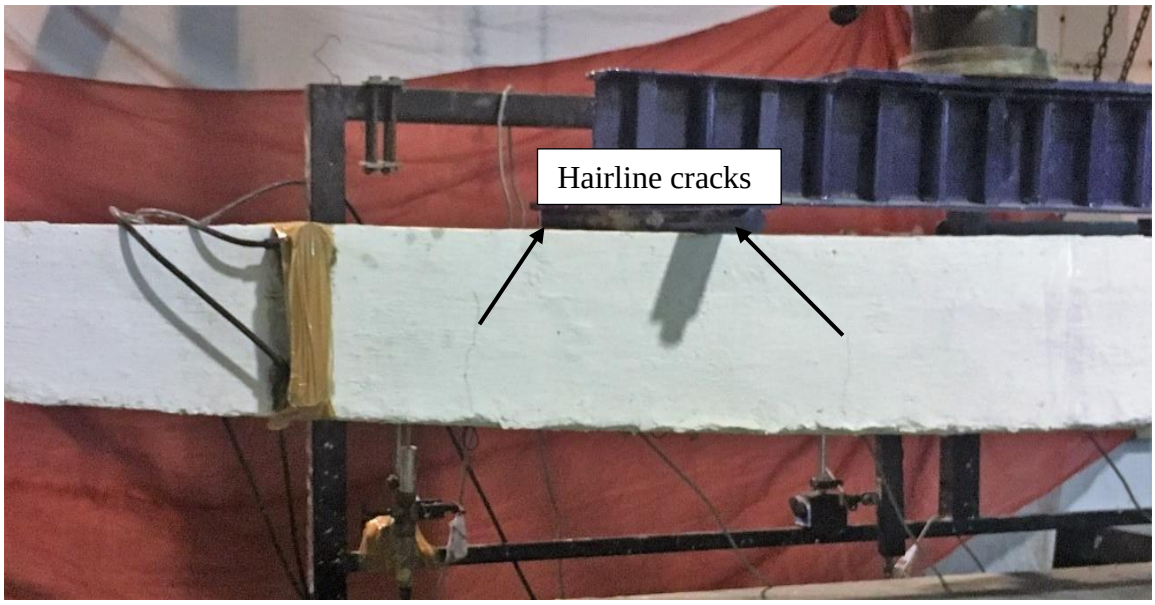

Fig.4.51 Hairline Cracks Appeared after the End of 2nd Cycle for CA

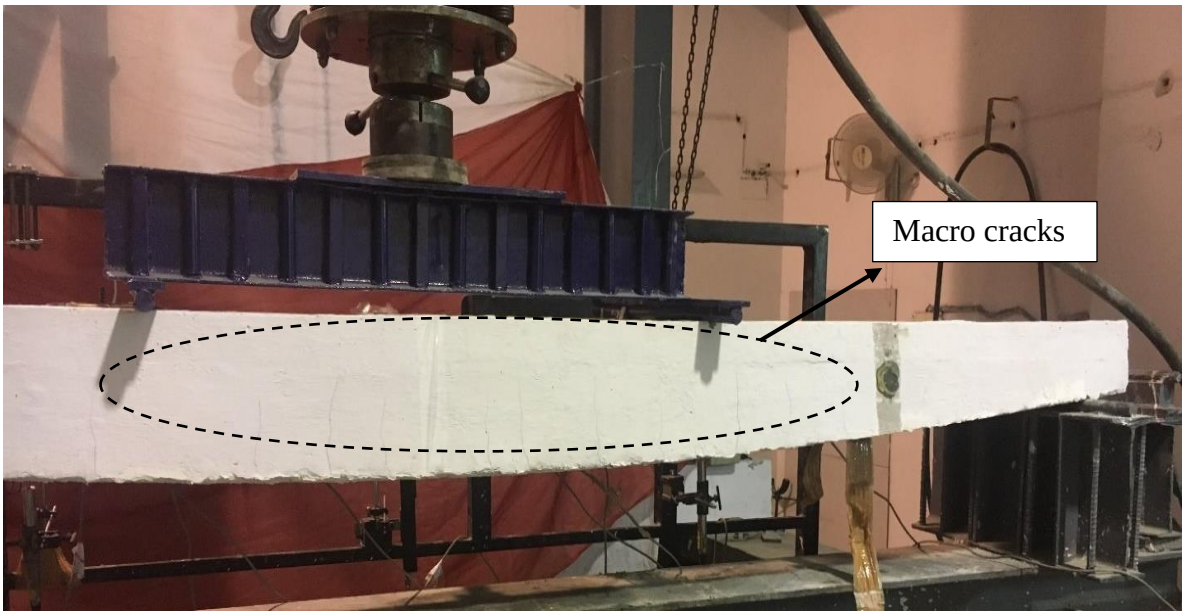

Fig.4.52 Cracks Appeared on the Surface of CA Slab

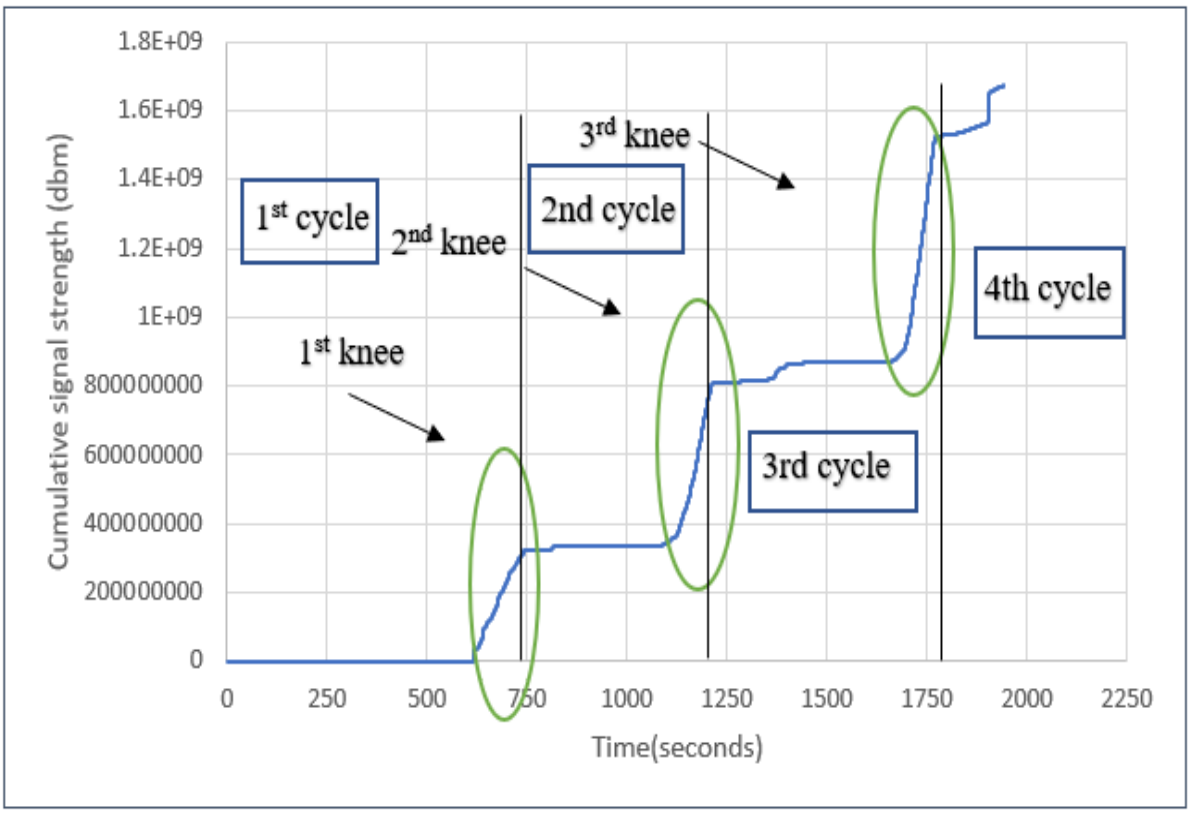

Fig.4.53 Cumulative Signal Strength vs Time for CA

Fig.4.54 (a) Hairline Cracks Appeared on the Surface of CA Slab at the End of 2nd Cycle

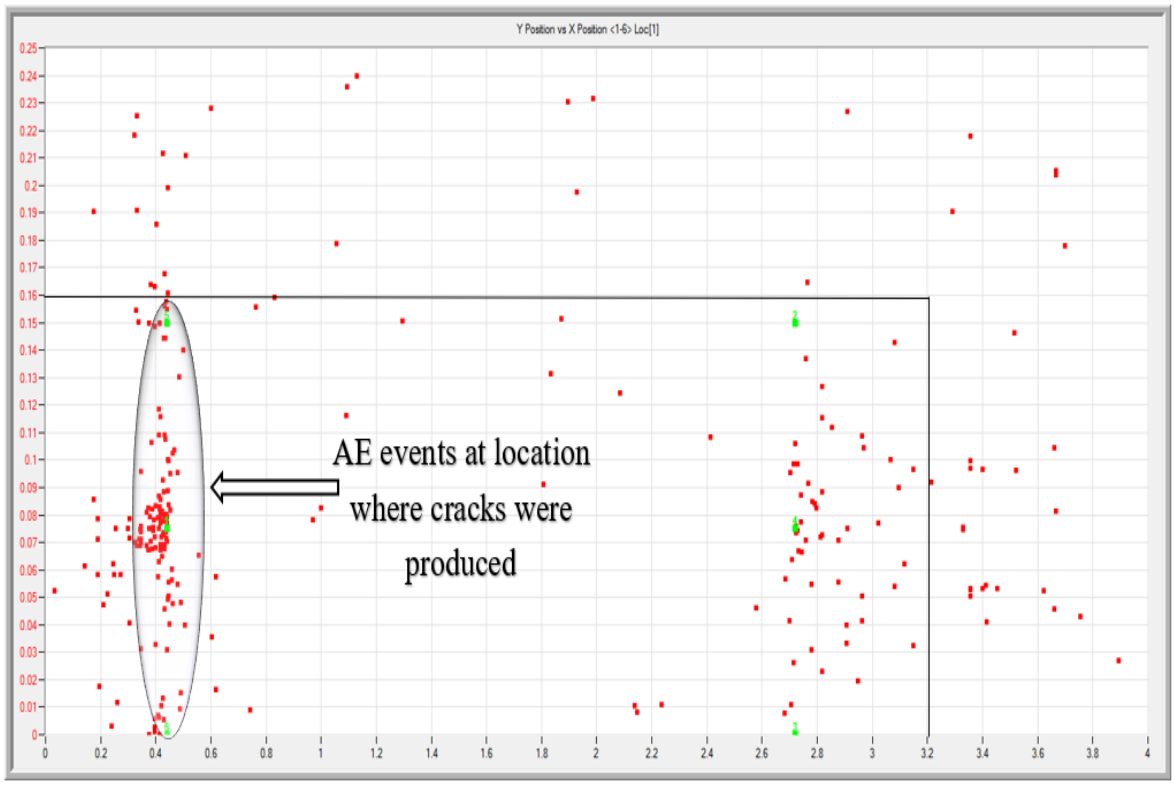

Fig.4.54 (b) AE Events at 2nd Cycle for Specimen CA

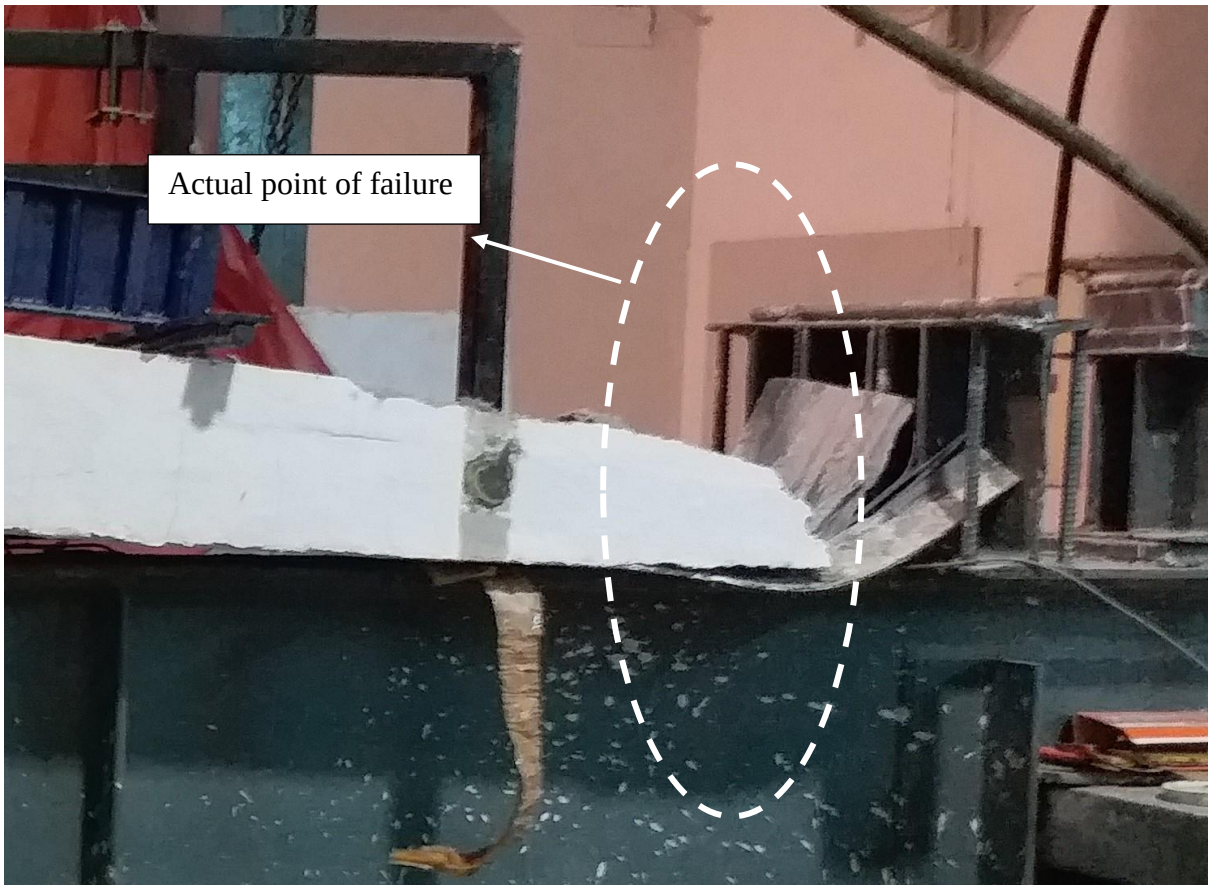

Fig.4.55 (a) Actual Cracked Specimen at Failure

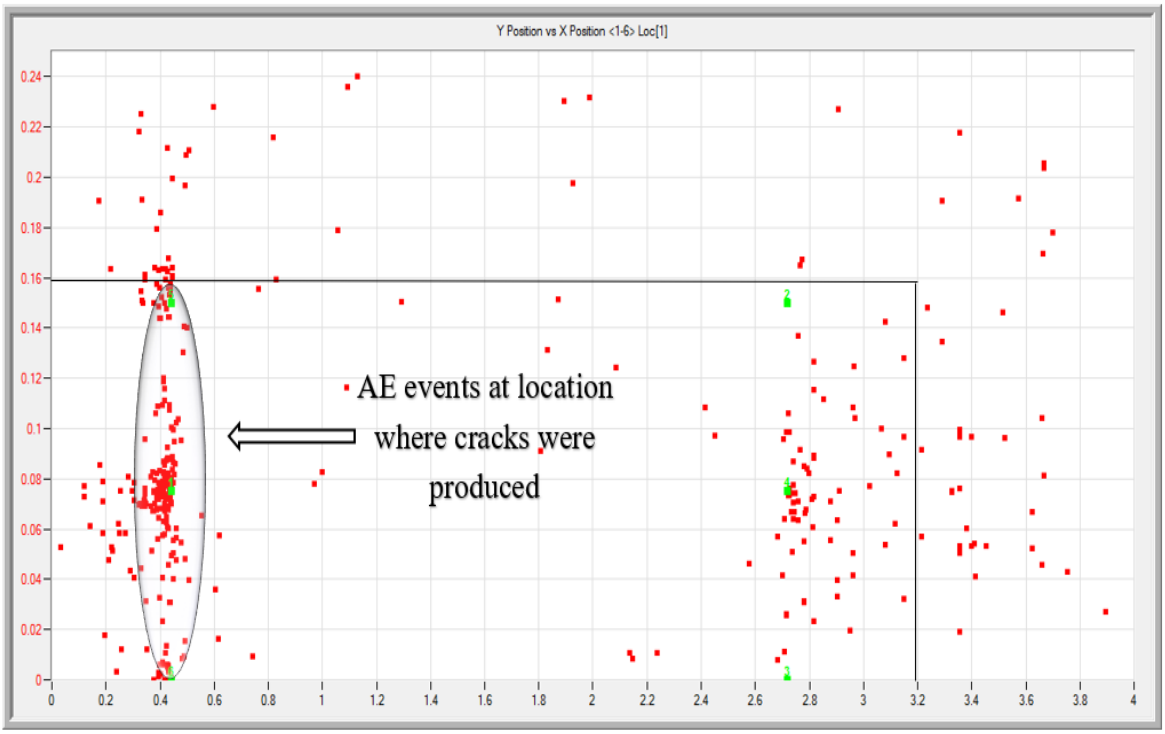

Fig.4.55 (b) AE Events at 4th Cycle for Specimen CA

4.6 ENERGY DISSIPATION CURVES

All the slab specimens (SA, CG an CA) were subjected to two-point cyclic loading flexural test. Continuous observation was carried out all through the test in order to check for crack initiation and propagation. For the slabs the loading cycle was applied with accretion of 30kN. For each slab, in order to calculate the energy absorption capacity under every loading cycle it is required to calculate the area under the load deflection curve for that loading cycle. In order to check the seismic properties of the structure it is important to calculate the energy dissipated by the structure as it act as an indicating factor. Structure with adequate amount of energy dissipated represents its ability to resist earthquake forces. Fig.4.62 shows the variation of relative energy absorption capacity with respect number of cycles for the 3 slab specimens. In order to obtain the cumulative energy dissipation capacity of slab specimen, energy absorption capacity during each loading cycle was added. Specimen which shows more energy dissipation performs in a better manner under seismic loads. Fig.4.63 represents the variation of cumulative energy absorption capacity with respect to number of cycle for all slab specimens. It was observed that energy dissipation for all the specimen was almost same but at later stage it was found out that adhesive coated specimen(CA) shows a little bit higher energy as compared to aggregate bonding specimen(CG).

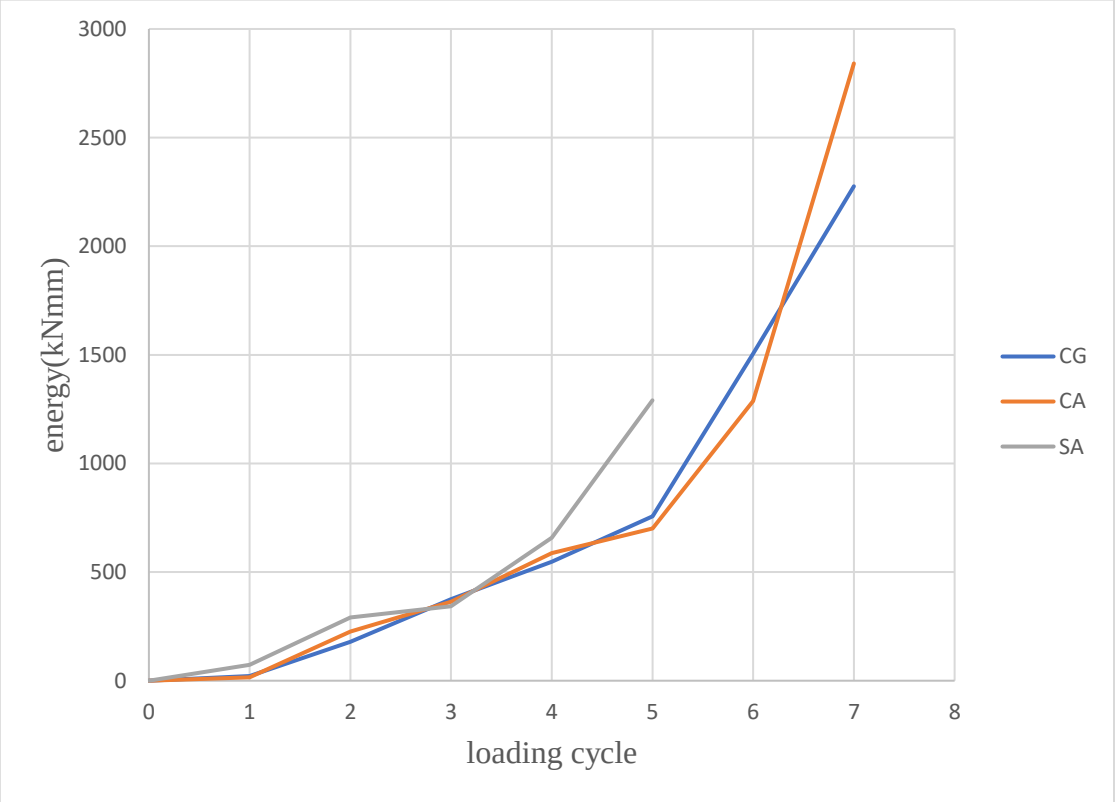

Fig.4.56 Comparison of Energy vs Loading Cycle of Specimen SA, CG and CA

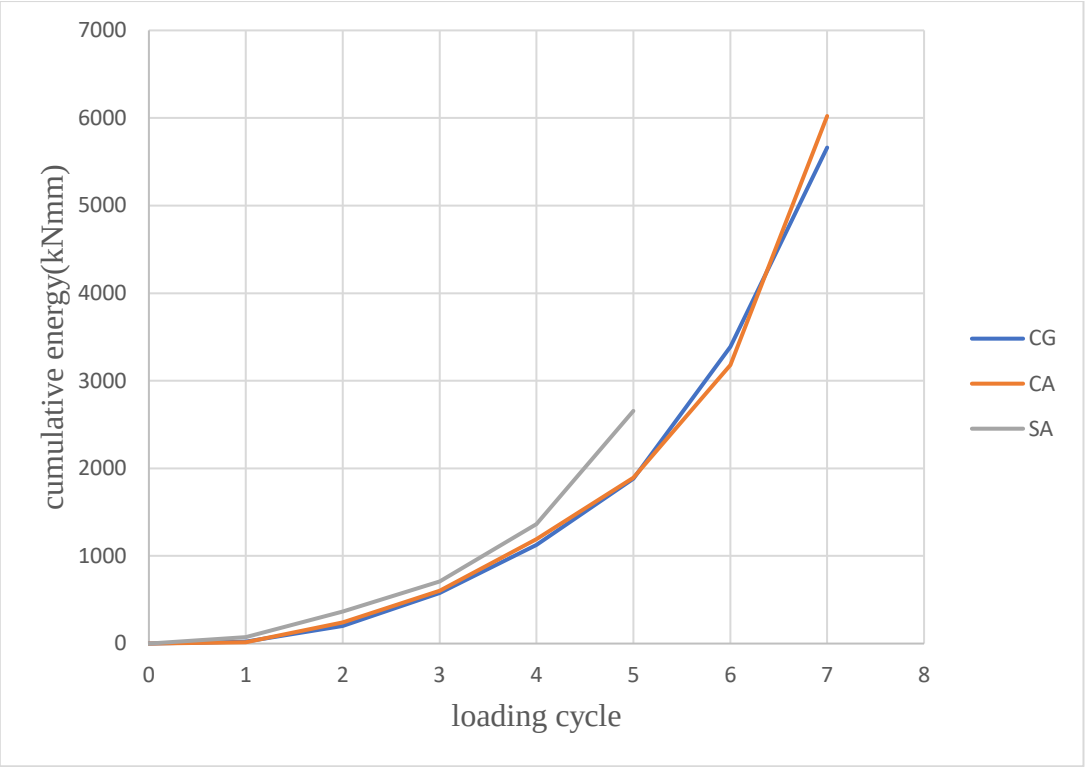

Fig.4.57 Comparison of Cumulative Energy vs Loading Cycle of Specimen SA, CG and CA

Table 4.1 Specimen Summary and Ultimate Load

Specimen	Initial cracking (kN)	Failure load (kN)	Maximum deflection(mm)	Failure mode
SA	42	144	58	Shear failure
CG	96	183.24	44	Shear failure
CA	114	201.36	48	Shear failure

CHAPTER 5

FINITE ELEMENT SIMULATION

5.1 GENERAL

A non-linear FEM program was used to validate experimental data numerically. In order to stimulate the performance of bond treated composite concrete-GFRP interface and also the flexible behaviour of the plank during casting stage, ATENA software was used in which a 3D finite element model was prepared.

5.2 FEM MODEL

A 3-D finite element model was prepared using ATENA software to simulate the behaviour of GFRP plank as formwork and as reinforcement. Both casting stage and flexural testing experiments were modelled to verify the results. The modelling details and the results obtained are present in this section

5.2.1 MATERIALS AND GEOMETRICAL MODELLING

Various material properties that were used for FEM analysis are mention in Table 5.1.

Table 5.1: Material Properties for FEM Analysis

Material	Material model in Atena	Important properties
Concrete	Non Linear Cementious 2	F_{ck}=50 MPa F_t=3.5 MPa
Epoxy	3D elastic isotropic	E=3.5 GPa
Glass fibre	Reinforcement	E=72 GPa
Steel	3D elastic isotropic	E=200 GPa
Bond treated FRP-concrete Interface	3 D interface	K_{nn} =3×10^5 MN/m^3 K_{tt} =10^5 MN/m^3 f_t=15 MPa

Shell macro elements were used in order to model GFRP form with 20 nodes quadratic 3D brick elements, especially for plate type structures modelling, in which thickness of one dimension is comparatively small than the other two. It is assumed that in shell macro elements,

after deformation there is no change in the cross-section, it remains plane after deformation. It is in agreement with in-plane and bending stiffness. The FRP consists of two parts out of which one is reinforcement (glass fibres) and the other is adhesive (3D elastic isotropic material) in which reinforcement is embedded. In the model, for modelling base plate using shell element the basic material used was adhesive having 35% fibre reinforcement ratio and fibre reinforcement ratio of about 30% for modelling stiffeners. The shell element allows for different material layers with different constituents. Mesh size was taken to be 15 mm for the shell elements. To distribute the load evenly at the two ends of the model, steel plates were used.

Modelling the bond between the concrete and the GFRP formwork is the most critical component. In order to model the bond at concrete GFRP interface a 3D Interface element was used. There are three different type of contact available in ATENA software:

(1) perfect connection

(2) no connection

(3) contact element.

So as to model the interface, it was required to define a pair of surface which will be located on both side of the interface. As far as original geometry is concerned the same position can be shared by the two different surfaces or they can be separated by a quasi-zero distance.

5.2.2 FEM MODELLING OF PLANK FOR CASTING STAGE TEST

Modelling of the plank was done in order to simulate the results of the deflection that occurred during the casting stage of both aggregate and adhesive bonded slabs. Shell element was used to model FRP plank with mesh size of 30mm in ATENA software. Fig.5.1 shows model of plank in ATENA software. The load that was applied on plank during casting stage was also applied on plank model. Fig.5.2 shows the comparison of load deflection plot obtained from experimentation and FEM simulation. It shows that they all follow almost similar path when load is applied and the final deflection was almost similar in the two cases.

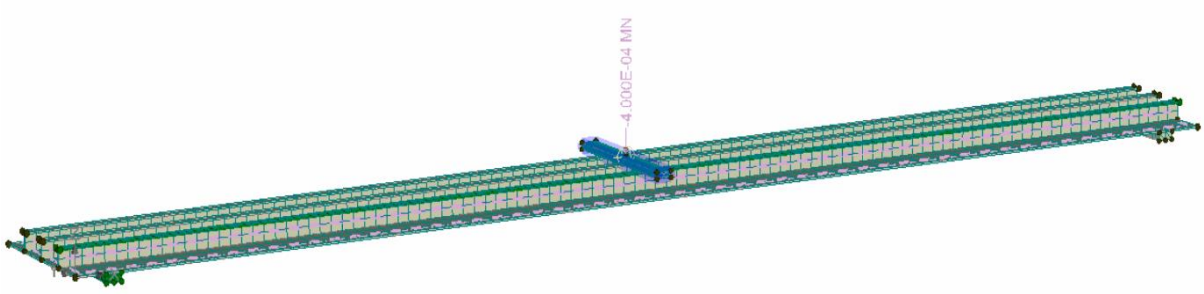

Fig.5.1 GFRP Plank Model

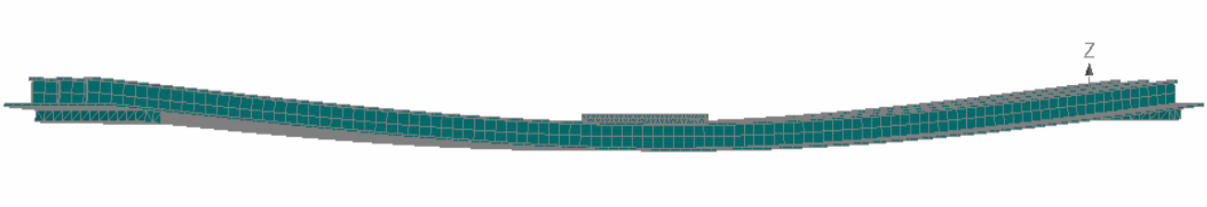

Fig.5.2 Deformed Shape of GFRP Plank Model

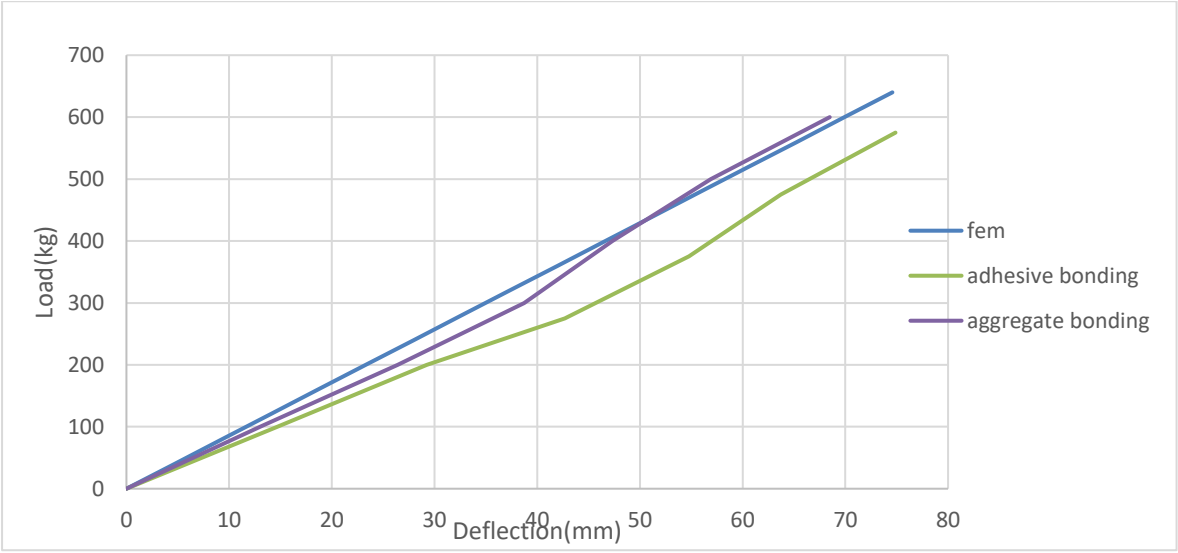

Fig.5.3 Comparison Between Experimental and FEM Results

5.3 FEM MODEL OF SLAB FOR FLEXURAL TESTS

Models and the comparison with experimental results are presented in the following sections. In ATENA software modelling of slab of span 3m with adhesive coating was done. Due to the symmetry of the structure in both the direction, modelling of only quarter section was done. Shell element was used to in modelling of with 100mm mesh size and to model concrete mesh

size of 20mm was used. Load was applied to slab with the help of steel prism. Load control mode of loading was adopted with each step increment of 4KN. Fig.5.3 shows FEM model for quarter section of 3m span beam.

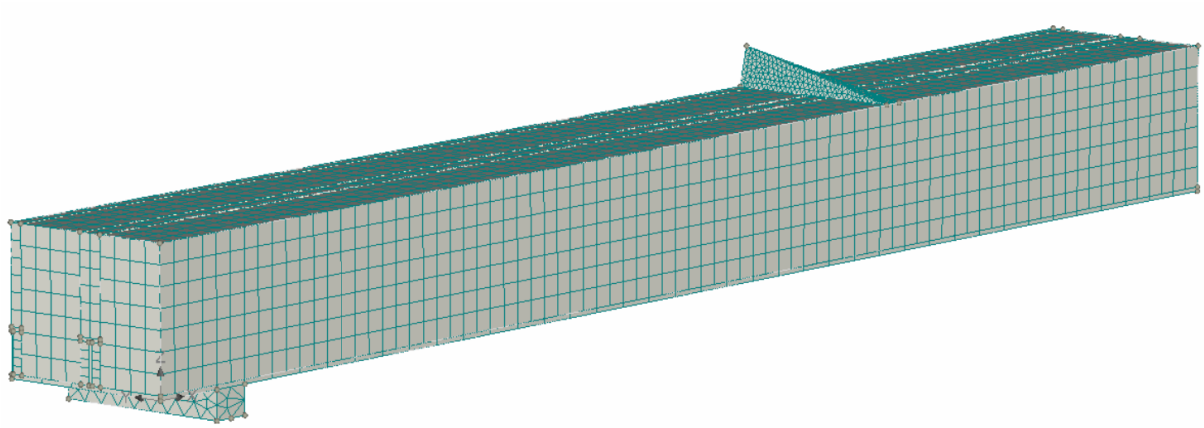

Fig.5.4 FEM Model for 3m Span Slab

Fig.5.4 shows comparison between load-deflection plot obtained from experimental and FEM simulations. It is evident that the FEM simulation closely agrees with the experimental curve. Fig.5.5 shows the failure mode obtained by FEM. In case of FEM model also, the failure occurred due to shear failure of concrete but there is slight difference in crack pattern of experimental test and FEM model. This difference is because of delamination of T sections during the experiment. The FEM simulation allows us to investigate the stresses inside the specimens and determine the cause of their failure. It was observed that flexure cracks start propagating at load 42 KN both experimentally and in FEM model. With increase in load further, number of flexural cracks increased and cracks propagated upward. This continued till 87 kN. With further increase in load no change in flexural crack pattern was observed both experimentally and in FEM model. Shear crack appeared at load around 120 kN and led to failure with failure mode as concrete shear failure along with debonding. In FEM model failure load (152 KN) is 10% more than that of experimental load. This difference is because of the delamination of the T sections from the base plate in the experimental work which led to early concrete shear failure. As in FEM model, cyclic loading is not provided, this resulted in lower stiffness in FEM model.

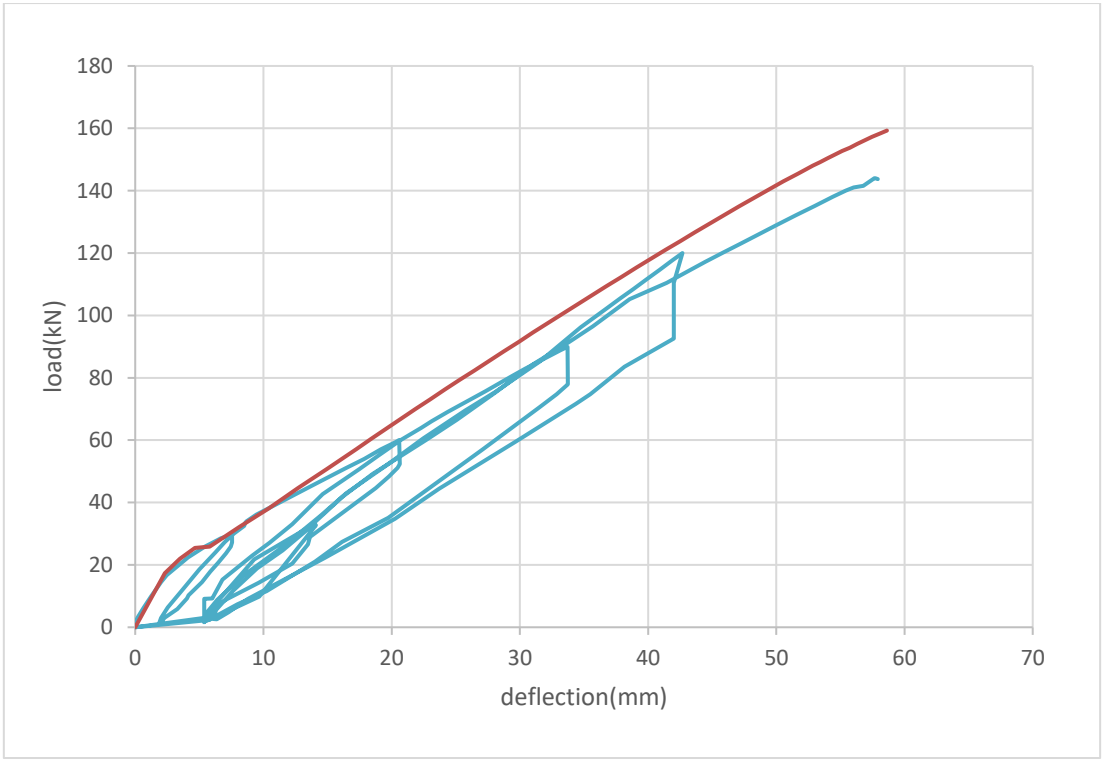

Fig.5.5 Comparison Between Experimental and FEM Results for 3m Span slab

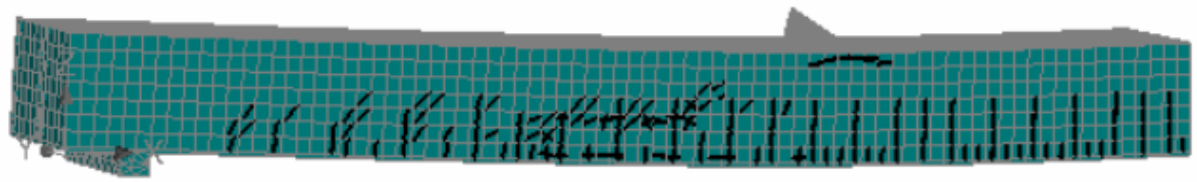

Fig.5.6 Crack Pattern for 3m Span Slab

CHAPTER 6

CONCLUSION

6.1 GENERAL

In this study pultruded GFRP planks were tested for their role as flexible SIP formwork for curved slabs. GFRP planks were tested for their performance as formwork for curved slabs through sand loading and wet concrete loading tests. Flexural performance of hybrid GPRP-concrete slabs was investigated using cyclic two point loading test with load cycle of 30kN.Comparison was made between flexural performance of curved slabs and straight slab. For achieving composite behavior between GFRP plank and cast-in-place concrete, two different bond techniques-adhesive bonding and aggregate bonding were investigated. Acoustic emission technique was also used for crack initiation and development in the casted specimen. FEM model using ATENA software was prepared for plank as formwork and as reinforcement.

6.2 CONCLUSIONS

From sand loading and concrete loading tests it was demonstrated that GFRP plank has desirable strength and stiffness to bear concrete loading as curved slab. Curved concrete slabs were cast with span of 3m with no intermediate supports for curved slabs and two intermediate supports for straight slabs. In case of straight slabs negligible deflection of 1.2mm was obtained and in case of curved slabs considerable deflection of 75mm (aesthetic point was obtained). Thus, loading tests it is evident that the selected GFRP plank can be used as SIP flexible formwork for straight as well as Load carrying capacity of curved slab is around 25% higher than straight slabs. This increase in load carrying capacity is due to increase in thickness in the central portion in case of curved slab. However, central deflection is higher in case of straight adhesive bonded slab as compared to curved slabs due to relatively low central thickness. Thus, straight adhesive bonded slabs shows more strain level in concrete as well as in GFRP plank when compared to curved slab specimens.

1. From the failure mode of all the three slabs, it was concluded that failure mode is brittle in case of both straight slabs and curved slabs. Initially many flexural cracks were obtained but ultimate failure was shear failure due to delamination of T ribs from the base plate. This resulted in shear failure of concrete.

2. AET parameters were very much efficient in investigating and monitoring the crack initiation as well as development of failure stages in GFRP-concrete composite systems. The surface mounted AE sensors on curved as well as on straight slabs gives an indication of AE activity taking place inside the concrete which can be related to the cracking process and maintenance of such GFRP-concrete composite systems.

3. Numerical validation of the experimental data was performed using non-linear finite elements method. A three-dimensional finite element model was prepared using software ATENA to simulate the behaviour of the bond treated GFRP-concrete interface. It was observed that strength and stiffness obtained through FEM model was on slightly higher side than the experimental ones. This could be due to perfect bond assumption in FEM model between FRP base plate and T ribs but in actual testing the failure was because of delamination between T ribs and base plate

6.3 SCOPE OFR FUTURE WORK

The work can be extended as follows:

1. The use of GFRP as a flexible formwork is new to the construction industry. Structural members with different configuration can be casted.
2. Concept of flexible formwork can be extended to the use of different type of formwork which can provide liberty to cast structural members of different configuration like fabric formwork.
3. Some advancements in technology can be done so that its failure could be ductile instead of brittle.
4. The associated main problem with the use of FRPs is the fire issue. Thus, the performance of proposed system under fire should be investigated

REFERENCES

Alagusundaramoorthy, P., Harik, I. E., & Choo, C. C. (2006). Structural behavior of FRP composite bridge deck panels. *Journal of Bridge Engineering*, *11*(4), 384-393.

Bank, L. C., Oliva, M. G., Bae, H. U., Barker, J. W., & Yoo, S. W. (2007). Pultruded FRP plank as formwork and reinforcement for concrete members. *Advances in Structural Engineering*, *10*(5), 525-535.

Berg, A. C., Bank, L. C., Oliva, M. G., & Russell, J. S. (2006). Construction and cost analysis of an FRP reinforced concrete bridge deck. *Construction and Building Materials*, *20*(8), 515-526.

Cheng, L., & Karbhari, V. M. (2005). Steel-Free Hybrid FRP Stiffened Panel-Concrete Deck System. *Special Publication*, *230*, 631-650.

Colombo, S., Forde, M. C., Main, I. G., & Shigeishi, M. (2005). Predicting the ultimate bending capacity of concrete beams from the "relaxation ratio" analysis of AE signals. *Construction and Building Materials*, *19*(10), 746-754.

Dieter, D., Dietsche, J., Bank, L., Oliva, M., & Russell, J. (2002). Concrete bridge decks constructed with fiber-reinforced polymer stay-in-place forms and grid reinforcing. *Transportation Research Record: Journal of the Transportation Research Board*, (1814), 219-226.

Fam, A., & Nelson, M. (2011). New bridge deck cast onto corrugated GFRP stay-in-place structural forms with interlocking connections. *Journal of Composites for Construction*, *16*(1), 110-117.

Goyal, R., Goyal, S., & Mukherjee, A. (2017). Pultruded fibre reinforced polymer planks as stay-in-place formwork for concrete structures. *Current Science (00113891)*, *113*(2).

Goyal, R., Mukherjee, A., & Goyal, S. (2016). An investigation on bond between FRP stay-in-place formwork and concrete. *Construction and Building Materials*, *113*, 741-751.

Goyal, R., Mukherjee, A., & Goyal, S. (2016). Bond between FRP formworks and concrete-effect of surface treatments and adhesives. *Steel and Composite Structures*, *20*(3), 671-692.

Grace, N., Jensen, E., Matsagar, V., & Penjendra, P. (2013). Performance of an AASHTO beam bridge prestressed with CFRP tendons. *Journal of Bridge Engineering*, *18*(2), 110-121.

Hadi, M. N. S. (2003). Retrofitting of shear failed reinforced concrete beams. *Composite Structures*, *62*(1), 1-6.

Hall, J. E., & Mottram, J. T. (1998). Combined FRP reinforcement and permanent formwork for concrete members. *Journal of Composites for Construction*, *2*(2), 78-86.

Honickman, H., & Fam, A. (2009). Investigating a structural form system for concrete girders using commercially available GFRP sheet-pile sections. *Journal of composites for construction*, *13*(5), 455-465.

Matta, F., Nanni, A., Ringelstetter, T. E., & Bank, L. C. (2006, December). Rapid construction of concrete bridge deck using prefabricated FRP reinforcement. In *CICE 2006, Third International Conference on FRP Composites in Civil Engineering* (pp. 13-15).

Mostafa, A., & Razaqpur, A. G. (2017). A nonlinear model for predicting intermediate crack-induced debonding in FRP-retrofitted beams in flexure. *Composite Structures*, *176*, 268-280.

Nair, A. (2006). Acoustic emission monitoring and quantitative evaluation of damage in reinforced concrete members and bridges.

Nelson, M. S., Fam, A. Z., Busel, J. P., Bakis, C. E., Nanni, A., Bank, L. C., ... & Hanus, J. (2014). Fiber-Reinforced Polymer Stay-in-Place Structural Forms for Concrete Bridge Decks: State-of-the-Art Review. *ACI Structural Journal*, *111*(5).

Nicoletta, B., Woods, J., Gales, J., & Fam, A. PERFORMANCE OF GFRP STAY-IN-PLACE FORMWORK FOR BRIDGE DECKS AFTER REAL AND SIMULATED FIRE DAMAGE.

Noël, M., & Fam, A. (2016). Design equations for concrete bridge decks with FRP stay-in-place structural forms. *Journal of Composites for Construction*, *20*(5), 04016024.

Oliva, M., Bank, L., Bae, H. U., Barker, J., & Yoo, S. W. (2007). FRP Stay-in-Place formwork and reinforcing for concrete highway bridge decks. *FRPRCS-8, Greece*, 1-10.

Orr, J. J., Darby, A., Ibell, T. J., & Evernden, M. (2014). Design methods for flexibly formed concrete beams.

Ramana, V. P. V., Kant, T. A. R. U. N., Morton, S. E., Dutta, P. K., Mukherjee, A. B. H. I. J. I. T., & Desai, Y. M. (2000). Behavior of CFRPC strengthened reinforced concrete beams with varying degrees of strengthening. *Composites Part B: Engineering*, *31*(6-7), 461-470.

Reising, R. M., Shahrooz, B. M., Hunt, V. J., Neumann, A. R., & Helmicki, A. J. (2004). Performance comparison of four fiber-reinforced polymer deck panels. *Journal of Composites for construction*, *8*(3), 265-274.

Sharma, A., Sharma, S., Sharma, S., & Mukherjee, A. (2018). Investigation of deterioration in corroding reinforced concrete beams using active and passive techniques. *Construction and Building Materials*, *161*, 555-569.

Sharma, A., Sharma, S., Sharma, S., & Mukherjee, A. (2018). Monitoring invisible corrosion in concrete using a combination of wave propagation techniques. *Cement and Concrete Composites*, *90*, 89-99.

Wu, K., Chen, B., & Yao, W. (2000). Study on the AE characteristics of fracture process of mortar, concrete and steel-fiber-reinforced concrete beams. *Cement and Concrete Research*, *30*(9), 1495-1500.